Interference modeling and performance analysis of asynchronous OFDM and FBMC wireless communication systems

Yahia Medjahdi

CONSERVATOIRE NATIONAL DES ARTS ET MÉTIERS

le cnam

École Doctorale Technologique et Professionnelle
CEDRIC/LAETITIA

THESE DE DOCTORAT

Présentée pour obtenir le Grade de Docteur
du Conservatoire National des Arts et Métiers

Discipline: Lasers, Métrologie, Communications
Spécialité: Communications et Electronique

Yahia Medjahdi

Modélisation d'Interférence et Analyse des Performances des Systèmes OFDM/FBMC pour les Communications sans fil Asynchrones.

Soutenue le 11 Juillet 2012 devant le jury composé de:

Rapporteurs

Faouzi Bader, CTTC, (Éspagne)
Luc Deneire, Université de Sophia-Antipolis I3S, (France)

Examinateurs

Pierre Siohan, Orange Labs, (France)
Jean-Baptiste Doré, CEA-LETI Minatec, (France)
Philippe Ciblat, TELECOM ParisTech, (France)

Directeurs :

Michel Terré, CNAM, (France)
Didier Le Ruyet, CNAM, (France)
Daniel Roviras, CNAM, (France)

Abstract

Multicarrier systems are widely used today due to their robustness to multipath effects and efficient implementation using FFT. Orthogonal Frequency Division Multiplexing (OFDM) system is a class of multicarrier modulation which consists of splitting up a wideband signal at a high symbol rate into several lower rate signals, each one occupying a narrower band. System performance improves because subcarriers experience flat fading channels and are orthogonal to one another. Recently, a number of papers have focused on a new alternative called Filter bank based multicarrier system (FBMC) which can offer a number of advantages over CP-OFDM system such as the improved spectral efficiency by not using a redundant CP and by having much better control of the out-of-band emission due to the time-frequency localized shaping pulses.

Furthermore, asynchronism inherently exists in several communication systems due to many factors e.g. the propagation delays and the spatial distribution of users. As one of the most challenging issue in design of communication systems, the asynchronism can harmfully affect the system performance by causing the so-called asynchronous interference.

In this dissertation, we investigate the impact of asynchronism on the performance of OFDM FBMC systems. First, we present a unified framework for multicarrier interference characterization and analysis in asynchronous environments. We propose a new family of interference tables that model the correlation between a given interfering subcarrier and the victim one, not only as a function of the spectral distance separating both subcarriers but also with respect to the timing misalignment between the subcarriers holders. These tables are derived for CP-OFDM, PHYDYAS-FBMC and IOTA-FBMC systems. Furthermore, the impact of the asynchronous interference on the average error rate and the average spectral efficiency of OFDM and FBMC systems is addressed. Based on computing the moment generating functions of the asynchronous interference power, simple new expressions for the exact evaluation of the average error rate and the average spectral efficiency are derived considering the frequency correlation fading between adjacent interfering subcarriers. These expressions significantly reduce the computation complexity of the performance evaluation.

For each technique two scenarios are examined: fully-loaded network and partially loaded ones. The accuracy of the obtained expressions has been validated through different simulation results. In contrast to OFDM, FBMC waveforms are demonstrated to be less sensitive to timing asynchronism, due to the better frequency localization of the used prototype filters.

Keywords: OFDM, FBMC, timing asynchronism, Interference, BER, Spectral efficiency

Résumé

Actuellement, les techniques multiporteuses sont largement utilisées dans les systèmes de transmission grâce à leur robustesse aux effets de trajets multiples et à leur implémentation efficace utilisant des FFTs. L'OFDM (orthogonal frequency division multiplexing) est un type de modulation multiporteuse qui consiste à subdiviser un flux de données à très haut débit en plusieurs flux élémentaires à bas-débit qui sont transmis sur différentes sous-porteuses orthogonales. Récemment, une technique multiporteuse à base de bancs de filtres (FBMC) a été proposée comme une alternative permettant d'offrir quelques avantages par rapport à l'OFDM. Un des principaux avantages est l'amélioration de l'efficacité spectrale grâce à l'absence du préfixe cyclique (CP) et aux formes d'onde bien localisées en temps et en fréquence.

Contrairement à ce qui est souvent supposé dans la littérature, l'asynchronisme existe intrinsèquement dans un bon nombre de systèmes de communication à cause de multiples facteurs tels que les délais de propagation et la distribution géographique des utilisateurs. Cet asynchronisme peut engendrer une perte d'orthogonalité entre les sous-porteuses qui peut se traduire par l'apparition d'interférences asynchrones causant à leurs tours une dégradation des performances du système. La modélisation de cette interférence présente un enjeu important dans la conception des systèmes de communication.

Dans cette thèse, nous analysons l'impact de la désynchronisation temporelle sur les performances de l'OFDM et de la FBMC. Tout d'abord, nous présentons un modèle global permettant la caractérisation et l'analyse de l'interférence dans les systèmes multiporteuses asynchrones. Une nouvelle famille de tables d'interférence est proposée tenant compte du décalage temporel ainsi que de la distance spectrale entre les sous-porteuses interférente et victime. Les termes de ces tables sont calculés pour CP-OFDM et FBMC avec les deux formes d'onde IOTA et PHYDYAS. L'impact de l'interférence asynchrone sur le taux d'erreur (BER) et sur l'efficacité spectrale de l'OFDM/FBMC est examiné. En se basant sur les fonctions génératrices des moments de la puissance d'interférence, nous avons établi des expressions analytiques simples du BER et de l'efficacité spectrale moyens. Ces dernières expressions réduisent d'une façon considérable la complexité de l'évaluation des performances. Cette étude théorique a été consolidée et validée par des résultats de simulation pour différents scénarios où nous avons démontré que contrairement à l'OFDM, les modulations FBMC sont moins sensible à la désynchronisation temporelle grâce à la bonne localisation des formes d'ondes utilisées.

Mots-clés : OFDM, FBMC, désynchronisation temporelle, Interférence, BER, Efficacité spectrale

Résumé des travaux de thèse

Motivation

Depuis quelques années, nous assistons à une métamorphose des applications pour les systèmes de communications sans-fil. En effet, les nouvelles applications telles que les visioconférences interactives avec partage de données en temps réel, les cours virtuels interactifs et la vidéo à la demande, sont en train de révolutionner les modèles de consommations en imposant des contraintes de débit de plus en plus élevé sur les systèmes de communications actuels.

Parmi les solutions étudiées pour répondre à ces contraintes de débit sans-cesse croissantes, les modulations multiporteuses (MCM) proposées depuis les années soixante se présentent comme candidates potentielles. En effet, l'idée de base des techniques multiporteuses consiste à subdiviser un flux de données à très haut débit en N flux élémentaires à un débit très bas qui sont transmis sur N sous-porteuses orthogonales. Le principal avantage est que même si les spectres des sous-porteuses se chevauchent, les signaux n'interfèrent pas entre eux grâce à l'orthogonalité [1]. De plus, le choix du nombre de sous-porteuses N doit assurer que la bande de chaque sous-canal soit plus petite que la bande de cohérence du canal de propagation. Ceci est équivalent à dire que l'étalement maximal des retards du canal est nettement inférieur à la période symbole T. Ainsi, chaque sous-canal subit un évanouissement plat et l'interférence entre symboles (ISI) devient négligeable [1], [2].

Actuellement, la technique multiporteuse OFDM (orthogonal frequency division multiplexing) est largement utilisée dans les systèmes de communications comme WiFi basé sur le standard IEEE 802.11, WiMax (Worldwide Interoperability for Microwave Access) [3], [4], [5] basé sur le standard IEEE 802.16 et LTE (Long Term Evolution) [3], [6]. Ce succès est la conséquence d'un nombre d'avantages offerts par l'OFDM :

- une efficace implémentation en utilisant la transformée de Fourier rapide (FFT),
- une robustesse aux effets des trajets multiples en utilisant un préfixe cyclique (CP),
- une simple égalisation utilisant un coefficient pour chaque sous-porteuse,
- une bonne efficacité spectrale permettant le recouvrement entre les spectres des différentes sous-porteuses.

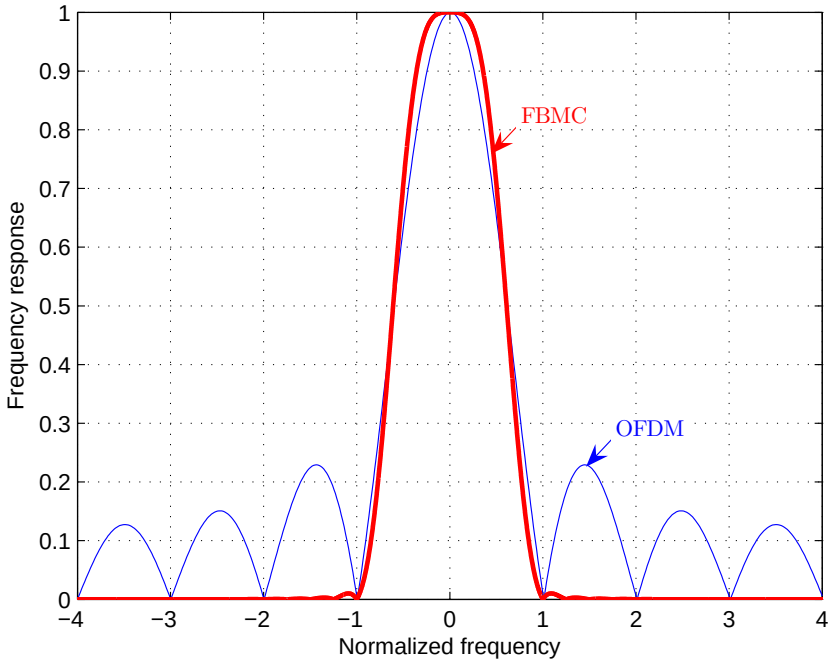

Réponses en fréquence de l'OFDM et de la FBMC

L'OFDM présente, cependant, deux inconvénients majeurs. D'une part, l'insertion du préfixe cyclique réduit l'efficacité spectrale puisque aucune information utile n'est transmise pendant la durée de ce préfixe cyclique. D'autre part, le niveau très élevé des lobes latéraux présents dans le spectre du filtre rectangulaire le rend non-compact et cause une perte additionnelle de l'efficacité spectrale.

Ces inconvénients ont stimulé de nombreux travaux de recherche. Afin de surmonter ces limitations en efficacité spectrale, une nouvelle couche physique basée sur les bancs de filtres a été proposée dans le projet européen PHYDYAS comme une alternative, très intéressante, à l'OFDM. En effet, une meilleure efficacité spectrale peut être réalisée en utilisant la modulation multiporteuse à base de banc de filtres (FBMC). Ceci est obtenu grâce à un choix judicieux d'une fonction prototype bien localisée dans l'espace temps/fréquence modulant chacune des sous-porteuses. De plus, les modulations FBMC peuvent atteindre une efficacité spectrale plus élevée grâce à l'absence du préfixe cyclique. En contre partie, une égalisation à la réception devient nécessaire afin d'éliminer les effets des trajets multiples [7, 8].

Dans la littérature, il est souvent supposé que les utilisateurs ou les stations de base, qui coexistent dans une même zone géographique, sont parfaitement synchronisés. En réalité, cette hypothèse n'est pas toujours vraie. Plusieurs scénarios, dans lesquels l'asynchronisme existe intrinsèquement, peuvent être cités tels que les réseaux Ad-hoc, les réseaux cognitifs ou opportunistes et les réseaux hétérogènes.

Cet asynchronisme peut engendrer une perte d'orthogonalité entre les sous-porteuses.

Cette perte d'orthogonalité peut se traduire par l'apparition des interférences asynchrones qui causent à leurs tours une dégradation des performances du système. La modélisation de cette interférence présente un enjeu important dans la conception des systèmes de communication. De nombreuses approches ont été examinées pour étudier ce problème. La densité spectrale de puissance (PSD) est couramment utilisée pour modéliser l'interférence en mesurant le rayonnement du signal en dehors de sa bande de fréquence autorisée [9], [10], [11]. Malheureusement, ce modèle peut conduire à des résultats erronés. Par exemple lorsque l'asynchronisme est absorbé par le préfixe cyclique dans le cas CP-OFDM. L'orthogonalité entre sous-porteuses est dans ce cas maintenue, alors que la modélisation PSD montre que l'interférence existe indépendamment du rang de la désynchronisation.

Objectifs de la thèse

Dans cette thèse, nous analysons l'impact de la désynchronisation temporelle sur les performances de l'OFDM et de la FBMC. En effet, nous allons :

- Estimer correctement la partie d'interférence introduite par la désynchronisation temporelle pour les systèmes OFDM.
- Proposer une extension de ce modèle englobant le cas FBMC qui, à notre connaissance, n'a jamais été pris en compte dans la littérature.
- En se basant sur le modèle proposé, établir les expressions analytiques du rapport signal-à-interférence-plus-bruit (SINR) pour les deux cas: OFDM et FBMC.
- Étudier l'impact de l'interférence sur les performances du système en établissant les expressions du taux d'erreur binaire (BER) et de l'efficacité spectrale dans les systèmes OFDM et FBMC.

Dans la suite, nous détaillons les travaux menés durant cette thèse :

Chapitre 2 - Introduction des techniques multiporteuses et des systèmes asynchrones

Dans ce chapitre, nous présentons le contexte et l'état de l'art lié aux différents concepts utilisés dans cette thèse. Tout d'abord, la technique OFDM est brièvement décrite. Ensuite, nous présentons la théorie fondamentale des techniques FBMC. En outre, l'implémentation polyphasée de l'émetteur/récepteur FBMC est exposée. Nous discutons finalement le problème d'asynchronisme dans les systèmes multiporteuses.

OFDM

Le schéma d'un système OFDM comporte un émetteur, un récepteur et un canal radio à travers lequel se fait la transmission. En amont à ce schéma, le flux de données haut-débit

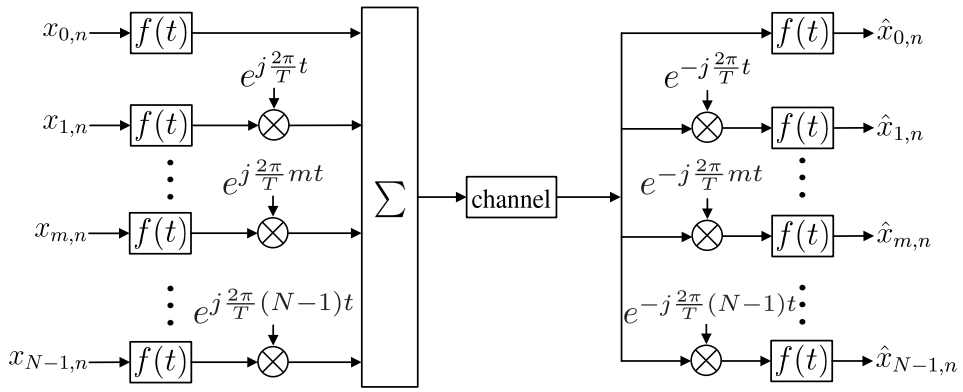

Le schéma de principe d'un système OFDM.

passe par un convertisseur série parallèle qui divise les données à son entrée en des flux de données parallèles à débit réduit. Chaque flux élémentaire est filtré par une fenêtre rectangulaire $f(t)$ et ensuite modulé sur une sous-porteuse m. À la réception, le signal est démodulé sur chaque sous-porteuse m puis passe par le filtre de réception $f(t)$. Dans un canal idéal, le signal reconstitué à la sortie du récepteur est égal à celui de l'entrée de l'émetteur c-à-d $x_{m,n} = \hat{x}_{m,n}$. Ainsi, on écrit la condition d'orthogonalité dans un système OFDM ayant une largeur spectrale de $1/T$ pour chaque sous-porteuse.

$$\int_{-\infty}^{+\infty} f(t-nT)f(t-n_0T)e^{j\frac{2\pi}{T}(m-m_0)t}dt = \delta_{m,m_0}\delta_{n,n_0}$$

où δ_{m,m_0} est le symbole de Kronecker.

On peut constater, à partir du schéma OFDM, que le signal transmis n'est rien d'autre que la transformée de Fourrier inverse du signal d'entrée. Par conséquent, pour récupérer les symboles $\hat{x}_{m,n}$, le récepteur exécute une simple transformée de Fourrier. Si le nombre de sous-porteuses N est une puissance de 2, il est connu que l'analyse et la synthèse de Fourrier peuvent être efficacement implémentées en utilisant la transformée de Fourier rapide (FFT) et la transformée de Fourier rapide inverse (IFFT), respectivement.

Dans un système OFDM classique, on reproduit, au début de chaque bloc OFDM, une copie de ses Δ derniers échantillons. Cette copie est appelée le préfixe cyclique (CP). Afin d'éliminer l'interférence introduite par les effets de trajets multiples, la longueur du préfixe cyclique doit être supérieure à l'étalement maximal du canal τ_{ds}. On peut aisément démontrer que l'utilisation du CP transforme la convolution entre le signal transmis et la réponse du canal en une convolution circulaire. Par conséquent, le signal à la sortie de la FFT devient :

$$y_{m_0,n_0} = H(m_0)x_{m_0,n_0}$$

où, $H(m_0) = \sum_{i=0}^{L-1} h_i e^{-j\frac{2\pi}{N}m_0 n_i}$ représente le gain complexe du canal de propagation sur la sous-porteuse m_0.

À cause de l'insertion du préfixe cyclique, la densité de symbole $\rho = T/(T+\Delta) < 1$. Afin de surmonter cette limitation, les modulations FBMC ont été proposées offrant une densité $\rho = 1$. Cependant, il a été démontré par le théorème de Balian-Low [12] qu'il est impossible d'avoir une forme d'onde bien localisée en temps et en fréquence satisfaisant à la fois la condition d'orthogonalité et une densité de symbole $\rho = 1$. Dans les modulations FBMC, la condition d'orthogonalité complexe a été relâchée en la limitant au domaine réel.

FBMC

L'idée principale de la FBMC/OQAM est de transmettre des symboles offset-QAM (OQAM) au lieu des symboles QAM (Quadrature Amplitude Modulation) conventionnels où un décalage d'une demi-période symbole $T/2$ est introduit entre la partie réelle et la partie imaginaire d'un symbole QAM donné. La seconde spécificité est que si la partie imaginaire est retardée de $T/2$ sur une sous-porteuse, c'est la partie réelle qui sera retardée sur la sous-porteuse suivante.
Le signal FBMC en temps continu et en bande de base peut être écrit sous la forme suivante:

$$s(t) = \sum_{m=0}^{N-1} \sum_{n=-\infty}^{+\infty} a_{m,n} f(t - nT/2) e^{j\frac{2\pi}{T}mt} e^{j\varphi_{m,n}}$$

où $a_{m,n}$ sont les symboles réels issus d'une modulation PAM (Pulse Amplitude Modulation), $f(t)$ est la réponse impulsionnelle du filtre prototype et la phase $\varphi_{m,n}$ est définie par :

$$\varphi_{m,n} = \frac{\pi}{2}(m+n) - \pi mn$$

Dans un canal parfait, le signal à la sortie du récepteur s'écrit comme suit :

$$\hat{a}_{m,n} = \sum_{m'=0}^{N-1} \sum_{n'=-\infty}^{+\infty} \int_{-\infty}^{+\infty} \mathrm{Re}\left[a_{m',n'} f(t - nT/2) f(t - n'T/2) e^{j\frac{2\pi}{T}(m'-m)t} e^{j(\varphi_{m',n'} - \varphi_{m,n})} dt \right]$$

Ainsi, la condition d'orthogonalité dans un système FBMC/OQAM ayant une largeur de $1/T$ pour chaque sous-porteuse est donnée par :

$$\int_{-\infty}^{+\infty} f(t - nT/2) f(t - n'T/2) \cos\left(\frac{2\pi}{T}(m'-m)t + \varphi_{m',n'} - \varphi_{m,n} \right) dt = \delta_{m,m'}\delta_{n,n'}$$

En présence des trajets multiples $h(t)$, le signal à l'entrée du récepteur devient :

$$r(t) = \sum_{m=0}^{N-1} \sum_{n=-\infty}^{+\infty} a_{m,n} e^{j\varphi_{m,n}} \sum_{i=0}^{L-1} h_i f(t - nT/2 - \frac{n_i}{N}T) e^{j\frac{2\pi}{T}m(t - \frac{n_i}{N}T)}$$

En général, la longueur du filtre prototype $f(t)$ est un multiple de la période symbole T. Par conséquent, la bande occupée par ce filtre est plus petite que la bande de cohérence du canal $B_c = 1/(2\tau_{\mathrm{ds}})$ [1], [13]. Ce qui implique :

$$f(t - nT/2 - \tau) \approx f(t - nT/2), \qquad \tau \in [0, \tau_{\mathrm{ds}}]$$

Le signal $r(t)$ peut donc être réécrit sous la forme suivante :

$$r(t) = \sum_{m=0}^{N-1} \sum_{n=-\infty}^{+\infty} a_{m,n} e^{j\varphi_{m,n}} f(t - nT/2) e^{j\frac{2\pi}{T}mt} H(m)$$

Étant donné que le filtre prototype est bien localisé en temps et en fréquence, l'intégrale $\int_{-\infty}^{+\infty} f(t - nT/2) f(t - n_0 T/2) e^{j\frac{2\pi}{T}(m-m_0)t} dt$ tend rapidement vers 0 avec l'augmentation de $|n - n_0|$ et $|m - m_0|$. Le signal à la sortie du filtre de réception de la sous-porteuse m_0 à l'instant n_0 est donc donné par:

$$y_{m_0,n_0} = H(m_0) \sum_{l \in \Omega_{\Delta m}} \sum_{n=-\infty}^{+\infty} a_{m,n} e^{j(\varphi_{m_0+l,n} - \varphi_{m_0,n_0})} \int_{-\infty}^{+\infty} f(t - nT/2) f(t - n_0 T/2) e^{j\frac{2\pi}{T}lt} dt$$

Finalement, le signal émis est reconstruit après la décision OQAM sous l'hypothèse d'une parfaite égalisation de canal.

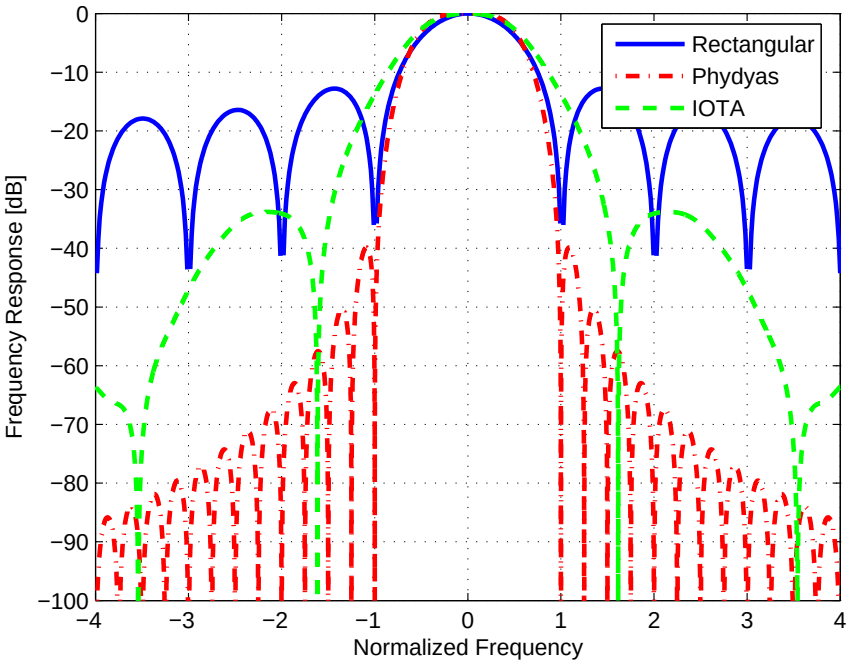

Les réponse en fréquence des formes d'ones: PHYDYAS et IOTA

Le transmultiplexeur FBMC peut être efficacement implémenté en utilisant la représentation polyphasée du filtre prototype. Cette implémentation se base sur le fait que le banc de filtre de synthèse (émetteur FBMC) et celui d'analyse (récepteur FBMC) sont composés d'un ensemble de versions décalées de la réponse fréquentielle du filtre prototype. Après certaines transformations, le banc de filtre de synthèse sera composé d'une IFFT en cascade

avec le réseau polyphasé du filtre $f(t)$. Le banc de filtre d'analyse est, quant à lui, réalisé par la mise en cascade du réseau polyphasé de $f(t)$ et d'une FFT.

Concernant le choix du filtre prototype, nous avons considéré dans cette thèse deux formes d'onde largement utilisées par la communauté : IOTA (Isotropic Orthogonal Transform Algorithm) qui est le résultat d'un algorithme d'orthogonalisation appliqué sur une fonction gaussienne [14], [15] et le filtre prototype de PHYDYAS proposé par Bellanger [16]. La propriété la plus importante de ces filtres est qu'ils sont bien localisés en temps et en fréquence.

L'asynchronisme dans les systèmes multiporteuses

En général, afin de préserver l'orthogonalité entre les sous-porteuse en OFDMA, les signaux des différents utilisateurs doivent arriver à l'entrée du récepteur d'une manière synchrone. Plusieurs techniques de synchronisation ont été proposées en OFDMA pour assurer l'alignement des signaux au niveau d'un récepteur. La plupart de ces techniques doivent être contrôlées en boucle fermée [17], ce qui exige l'estimation des différents temps d'arrivées par le récepteur.
Dans cette section, nous décrivons quelques scénarios où le synchronisme temporel ne peut, malheureusement, pas être garanti. Parmi ces scénarios, nous avons :

Les réseaux Ad-hoc Contrairement aux réseaux cellulaires classiques, les utilisateurs dans les réseaux Ad-hoc peuvent communiquer entre eux sans passer par une station de base centrale. Par conséquent, l'implémentation des techniques de synchronisation en OFDMA au niveau de chaque utilisateur serait très coûteuse. Dans ce cas, la méthode la plus adaptée consiste à étendre le préfixe cyclique au-delà de ce qui est nécessaire pour éliminer l'interférence causée par les effets des trajets multiples [17]. Néanmoins, cette solution augmente la redondance et diminue de ce fait le débit effectif du système.

Les réseaux radio-cognitifs Le problème de synchronisation dans ces réseaux est plus difficile parce que les utilisateurs primaires et secondaires (ou cognitifs) transmettent leurs signaux indépendamment les uns des autres.

Dans le chapitre suivant, l'impact de l'asynchronisme sur les systèmes multiporteuses sera étudié et analysé.

Chapitre 3 - Modélisation d'interférence asynchrone

L'interférence est une des causes les plus importantes entraînant la dégradation de la qualité de service dans les systèmes de communication sans-fil. Dans ce chapitre, nous présentons un modèle global pour la caractérisation et l'analyse de l'interférence dans les systèmes multiporteuses asynchrones. Cette interférence est la conséquence de la perte de l'orthogonalité entre les différentes sous-porteuses. Nous expliquons tout d'abord le concept général des tables d'interférence. Nous développons ensuite le calcul théorique des termes d'interférence

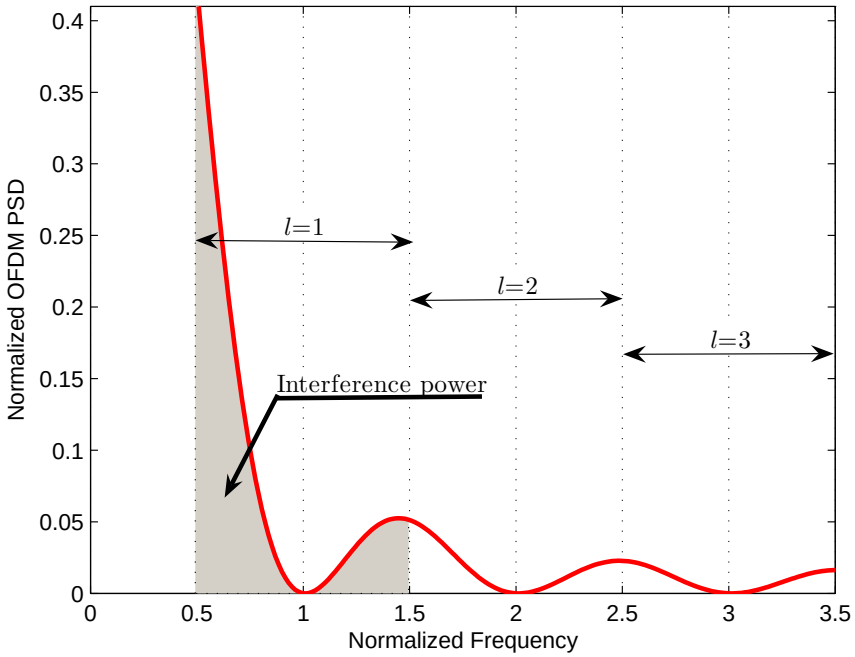

La PSD d'une sous-porteuse OFDM

pour l'OFDM et la FBMC et nous présentons une extension de ce modèle en considérant les canaux sélectifs en fréquence. Enfin, quelques résultats de simulations sont analysés.

Le concept général des tables d'interférence

La densité spectrale de puissance (PSD) est souvent utilisée pour analyser l'interférence causée par un système sur un autre [9], [10]. Selon [10], l'interférence mutuelle normalisée entre deux systèmes qui partage une bande de fréquence donnée est définie par :

$$I(l) = \int_{(l-1/2)\Delta f}^{(l+1/2)\Delta f} \Phi(f) df$$

où :

- l est la distance spectrale entre les deux sous-porteuses interférente et victime.
- Δf est la largeur d'une sous-porteuse
- $\Phi(f)$ est la densité spectrale de puissance qui dépend de la forme d'onde utilisée.

Dans le cas d'OFDM, la PSD normalisée est donnée par [10] :

$$\Phi_{\mathrm{OFDM}}(f) = T_{\mathrm{OFDM}} \left(\frac{sin(\pi f T_{\mathrm{OFDM}})}{\pi f T_{\mathrm{OFDM}}} \right)^2$$

où $T_{\mathrm{OFDM}} = T + \Delta$; Δ étant la durée du préfixe cyclique.
En ce qui concerne les systèmes FBMC, la PSD a été calculée dans [9], pour les deux formes d'onde : IOTA et PHYDYAS,

$$\Phi_{\mathrm{IOTA}}(f) = (f_{1,\sqrt{2}/2,\sqrt{2}/2})^2$$

où $f_{1,\sqrt{2}/2,\sqrt{2}/2}$ représente la réponse impulsionnelle du filtre IOTA qui est égale à sa transformée de Fourrier.

$$\Phi_{\mathrm{PHYDYAS}}(f) = (F(f))^2$$

où $F(f)$ est la racine carrée de la réponse en fréquence du filtre prototype de PHYDYAS.

On peut constater que l'interférence calculée par le modèle PSD ne dépend pas du décalage temporel entre les signaux transmis par les deux systèmes. Cependant dans un système CP-OFDM, l'orthogonalité entre les différents signaux transmis est maintenue tant que la désynchronisation ne dépasse pas la durée du préfixe cyclique. Cet exemple met en évidence les limites du modèle PSD.

Tables d'interférence: OFDM et FBMC

Après avoir introduit le concept général de l'estimation d'interférence, nous proposons une nouveau modèle qui tient compte de la désynchronisation entre l'interféreur et le récepteur victime. Ce modèle est appelé "les tables d'interférence instantanées". Nous notons ces tables par $I(\tau, l)$ pour l'OFDM et la FBMC. Elles peuvent être définie comme :

CP-OFDM:

$$I(\tau,l) = \begin{cases} \delta(l) & \tau \in [0,\Delta] \\ \left[(T+\Delta-\tau)^2 + (\tau-\Delta)^2\right]/T^2 & \tau \in [\Delta, T+\Delta], l = 0 \\ \left|\frac{\sin(\pi l(T+\Delta-\tau)/T)}{\pi l}\right|^2 + \left|\frac{\sin(\pi l(\tau-\Delta)/T)}{\pi l}\right|^2 & \tau \in [\Delta, T+\Delta], l \neq 0 \end{cases}$$

Ces tables d'interférence montrent que l'orthogonalité entre les sous-porteuses interférente et victime est maintenue quand le décalage temporel τ est inférieur à la durée du CP Δ. Ces tables montrent aussi que la puissance d'interférence change en fonction de la distance spectrale l et la désynchronisation τ.

FBMC:

De la même manière, nous avons calculé les tables d'interférence en FBMC,

$$I(\tau, l) = \mathbb{E}_{a_{m,n},\varphi}\left[|y_{tot}(\tau,\varphi)|^2\right]$$

où $y_{tot}(\tau,\varphi)$ représente le signal après la décision OQAM, résultant d'un signal transmis qui a subi un retard τ et un déphasage φ :

$$y_{tot}(\tau,\varphi) = \mathrm{Re}\left\{y_{m_0,n_0}(\tau,\varphi)\right\} + j\mathrm{Re}\left\{y_{m_0,n_0+1}(\tau,\varphi)\right\}$$

avec $y_{m_0,n_0}(\tau,\varphi)$ est le signal complexe à la sortie du filtre de réception qui est donné en fonction de la désynchronisation τ par :

cas 1: $(n_0-n)\frac{T}{2} < \tau$

$$y_{m_0,n_0}(\tau,\varphi) = \sum_{n=\lfloor \frac{-\tau}{T/2}\rfloor+n_0+1}^{2K+n_0-1} a_{m,n} e^{j(\varphi+\varphi_{m,n}-\varphi_{m_0,n_0})} e^{-j\frac{2\pi}{T}m\tau} \Psi(t,\tau,l)\Big|_{t=\tau}^{KT+(n_0-n)\frac{T}{2}}$$

cas 2: $\tau < (n_0-n)\frac{T}{2}$

$$y_{m_0,n_0}(\tau,\varphi) = \sum_{n=-2K+n_0+1}^{n_0+\lceil \frac{-\tau}{T/2}\rceil-1} a_{m,n} e^{j(\varphi+\varphi_{m,n}-\varphi_{m_0,n_0})} e^{-j\frac{2\pi}{T}m\tau} \Psi(t,\tau,l)\Big|_{t=(n_0-n)\frac{T}{2}}^{KT+\tau}$$

À travers ces exemples de tables d'interférence, nous pouvons voir qu'il n'y a pratiquement pas d'interférence quand la distance spectrale $l > 1$ pour PHYDYAS et $l > 2$ pour IOTA. De plus, nous pouvons constater que l'interférence significative en FBMC est quasiment invariable par rapport à la désynchronisation τ. Contrairement aux formes d'onde FBMC, l'interférence asynchrone en OFDM reste significative même pour une distance spectrale $l = 6$.
Nous avons également comparé les tables d'interférence moyennes avec les tables calculées par la PSD. Nous pouvons voir que la différence des niveaux d'interférence croît proportionnellement à la distance spectrale l. Mais, cette différence est négligeable en FBMC quand le niveau d'interférence est élevé.

L'interférence asynchrone dans un canal sélectif en fréquence

En présence d'un canal sélectif en fréquence, nous avons démontré que la puissance de l'interférence asynchrone peut être calculée par :

$$P_{\text{interf}}(m_0,\tau) = d^{-\beta} P_{\text{trans}}(m) I(\tau, |m-m_0|) |H(m)|^2$$

où :

- d est la distance entre l'interféreur et le récepteur d'intérêt,

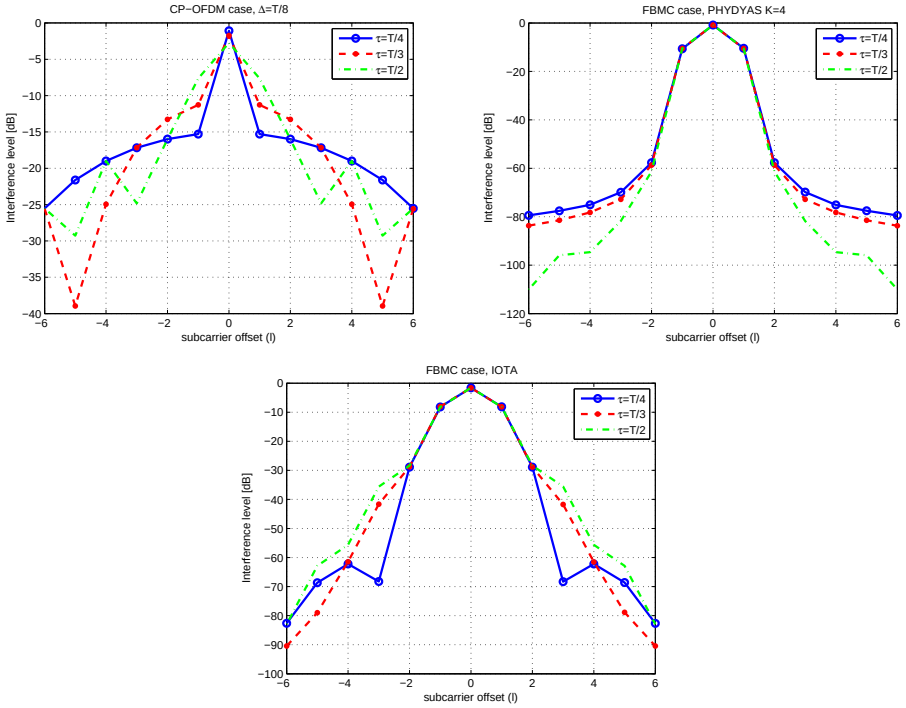

Les tables instantanées d'OFDM, FBMC-PHYDYAS et FBMC-IOTA pour $\tau = T/4, T/3, T/2$

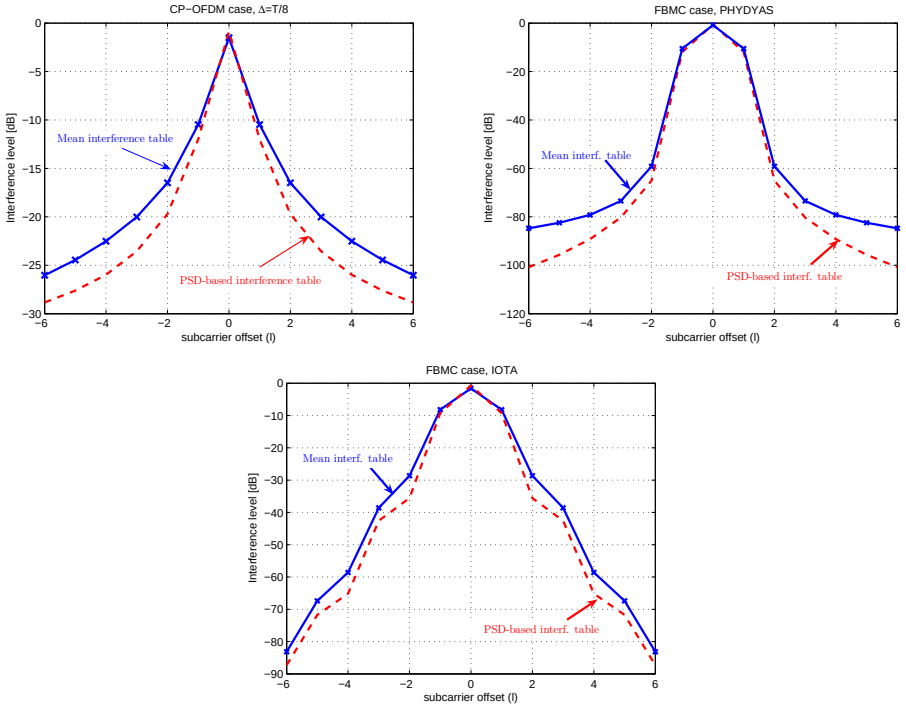

Comparaison entre la table d'interférence moyenne et la table calculée par la PSD

- β est l'exposant de l'affaiblissement de propagation,
- $P_{\text{trans}}(m)$ est la puissance transmise sur la sous-porteuse m,
- $I(\tau, |m - m_0|)$ est le coefficient de la table d'interférence qui correspond à un décalage temporel τ et une distance spectrale $|m - m_0|$,
- $|H(m)|^2$ est le gain en puissance du canal entre l'interféreur et le récepteur d'intérêt sur la sous-porteuse m.

Validation du modèle proposé

Afin de valider le modèle proposé, nous avons réalisé plusieurs simulations sur le scénario présenté dans la figure ci-après. Nous considérons la voie montante d'une transmission OFDM/FBMC dans un réseau à 2 cellules. L'utilisateur de référence MU_0 est situé à une distance d_0 de sa station de base BS_0. L'interféreur MU_1 communique avec BS_1 et il est situé à une distance d de BS_0. La puissance d'émission de chaque utilisateur doit assurer un rapport signal à bruit (SNR) de 20 dB. Les blocs de sous-porteuses $\mathcal{F}_0$ et $\mathcal{F}_1$ sont alloués respectivement à MU_0 et MU_1.
La propagation des signaux transmis suit le modèle Pedestrian-A. Le choix de ce modèle est basé sur l'hypothèse que chaque sous-porteuse subit un évanouissement plat. De plus, le modèle de propagation considéré inclut l'affaiblissement de propagation qui tient compte de la position de l'utilisateur par rapport à la station de base de référence BS_0. Cet affaiblissement est exprimé par :

$$\Gamma_{\text{loss}}(d) = 128.1 + 37.6 \log_{10}(d[km])[dB]$$

D'autre part, nous avons considéré un système avec $N = 1024$ sous-porteuses et une fréquence d'échantillonnage de 10 MHz. La densité spectrale du bruit thermique considéré est $N_0 = -174$ dBm/Hz.

Chaque usager est supposé parfaitement synchronisé avec sa station de base mais pas synchronisé avec l'autre BS. À cause de la désynchronisation entre MU_1 et BS_0, les signaux transmis par MU_0 et MU_1 ne sont pas orthogonaux. Cette perte d'orthogonalité génère de l'interférence qui dégrade à son tour le SINR. Ce dernier peut s'exprimer pour une sous-porteuse $m \in \mathcal{F}_0$ par :

$$\text{SINR}(m) = \frac{d_0^{-\beta} P_{\text{trans}}(m) \left|H_0(m)\right|^2}{\sum\limits_{m' \in \mathcal{F}_1} d^{-\beta} P_{\text{trans}}(m') I(\tau, |m' - m|) \left|H_1(m')\right|^2 + N_0 \Delta f}$$

où Δf est la largeur de la sous-porteuse m_0.
Il est à noter que le coefficient $I(\tau, |m' - m|)$ est calculé par les deux méthodes : PSD et le modèle proposé.
L'objectif de cette section est d'évaluer le SINR moyen ainsi que l'efficacité spectrale exprimés respectivement par :

$$\text{SINR}_{\text{average}}(m) = \mathbb{E}\left[\text{SINR}(m)\right]$$

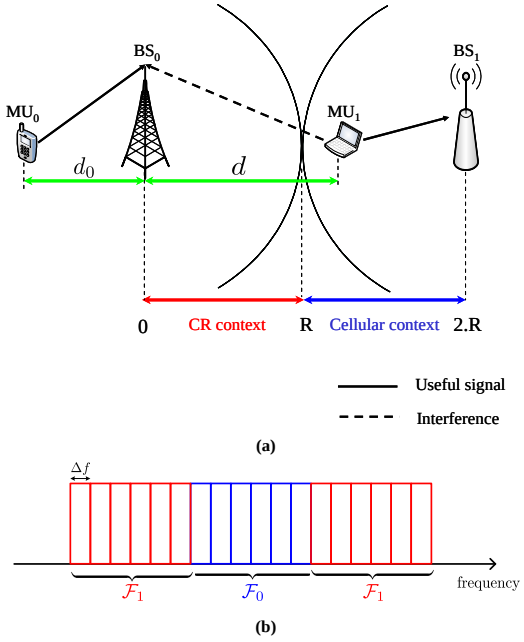

la voie montante d'un réseau OFDM/FBMC à deux cellules

$$C_{\text{average}}(m) = \mathbb{E}\left[\log_2\left(1 + \text{SINR}(m)\right)\right]$$

où $\mathbb{E}[.]$ représente l'espérance mathématique calculée sur toutes les réalisations de $H_0(m)$ et de $\{H_1(m'), m' \in \mathcal{F}_1\}$ et sur toutes les valeurs de désynchronisation τ qui est uniformément distribuée sur $[0, T]$.
Deux contextes sont analysés :

- **Le contexte cellulaire classique**: quand $d \in [R, 2R]$
- **Le contexte radio cognitif**: quand $d \in [0, R]$

Dans les figures ci-après, l'évolution du SINR en fonction de d/R est représentée dans les cas CP-OFDM, FBMC-PHYDYAS et FBMC-IOTA. Trois méthodes sont utilisées pour l'estimation du SINR dans chaque cas : les tables instantanées (ligne), les tables PSD (points .) et les simulations numériques (croix x). Nous pouvons voir que les résultats obtenus par les tables instantanées correspondent parfaitement aux résultats obtenus par la méthode numérique. Cependant, les résultats obtenus par le modèle PSD sont inexactes notamment dans le contexte radio cognitif.
Dans le contexte cognitif, on constate, en effet, une très forte degradation du SINR pour l'OFDM par rapport au SNR cible de 20 dB. Ceci est justifié par le niveau élevé de la puissance de l'interférence présente sur l'ensemble des sous-porteuses $m \in \mathcal{F}_0$. En revanche, une faible perte en SNR est observée dans le cas FBMC. Un tel résultat peut s'expliquer par le fait qu'uniquement une sous-porteuse (2 sous-porteuse dans le cas FBMC-IOTA) sur

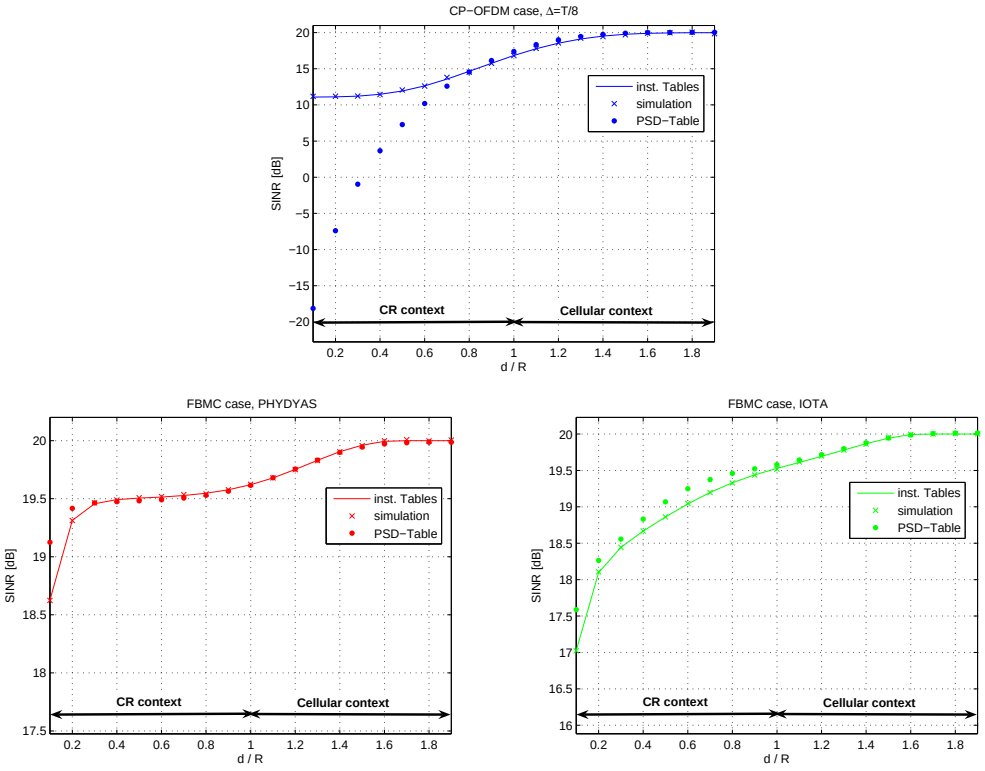

Le SINR moyen en fonction de la distance d entre $\mathbf{MU}_1$ et $\mathbf{BS}_0$, $\tau \in [0, T]$

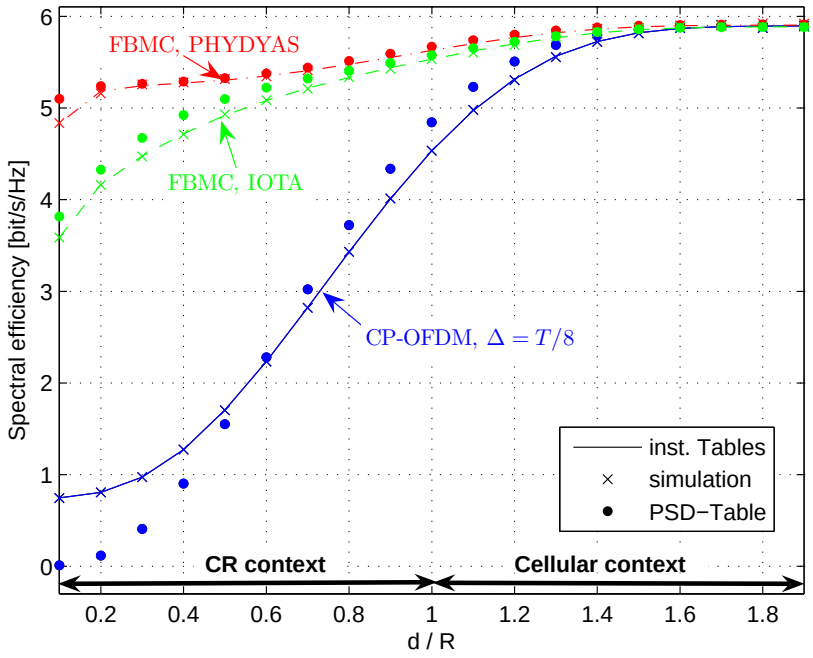

L'efficacité spectrale en fonction de la distance d entre $\mathbf{MU}_1$ et $\mathbf{BS}_0$, $\tau \in [0, T]$

chaque extrémité de $\mathcal{F}_0$ est affectée par l'interférence.
Dans le contexte cellulaire, l'interféreur MU_1 est suffisamment loin de BS_0. Ceci implique que la puissance provenant de MU_1 à BS_0 est réduite par l'important affaiblissement de propagation. Par conséquent, l'impact de l'interférence asynchrone est mois significatif dans ce contexte pour toutes les formes d'ondes. Par ailleurs, les SINRs de l'OFDM et de FBMC convergent vers le SNR cible pour les valeurs élevées de d. L'interférence est dans ce cas négligeable devant le bruit.
L'effet de l'interférence asynchrone sur l'efficacité spectrale a également été examiné, dans la figure ci-avant. Ces résultats confirment la bonne estimation de l'efficacité spectrale par le modèle proposé et montrent une meilleure performance dans le cas FBMC par rapport à l'OFDM. On peut voir aussi que l'efficacité spectrale des deux modulations OFDM et FBMC tends vers le même palier à cause de la prédominance du bruit. On rappelle que le debit effectif de l'OFDM est inférieur à celui présenté dans ces résultats à cause de la redondance introduite par le CP dans chaque bloc OFDM.

La méthode d'estimation de l'interférence asynchrone proposée dans ce chapitre présente une alternative plus efficace à l'évaluation numérique directe. Il est donc intéressant de souligner que la méthode proposée est une méthode semi-analytique. Ce qui signifie que nous avons toujours besoin de simuler les réalisations des différents canaux (utile et canaux d'interférence). Par conséquent, on peut voir que la complexité de l'évaluation des performances demeure importante, en particulier lorsque le nombre des interféreurs est important.

Dans les deux chapitres suivants, nous développons de nouvelles expressions analytiques qui réduisent considérablement la complexité de l'évaluation des performance : taux d'erreur et efficacité spectrale.

Chapitre 4 - Analyse des taux d'erreurs de l'OFDM et la FBMC dans les systèmes asynchrones

Le taux d'erreur d'une transmission donnée est un critère fréquemment utilisé pour analyser l'impact de l'interférence sur les performances du système. Dans ce chapitre, nous développons une expression analytique du taux d'erreur (BER) dans des systèmes OFDM et FBMC asynchrones. Tout d'abord, nous analysons le SINR. Nous nous intéressons par la suite au calcul des expressions du BER. Enfin, quelques résultats de simulation sont discutés.

Analyse de l'interférence et du SINR

Considérons un récepteur (récepteur d'intérêt) qui communique de manière synchrone avec son émetteur correspondant. D'autres émetteurs, qui coexistent dans la même zone géographique, transmettent d'une façon asynchrone par rapport au récepteur d'intérêt. On peut exprimer le signal composite à l'entrée du récepteur d'intérêt par la somme du signal

utile et des signaux interférants provenant des autres émetteurs :

$$r(t) = \underbrace{d_0^{-\beta/2} s_0(t) * h_0(t)}_{\text{desired signal}} + \underbrace{\sum_{k=1}^{K} d_k^{-\beta/2} s_k(t-\tau_k) * h_k(t)}_{\text{interference signal}} + n(t)$$

où :

- K est le nombre d'émetteurs interféreurs,
- d_0 est la distance entre le récepteur d'intérêt et son émetteur,
- d_k représente la distance entre un interféreur k et le récepteur d'intérêt,
- $s_0(t)$ est le signal transmis par l'émetteur d'intérêt,
- $s_k(t)$ est le signal d'interférence transmis par le k-ème émetteur,
- $h_k(t)$ et τ_k représentent, respectivement, le canal de propagation et le décalage temporel entre l'émetteur k et le récepteur d'intérêt,
- $n(t)$ est le bruit blanc additif gaussien (AWGN)
- β est l'exposant de l'affaiblissement de propagation.

En se basant sur le modèle d'interférence proposé dans le chapitre précédent, on peut exprimer la puissance de l'interférence totale qui affecte la m-ème sortie du récepteur de référence par

$$P_{\text{interf}}(m, \{\tau_k, k = 1, ..., K\}) = \sum_{k=1}^{K} \sum_{m' \in \mathcal{F}_k} d_k^{-\beta} P_{trans}(m') I(\tau_k, |m' - m|) \left|H_k(m')\right|^2$$

où :

- $\mathcal{F}_k$ désigne l'ensemble des sous-porteuses utilisées par l'émetteur k
- $P_{trans}(m')$ est la puissance émise sur la sous-porteuse interférente m'
- $\left|H_k(m')\right|^2$ est le gain en puissance du canal entre l'interféreur k et le récepteur d'intérêt sur la sous-porteuse m'.

Comme nous l'avons indiqué précédemment, le récepteur d'intérêt est supposé parfaitement synchronisé avec son émetteur. Par conséquent, la puissance du signal utile est donnée par

$$P_{\text{desired}}(m) = d_0^{-\beta} P_{trans}(m) \left|H_0(m)\right|^2$$

Cette hypothèse est vraie, dans le cas OFDM, tant que le préfix cyclique Δ est plus grand que l'étalement maximal du canal τ_{ds}. Dans le cas FBMC, le gain du canal est considéré plat sur chaque sous-porteuse si le nombre des sous-porteuses est très élevé. Etant donné que le but de ce chapitre est d'analyser la sensibilité de l'OFDM et de FBMC à la désynchronisation

temporelle, nous allons supposer que chaque sous-porteuse subit un évanouissement plat. Ceci est vrai dans les cas des canaux modérément sélectifs en fréquence.

Le SINR instantané est donc donné par :

$$\mathrm{SINR}(m) = \frac{d_0^{-\beta} P_{trans}(m) \left|H_0(m)\right|^2}{\sum_{k=1}^{K} \sum_{m' \in \mathcal{F}_k} d_k^{-\beta} P_{trans}(m') I(\tau_k, |m'-m|) \left|H_k(m')\right|^2 + N_0 \Delta f}$$

où N_0 représente la densité spectrale du bruit et Δf est la largeur de la sous-porteuse m. Pour des raisons de simplicité, nous réécrivons le SINR comme suit :

$$\mathrm{SINR}(m) = \frac{\left|H_0(m)\right|^2}{\sum_{k=1}^{K} \sum_{m' \in \mathcal{F}_k} A_{k,m,m'} \left|H_k(m')\right|^2 + b}$$

avec

$$A_{k,m,m'} = \left[\frac{d_k}{d_0}\right]^{-\beta} \frac{P_{trans}(m')}{P_{trans}(m)} I(\tau_k, |m'-m|)$$

$$b = \frac{N_0 \Delta f}{d_0^{-\beta} P_{trans}(m)}$$

Analyse du BER moyen

Dans la littérature, le BER de la QPSK est donné par [18] :

$$\mathrm{BER}(\mathrm{SNR}) = \frac{1}{2}\mathrm{erfc}\left(\sqrt{\frac{1}{2}\mathrm{SNR}}\right)$$

Il est à souligner que nous avons considéré des décalage τ_k constants dans le calcul des coefficients $A_{k,m,m'}$. Connaissant l'ensemble des variables aléatoires $\mathcal{H} = \{H_0(m), H_k(m'), k \in \{1, ..., K\}, m' \in \mathcal{F}_k\}$, on peut exprimer le BER conditionnel en présence de l'interférence par :

$$\mathrm{BER}(\mathrm{SINR})|_{\mathcal{H}} = \frac{1}{2}\mathrm{erfc}\left(\frac{1}{2}\frac{\left|H_0(m)\right|^2}{\sum_{k=1}^{K} \sum_{m' \in \mathcal{F}_k} A_{k,m,m'} \left|H_k(m')\right|^2 + b}\right)^{1/2}$$

Par conséquent, le BER moyen est donné par :

$$\mathrm{BER}_{\mathrm{average}} = \mathbb{E}_{\mathcal{H}}\left[\mathrm{BER}(\mathrm{SINR})|_{\mathcal{H}}\right] = \mathbb{E}_{\mathcal{H}}\left[\frac{1}{2}\mathrm{erfc}\left(\frac{1}{2}\frac{\left|H_0(m)\right|^2}{\sum_{k=1}^{K} \sum_{m' \in \mathcal{F}_k} A_{k,m,m'} \left|H_k(m')\right|^2 + b}\right)^{1/2}\right]$$

L'approche directe du calcul du BER moyen mène à une intégrale multiple qui est souvent difficile à calculer analytiquement. Afin de réduire la complexité du calcul, nous utilisons le lemme suivant [19],

Lemme Soit x une variable aléatoire gamma de moyenne unitaire et de paramètre α et soit c une constante positive. Soit g une variable aléatoire positive et indépendante de x. On a alors,

$$\mathbb{E}_{x,y}\left[\operatorname{erfc}\left(\frac{x}{g+c}\right)^{1/2}\right] = 1 - \frac{2}{\pi}\frac{\Gamma\left(\alpha+\frac{1}{2}\right)}{\Gamma(\alpha)}\int_0^{+\infty}\frac{e^{-z}}{\sqrt{z}}{}_1F_1\left(1-\alpha;\frac{3}{2};z\right)\mathcal{M}_g(\alpha z)e^{-z\alpha c}dz$$

où :

- $\Gamma(\alpha) = \int_0^{+\infty} z^{\alpha-1}e^{-z}dz$ est la fonction Gamma (définie pour $\alpha \in \mathbb{C}$ et $\mathrm{Re}(\alpha) > 0$) [20],
- ${}_1F_1(a;b;z) = \frac{\Gamma(b)}{\Gamma(b-a)\Gamma(a)}\int_0^1 e^{zu}u^{a-1}(1-z)^{b-a-1}du$ ($\mathrm{Re}(a) > 0$ et $\mathrm{Re}(b) > 0$) est la fonction hypergéométrique confluente de première espèce [20],
- $\mathcal{M}_g(z) = \mathbb{E}_g\left[e^{-zg}\right]$ est la fonction génératrice des moments (MGF) de g.

Après quelques transformations de l'expression du BER moyen, on obtient :

$$\mathrm{BER}_{\text{average}} = \frac{1}{2} - \frac{1}{2\sqrt{\pi}}\int_0^{+\infty}\frac{e^{-z(1+2b)}}{\sqrt{z}}\mathcal{M}_g(z)dz$$

où g représente la variable aléatoire de la puissance de l'interférence totale,

$$g = 2\sum_{k=1}^{K}\sum_{m'\in\mathcal{F}_k}A_{k,m,m'}g_{k,m'}$$

ici $g_{k,m'} = |H_k(m')|^2$.
Pour une analyse complète du BER, nous allons développer le calcul dans 2 cas :

Le cas multi-interféreurs complètement chargés

Comme les signaux transmis par les différents interféreurs sont indépendants, la MGF de g sera le produit des MGFs $\mathcal{M}_k(z)$ où :

$$\mathcal{M}_k(z) = \mathbb{E}_{\{g_{k,m'},m'\in\mathcal{F}_k\}}\left[e^{-2z\sum\limits_{m'\in\mathcal{F}_k}A_{k,m,m'}g_{k,m'}}\right]$$

Comme les sous-porteuses m' appartiennent au même bloc de sous-porteuses $\mathcal{F}_k$, leurs gains $g_{k,m'}$ sont corrélés.
Soit $\mathbf{\Omega}_k$ la matrice de corrélation des variables $\{g_{k,m'}, m' \in \mathcal{F}_k\}$. Selon [21], la MGF $\mathcal{M}_k(z)$ est donnée par :

$$\mathcal{M}_k(z) = \left|\mathbf{I}_{L_k} + 2\mathbf{D}_k^A\,\mathbf{\Omega}_k\,z\right|^{-1}$$

où :

- $\mathbf{I}_{L_k}$ est la matrice identité de dimensions $L_k \times L_k$ et L_k représente le cardinal de l'ensemble $\mathcal{F}_k$
- $\left|\mathbf{I}_{L_k} + 2\mathbf{D}_k^A\, \mathbf{\Omega}_k\, z\right|$ désigne le déterminant de la matrice $\mathbf{I}_{L_k} + 2\mathbf{D}_k^A\, \mathbf{\Omega}_k\, z$
- $\mathbf{D}_k^A$ est matrice diagonale avec,

$$\mathbf{D}_k^A(i,i) = A_{k,m,i} \qquad i \in \mathcal{F}_k$$

Finalement, le BER moyen peut s'écrire sous la forme suivante :

$$\mathrm{BER}_{\mathrm{average}} = \frac{1}{2} - \frac{1}{2\sqrt{\pi}} \int_0^{+\infty} \frac{e^{-z(1+2b)}}{\sqrt{z}} \prod_{k=1}^{K} \left|\mathbf{I}_{L_k} + 2\mathbf{D}_k^A\, \mathbf{\Omega}_k\, z\right|^{-1} dz$$

Dans le cas des canaux à évanouissement plat, le BER moyen devient :

$$\mathrm{BER}_{\mathrm{average}} = \frac{1}{2} - \frac{1}{2\sqrt{\pi}} \int_0^{+\infty} \frac{e^{-z(1+2b)}}{\sqrt{z}} \prod_{k=1}^{K} \left(1 + 2 \sum_{m' \in \mathcal{F}_k} A_{k,m,m'} z\right)^{-1} dz$$

Si les gains sur les sous-porteuses interférentes sont complètement décorrélés, le BER moyen peut s'écrire comme suit :

$$\mathrm{BER}_{\mathrm{average}} = \frac{1}{2} - \frac{1}{2\sqrt{\pi}} \int_0^{+\infty} \frac{e^{-z(1+2b)}}{\sqrt{z}} \prod_{k=1}^{K} \prod_{m' \in \mathcal{F}_k} \left(1 + 2A_{k,m,m'} z\right)^{-1} dz$$

Le cas multi-interféreurs partiellement chargés

Dans le cas précédent, nous avons calculé le BER moyen dans un scénario complètement chargé. Il est possible qu'un interféreur passe par des périodes de silence (d'inactivité). On peut modéliser l'activité d'un interféreur k par une variable aléatoire de Bernoulli Q_k avec une densité de probabilité

$$p(Q_k) = \begin{cases} \alpha_k & Q_k = 1 \\ 1 - \alpha_k & Q_k = 0 \end{cases}, \quad k \in \{1, ..., K\}$$

La variable g devient alors :

$$g = 2 \sum_{k=1}^{K} Q_k A_{k,m,m'} g_{k,m'}$$

Par conséquent, la MGF $\mathcal{M}_g(z)$ est exprimé par :

$$\begin{aligned} \mathcal{M}_g(z) &= \prod_{k=1}^{K} \left(1 - \alpha_k + \alpha_k \mathcal{M}_k(z)\right) \\ &= \prod_{k=1}^{K} \left(1 - \alpha_k + \alpha_k \left|\mathbf{I}_{L_k} + 2\,\mathbf{\Omega}_k\, \mathbf{D}_k^A z\right|^{-1}\right) \end{aligned}$$

Le BER moyen peut alors s'écrire :

$$\mathrm{BER}_{\mathrm{average}} = \frac{1}{2} - \frac{1}{2\sqrt{\pi}} \int_0^{+\infty} \frac{e^{-z(1+2b)}}{\sqrt{z}} \prod_{k=1}^{K} \left(1 - \alpha_k + \alpha_k \left|\mathbf{I}_{L_k} + 2\,\mathbf{\Omega}_k\,\mathbf{D}_k^A z\right|^{-1}\right) dz$$

Le modèle du système

Dans cette section, nous décrivons le modèle du système considéré dans les simulations réalisée dans les Chapitres 4 et 5. Nous considérons la voie descendante d'une transmission OFDM/FBMC dans un réseau cellulaire à 12 cellules. L'utilisateur de référence est situé à la position de coordonnées (u, v). Soit la station de base k située à (u_k, v_k), la distance entre cette BS et l'utilisateur de référence est donnée par :

$$d_k = \sqrt{(u_k - u)^2 + (v_k - v)^2}$$

Le facteur de réutilisation des fréquences est égal à $1/7$. Dans ce schéma, nous avons considéré une bande de garde de δ sous-porteuses entre les différents bloc de sous-porteuses. Le Rayon de la cellule est fixé à $R = 1$km. Nous avons par ailleurs considéré un système à

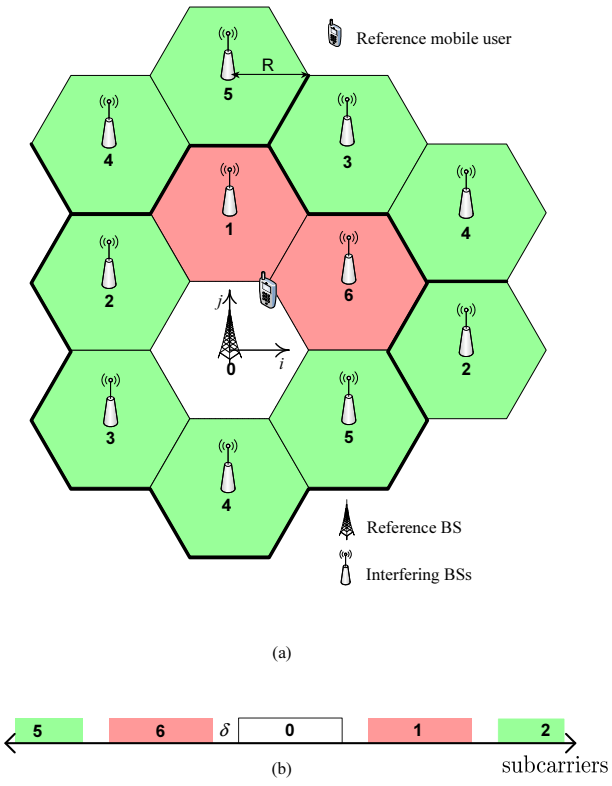

La voie descendante d'un réseau OFDM/FBMC à 12 cellules

$N = 1024$ sous-porteuses. Les données transmises sont modulées en QPSK et la fréquence

d'échantillonnage est égale à 10 MHz. Le bruit thermique est caractérisé par une densité spectrale de puissance égale à -174 dBm/Hz. La durée du CP est fixée à $\Delta = T/8$, et la taille de chaque bloc de sous-porteuse est égale à 18 sous-porteuses. Tous les résultats sont comparés aux résultats du scénario optimal où il n'y a pas d'interférence asynchrone.

Résultats de simulation

Dans la figure ci-après, les BERs moyens de l'OFDM et de la FBMC sont tracés en fonction du SNR dans le cas d'un réseau complètement chargé sans bande de garde ($\delta = 0$). La désynchronisation τ est supposée être uniformément répartie sur l'intervalle $[0, T]$. Nous pouvons voir que les résultats de simulation correspondent parfaitement aux résultats obtenus par l'expression analytique développée précédemment. Une sévère dégradation du BER est constatée sur toutes les formes d'ondes à cause de la désynchronisation. Nous remarquons également que plus le SNR est grand, plus cette dégradation devient significative. Ceci peut s'expliquer par le fait que le bruit est, dans ce cas, négligeable devant l'interférence causée par les autres stations de base, ce qui mène à un palier d'erreur. Toutefois, le BER de la FBMC asynchrone est inférieur à celui de l'OFDM. Ce gain est dû au fait que seulement une sous-porteuse (cas de PHYDYAS) ou deux sous-porteuses (cas d'IOTA) sont affectées par l'interférence sur chaque bord. Alors qu'en OFDM, l'ensemble des sous-porteuses souffrent d'une forte interférence asynchrone causée par un nombre important de sous-porteuses interférentes.
Dans les figures ci-après, nous avons le BER moyens de l'OFDM et de la FBMC en fonction du SNR avec différents intervalles de désynchronisation: $[0, T/7]$ correspondant au scénario (a), $[0, T/4]$ pour le scénario (b) et $[0, T]$ pour le scénario (c).
En OFDM, la dégradation est très importante quand l'intervalle de désynchronisation est large. En effet, quand $\tau \leq \Delta$, les différentes sous-porteuses sont orthogonales. Au delà du préfixe cyclique, une très forte interférence, provoquée par la perte d'orthogonalité, affecte les performances du système. Comme la désynchronisation est uniformément répartie, la probabilité d'avoir les performances du cas optimal est égale à (Δ/τ_{max}). De ce fait, plus τ_{max} est grand, plus la probabilité d'orthogonalité entre les sous-porteuses est faible.
Concernant le cas FBMC, on peut conclure que les deux formes d'ondes PHYDYAS et IOTA ne sont pas sensibles à la largeur de l'intervalle de désynchronisation. Ceci est dû au fait que l'interférence significative (supérieure ou égale à $-30\ dB$) est quasiment invariable par rapport au décalage τ.
Nous avons également étudié l'impact de la taille de la bande de garde δ sur les performances du système. Différentes valeurs de $\delta = 0, 1, 2, 5, 20$ ont été considérées. La désynchronisation est uniformément distribuée sur $[0, T]$. Comparant les différentes courbes de l'OFDM, on peut voir une amélioration des performances en augmentant δ. Cependant, il y a toujours un écart par rapport à l'optimal même pour une bande de garde de 20 sous-porteuses.
Contrairement à l'OFDM, les formes d'ondes FBMC offrent pratiquement les performances du cas optimal pour $\delta = 1$ dans le cas PHYDYAS et $\delta = 2$ dans le cas IOTA. Ceci est dû au fait que l'interférence ne dépasse pas -60 dB quand le bloc des sous-porteuses d'intérêt est

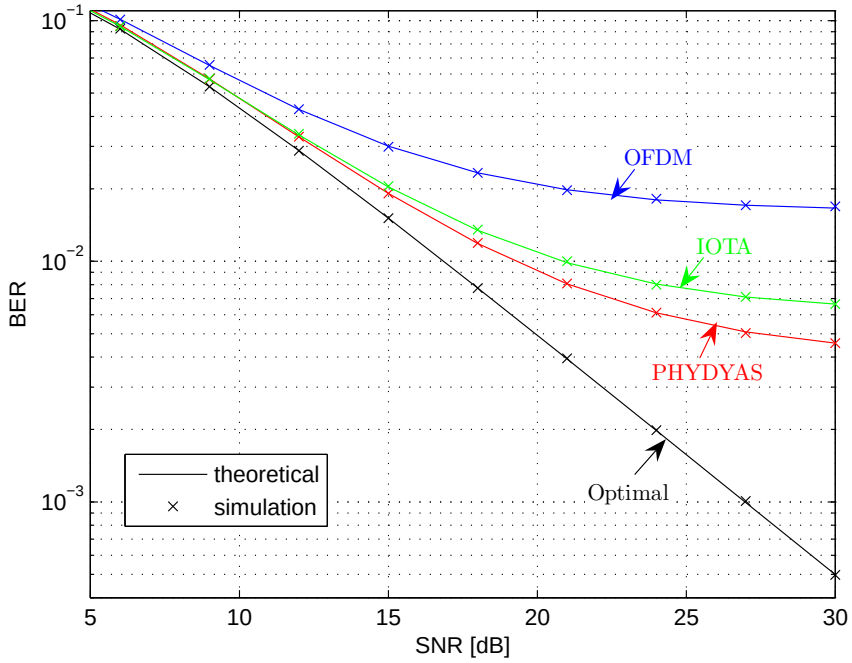

Les BERs moyens d'OFDM/FBMC en fonction du SNR pour $\tau \in [0, T]$, sans bande de garde $\delta = 0$

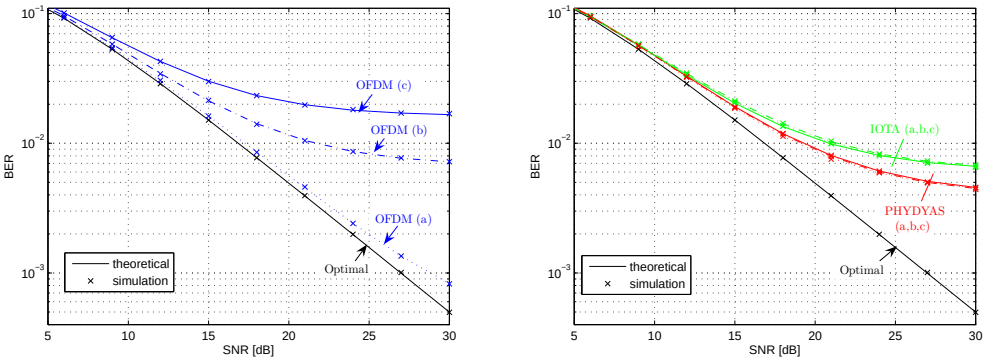

Les BERs moyens d'OFDM/FBMC dans les cas suivants : optimal (a). $\tau \in$[0,T/7] (b). $\tau \in$[0,T/4] (c). $\tau \in$[0,T], sans bande de garde $\delta =$0

séparé des autres blocs par une sous-porteuse dans le cas PHYDYAS ou 2 sous-porteuses dans le cas IOTA.

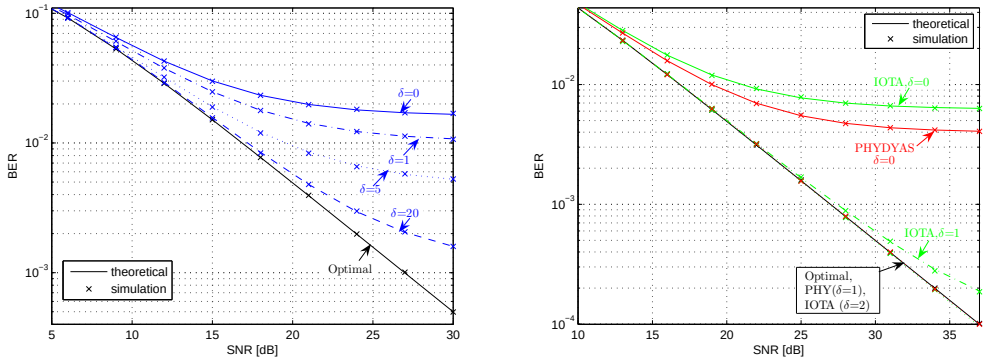

Les BERs moyens d'OFDM/FBMC en fonction du SNR pour δ = 0, 1, 2, 5 and 20, avec τ ∈[0,T]

Dans les deux dernières figures, les BERs moyens de l'OFDM/FBMC sont tracés en fonction du facteur de charge α pour deux niveaux de SNR : 20 dB et 25 dB. La désynchronisation τ est uniforme sur $[0, T]$. Nous pouvons constater que le BER est proportionnel à α. On voit également que les modulations FBMC garde leurs supériorités par rapport à l'OFDM. De plus, la parfaite correspondance entre la théorie et la simulation valide l'expression obtenue du BER dans le cas partiellement chargé.

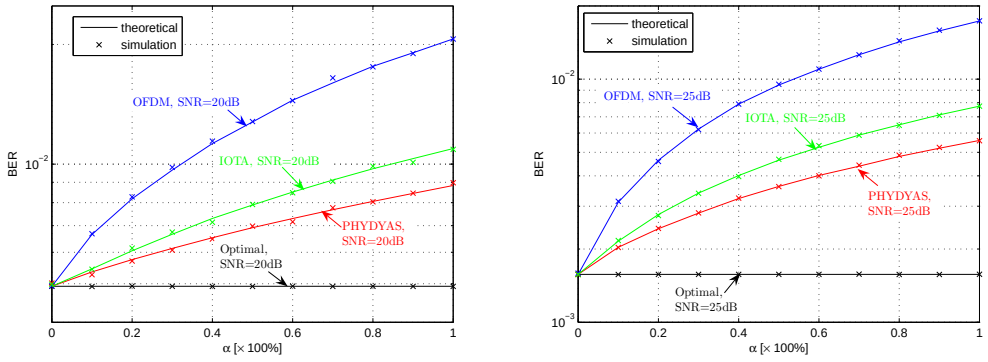

Les BERs moyens en fonction du facteur de charge α pour SNR = 20 et 25 dB, avec τ ∈[0,T]

Chapitre 5 - Analyse de l'efficacité spectrale de l'OFDM et la FBMC dans les systèmes asynchrones

L'efficacité spectrale représente un des critères fondamentaux dans l'évaluation des performances d'un système donné. Dans ce chapitre, nous développons une expression analytique de l'efficacité spectrale en tenant compte de l'interférence asynchrone. Nous terminons par analyser quelques résultats de simulation.

Analyse de l'efficacité spectrale moyenne

Suivant le même raisonnement adopté dans le chapitre précédent, l'efficacité spectrale conditionnelle, considérant l'ensemble des variables aléatoires $\mathcal{H} = \{H_0(m), H_k(m'), k \in \{1, ..., K\}, m' \in \mathcal{F}_k\}$ connues, peut s'exprimer comme suit :

$$C(\text{SINR})|_{\mathcal{H}} = B \log_2 \left(1 + \frac{|H_0(m)|^2}{\sum\limits_{k=1}^{K} \sum\limits_{m' \in \mathcal{F}_k} A_{k,m,m'} |H_k(m')|^2 + b} \right)$$

Par conséquent, l'efficacité spectrale moyenne est donnée par :

$$C_{\text{average}} = \mathbb{E}_{\mathcal{H}} \left[B \log_2 \left(1 + \frac{|H_0(m)|^2}{\sum\limits_{k=1}^{K} \sum\limits_{m' \in \mathcal{F}_k} A_{k,m,m'} |H_k(m')|^2 + b} \right) \right]$$

L'approche directe pour calculer cette moyenne mène à une intégrale multiple trop complexe

$$C_{\text{average}} = B \int\limits_{\mathcal{H}} \log_2 \left(1 + \frac{|H_0(m)|^2}{\sum\limits_{k=1}^{K} \sum\limits_{m' \in \mathcal{F}_k} A_{k,m,m'} |H_k(m')|^2 + b} \right) p(\mathcal{H}) d\mathcal{H}$$

où $p(\mathcal{H})$ représente la densité de probabilité du vecteur $\mathcal{H}$.
Les fonctions génératrices des moments (MGF) constituent un outil très efficace dans l'analyse des performances pour les canaux à évanouissement [22], [19]. En utilisant le lemme [19] suivant, le calcul de l'efficacité spectrale moyenne se réduit à une seule intégrale.

Lemme Soit x une variable aléatoire avec une distribution gamma de moyenne unitaire et de paramètre α. Soit c une constante positive et g une variable aléatoire positive et indépendante de x. Alors,

$$\mathbb{E}_{x,g} \left[\ln \left(1 + \frac{x}{g + c} \right) \right] = \int\limits_{0}^{+\infty} \left[\frac{1}{z} - \frac{1}{z(1+z)^{\alpha}} \right] \mathcal{M}_g(\alpha z) e^{-z\alpha c} dz$$

Par conséquent, l'efficacité spectrale moyenne devient :

$$C_{\text{average}} = B\log_2(e)\int_0^{\infty}\frac{e^{-zb}}{1+z}\mathcal{M}_g(z)dz$$

De la même manière, nous distinguons deux cas principaux :

Le cas multi-interféreurs complètement chargés

L'efficacité spectrale dans ce cas est donnée par :

$$C_{\text{average}} = B\log_2(e)\int_0^{+\infty}\frac{e^{-zb}}{1+z}\prod_{k=1}^{K}\left|\mathbf{I}_{L_k}+\mathbf{D}_k^A\,\mathbf{\Omega}_k\,z\right|^{-1}dz$$

Le cas multi-interféreurs partiellement chargés

Quand le système est partiellement chargé avec un facteur $\alpha \in [0,1]$, l'expression de l'efficacité spectrale devient :

$$C_{\text{average}} = B\log_2(e)\int_0^{+\infty}\frac{e^{-zb}}{1+z}\prod_{k=1}^{K}\left(1-\alpha_k+\alpha_k\left|\mathbf{I}_{L_k}+\,\mathbf{\Omega}_k\,\mathbf{D}_k^A z\right|^{-1}\right)dz$$

Résultats de simulation

Dans la section précédente, nous avons développé les expressions de l'efficacité spectrale en présence de l'interférence asynchrone. Contrairement à l'approche directe complexe, les expressions obtenues constituent une approche plus simple dans le calcul de l'efficacité spectrale moyenne. Dans cette section, nous présentons quelques résultats de simulation pour la voie descendante des systèmes OFDM et FBMC. Le reste des paramètres de simulation est identique à ceux donnés dans le chapitre précédent. Il est à noter que tous les résultats sont comparés au cas optimal où l'orthogonalité entre les différentes sous-porteuses est maintenue.

Dans la première figure, l'efficacité spectrale calculée théoriquement est comparée à celle obtenue par simulation. Nous avons considéré une configuration sans bande de garde entre les différents bloc de sous-porteuses ($\delta = 0$) avec une désynchronisation uniformément distribuée sur $[0, T]$. Dans cette figure, l'efficacité spectrale moyenne de l'OFDM et de la FBMC est tracée en fonction du SNR pour l'expression théorique et les résultats de simulation. Nous pouvons voir que les résultats théoriques correspondent parfaitement à ceux obtenus par simulation. Nous constatons également une dégradation significative des performances pour les valeurs élevées du SINR. Les courbes tracées montrent également un palier de l'efficacité spectrale pour l'OFDM quand le SNR est élevé. Ce comportement peut être expliqué par la prédominance de l'interférence asynchrone causée par les différentes BS sur le niveau de bruit considéré. D'autre part, les modulations FBMC offrent des meilleures performances par rapport à l'OFDM. Ce gain important est dû au fait que toutes les sous-porteuses en OFDM souffrent d'une forte interférence alors que seulement une ou deux

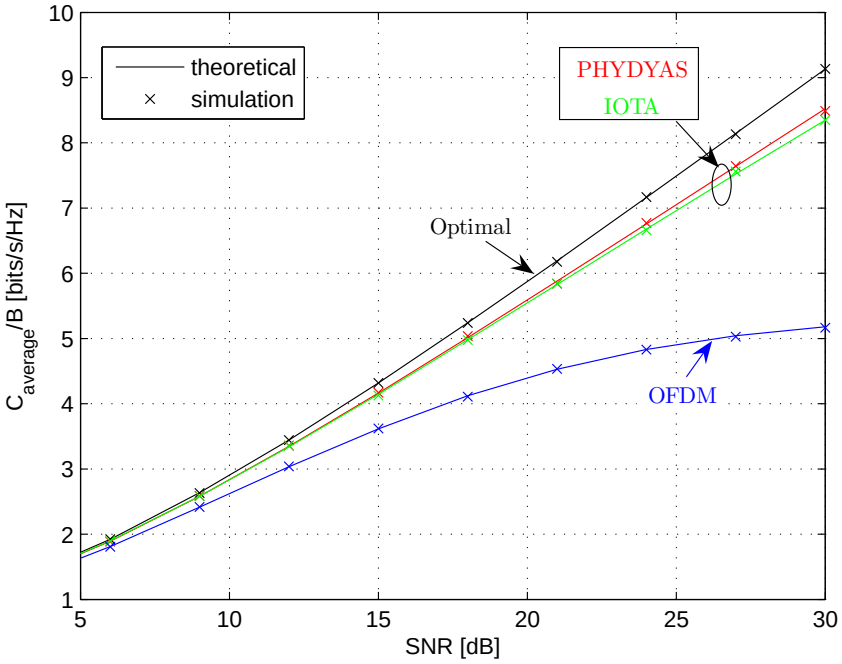

Les efficacités spectrales moyennes d'OFDM/FBMC en fonction du SNR pour $\tau \in [0, T]$, sans bande de garde $\delta = 0$

sous-porteuses sont affectées par l'interférence en FBMC. Concernant le scénario optimal, les deux modulations offrent les mêmes performances. Mais si on considère la redondance introduite par le CP en OFDM, le débit réel des modulations FBMC est plus grand que celui de l'OFDM.

Les figures ci-dessous, montrent l'effet de la largeur de l'intervalle de désynchronisation sur

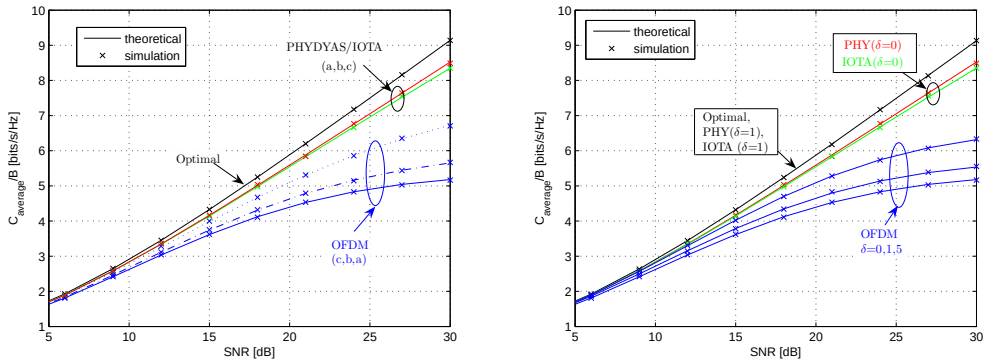

Les efficacités spectrales moyennes d'OFDM/FBMC dans les cas suivants : optimal (a). $\tau \in$[0,T/7] (b). $\tau \in$[0,T/4] (c). $\tau \in$[0,T], sans bande de garde δ =0 et pour δ = 0, 1, 2, 5 and 20, avec $\tau \in$[0,T]

les performances des deux modulations OFDM et FBMC. En OFDM, la dégradation est moins importante pour de faibles désynchronisations. Ce comportement est dû au fait que l'OFDM parvient à maintenir l'orthogonalité entre les sous-porteuses quand la désynchronisation est absorbée par le CP. Comme nous avons considéré une désynchronisation uniforme sur $[0, \tau_{\max}]$, la probabilité d'avoir les performances optimales est donnée par $\Delta/\tau_{\max}$. Donc plus $\tau_{\max}$ est proche de Δ, plus l'OFDM est proche de l'optimal. De l'autre côté, les modulations FBMC se montrent insensibles à la désynchronisation. On peut expliquer cette insensibilité par le fait que l'interférence la plus significative en FBMC est quasiment invariable par rapport à la désynchronisation.

Jusqu'à maintenant nous avons négligé l'impact des bandes de garde. Dans les figures suivantes, nous examinons les variations des performances en fonction de la taille de la bande de garde δ. La désynchronisation ici est considérée uniformément distribuée sur $[0, T]$. Comme la distance spectrale influe sur l'interférence, nous allons calculer l'efficacité spectrale uniquement sur les sous-porteuses actives. Comparant les différentes courbes, nous constatons qu'il y a une amélioration des performances avec l'augmentation de δ. Cependant, un écart entre les performances de l'OFDM par rapport au cas optimal est toujours observé. À l'opposé de l'OFDM, les modulations FBMC sont capables d'atteindre les performances optimales pour une bande de garde $\delta = 1$ ou 2 sous-porteuses, respectivement pour PHYDYAS et IOTA.

Finalement, l'effet de la charge du réseau sur les performances du système est exposé dans les figures suivantes. Deux niveaux de SNR sont considéré 20 et 25 dB. Les courbes montrent que l'efficacité spectrale est inversement proportionnelle au facteur de charge α. Quand

$\alpha = 0$, les deux modulations offrent les même performances. Néanmoins, les courbes divergent avec l'augmentation de α. Les résultats obtenus confirment la supériorité des modulations FBMC par rapport à l'OFDM.

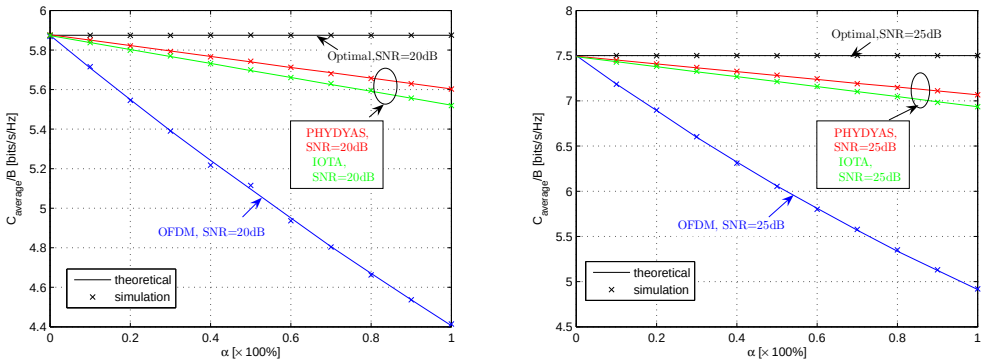

Les efficacités spectrales moyennes en fonction du facteur de charge α pour SNR = 20 et 25 dB, avec $\tau \in$[0,T]]

Conclusion

Le principal objectif de cette thèse est d'analyser l'impact de la désynchronisation temporelle sur les performances des systèmes OFDM et FBMC.

Dans le chapitre 3, Nous avons démontré que la désynchronisation peut causer une perte d'orthogonalité entre les sous-porteuses. Cette perte d'orthogonalité se traduit par l'apparition de l'interférence asynchrones. Nous avons introduit le concept général des tables d'interférence et calculé ces tables pour le modèle PSD. Comme ce modèle ne tient pas compte de la désynchronisation entre le signal d'interférence et le signal utile, nous avons proposé de nouvelles tables appelées tables instantanées. En utilisant ces dernières, nous avons établi une méthode semi-analytique pour évaluer le SINR moyen et l'efficacité spectrale. Contrairement au modèle PSD qui présente une large imprécision, le modèle proposé à été validé à travers différents résultats de simulation.

Dans les chapitres 4 et 5, nous avons étudié le BER et l'efficacité spectrale en présence de l'interférence asynchrone. Tout d'abord, l'expression analytique du SINR instantané a été calculée. Nous avons démontré ensuite que l'approche directe du calcul du BER mène à des intégrales multiples complexes qui difficiles à évaluer. En se basant sur les fonctions génératrices des moments de la puissance d'interférence, nous avons développé des expressions simples du BER et de l'efficacité spectrale moyens. Ces dernières expressions réduisent d'une façon considérable la complexité de l'évaluation des performances.
Cette étude théorique a été consolidée et validée par plusieurs résultats de simulation où nous avons démontré que :

- l'asynchronisme entre l'interféreur et le récepteur de référence cause une sévère dégradation dans les performances du système OFDM. Un tel résultat est expliqué par la forte interférence qui apparaît suite à la perte d'orthogonalité entre les sous-porteuses du système,
- grâce à la bonne localisation des formes d'ondes IOTA et PHYDYAS, les modulations FBMC sont moins sensible à la désynchronisation par rapport à l'OFDM,
- les modulations FBMC peuvent atteindre les performances optimales en prévoyant une bande de garde de une (PHYDYAS) ou deux (IOTA) sous-porteuses,
- la modulation OFDM est meilleure quand l'asynchronism temporel τ n'est pas important.

Contents

List of Figures

List of Tables

Nomenclature

Abbreviations and Acronyms

AWGN	Additive White Gaussian Noise
AFB	Analysis Filter Bank
BER	Bit Error Rate
BS	Base Station
CIR	Channel Impulse Response
CMT	Cosine modulated MultiTone
CR	Cognitive Radio
CP	Cyclic Prefix
DAB	Digital Audio Broadcasting
DVB	Digital Video Broadcasting
DFT	Discrete Fourier Transform
DSL	Digital Subscriber Line
EGF	Extended Gaussian Function
FBMC	Filter Bank based MultiCarrier
FDMA	Frequency Division Multiple Access
FIR	Finite Impulse Response
FFT	Fast Fourier Transform
FMT	Filtered MultiTone
ICI	Inter-Carrier-Interference
IEEE	Institute of Electrical and Electronics Engineers
i.i.d.	independent and identically distributed
IDFT	Inverse Discrete Fourier Transform
IFFT	Inverse Fast Fourier Transform
IOTA	Isotropic Orthogonal Transfer Algorithm
ISI	Inter-Symbol-Interference
MCM	MultiCarrier Modulations
MGF	Moment Generating Function
MMSE	Minimum Mean Square Error
MU	Mobile User

NPR	Near Perfect Reconstruction
OFDM	Orthogonal Frequency Division Multiplexing
OFDMA	Orthogonal Frequency Division Multiple Access
OQAM	Offset Quadrature Amplitude Modulation
PAM	pulse amplitude modulation
PDF	Probability Density Function
PHYDYAS	PHYsical layer for DYnamic spectrum AccesSand cognitive radio
PPN	PolyPhase Network
PR	Perfect Reconstruction
PSD	Power Spectral Density
QAM	Quadrature Amplitude Modulation
QoS	Quality of Service
QPSK	Quadrature Phase Shift Keying
RV	Random Variable
SFB	Synthesis Filter Bank
SMT	Staggered MultiTone
SINR	Signal-to-Interference-plus-Noise Ratio
SNR	Signal-to-Noise Ratio
SRRC	Square Root Raised Cosine
VSB	Vestigial SideBand
WiMAX	Worldwide Interoperability for Microwave Access
WLAN	Wireless Local Area Network
WMAN	Wireless Metropolitan Area Network

Notations

$\mathbb{N}$	The set of positive integer elements.
$\mathbb{R}$	The set of real elements.
$\mathbb{C}$	The set of complex elements.
$\ln(\cdot)$	The natural logarithm.
$\log_2(\cdot)$	The base 2 logarithm.
$\mathrm{Re}\{x\}$	Real part of the complex value x.
$\mathrm{Im}\{x\}$	Imaginary part of the complex value x.
x^*	Complex conjugate of the complex value x.
$\lvert x\rvert$	The absolute value of a scalar.
$\lfloor x \rfloor$	The floor operator, i.e. the largest integer less than or equal to x.
$\lceil x \rceil$	The ceil operator, i.e. the smallest integer greater than or equal to x.
$\lvert\Omega\rvert$	The cardinality of the set Ω, i.e. the number of elements in the finite set Ω.
$\mathbb{E}\{\cdot\}$	The expectation operator.
$\mathbf{I}_n$	The identity matrix of size n.
$\mathbf{D}_k^A$	The diagonal matrix containing elements of the vector A_k.
$\delta(t)$	Dirac delta function.
$*$	Convolution operator.
$E(n, z)$	Exponential integral function.
${}_1F_1(;;)$	Confluent hypergeometric function of the first kind.

Thesis Specific Notations

The following list is not exhaustive, and consists of the most relevant notations used in the dissertation.

Notations specific to Chapter 2:

T	Symbol duration.
τ_{ds}	Maximum delay spread of the channel.
B	Frequency bandwidth.
N	Total number of subcarriers.
$x_{m,n}$	n-th complex input symbol of the m-th subcarrier.
$x_{m,n}^I$	In-phase component of $x_{m,n}$.
$x_{m,n}^Q$	Quadrature-phase component of $x_{m,n}$.
$\hat{x}_{m,n}$	n-th complex recovered symbol of the m-th subcarrier.
$f_T t$	Transmit pulse shape.
$f_R t$	Receive pulse shape.
Δ	Cyclic prefix duration.
B_c	Coherence bandwidth of the channel.
$H(m)$	Complex channel gain at subcarrier m.
β	Roll-off factor of SRRC filter.
K	Overlapping factor of the prototype filter.

Notations specific to Chapter 3:

$\Phi(f)$	Power spectral density.
Δf	Subcarrier spacing.
τ	Timing offset.
φ	Phase offset.
$I(\tau, l)$	Interference table coefficient for a timing offset τ and a spectral distance l.
$P_{\text{trans}}(m)$	Transmitted power on the m-th subchannel.
$P_{\text{interf}}(m)$	Interference power in the m-th subchannel.

Notations specific to Chapters 4 and 5:

d_k	Distance between the k-th BS and the reference mobile user.
h_k	Channel impluse response between the k-th BS and the reference mobile user.
$n(t)$	Additive white Gaussian noise .
K	Total number of neighboring cells.
β	Path-loss exponent.

$\mathcal{F}_k$	Set of subcarriers assigned to k-th BS.
τ_k	Timing offset between the k-th BS and the reference mobile user.
N_0	Noise power spectral density.
B_{sc}	Subchannel bandwidth.
g	Total interference power random variable.
$\mathcal{M}_g(z)$	MGF of the random variable g.
$\mathbf{\Omega}_k$	Correlation matrix of the RVs $\{g_{k,m},\ m \in \mathcal{F}_k\}$.
δ	Size of guard-band between two neighboring subcarrier blocks.
α	Load factor of the multi-cell network.

Chapter 1

Introduction

1.1 Background and motivation

Today, we witness a metamorphosis of applications for wireless communications. In fact, image, music and video sharing between users are reshaping consumption models and imposing higher and higher data rate constraints on today's communication systems.

Multicarrier techniques are promising and potential candidates to achieve these high required data rates. Indeed, the key idea of multicarrier techniques is to divide the high data-rate stream into N low-rate substreams that are transmitted on N orthogonal subcarriers. The main advantage here is that the subcarriers are selected to be orthogonal, in such a way that their spectra overlap but without causing interference to the other subcarriers [1]. Moreover, the number N must be as large as the bandwidth of each subchannel is smaller than coherence bandwidth of the propagation channel, that is, the maximum delay spread of the channel τ_{ds} is much lower than the symbol duration T. Consequently, each subchannel experiences a flat fading and the intersymbol interference in each subchannel becomes very small [1], [2].

Orthogonal Frequency Division Multiplexing (OFDM) is the most widespread multicarrier modulation scheme and it has been considered as fundamental part in a number of wireless communication systems such as WiFi based on the IEEE 802.11 standard, WiMax (Worldwide Interoperability for Microwave Access) [3], [4], [5] based on the IEEE 802.16 standard, Long Term Evolution (LTE) [3], [6], LTE-advanced, ... etc. This is due to a number of advantages such as:

- its efficient FFT-based implementation
- its robustness to multi-path effects by adding a cyclic prefix that significantly reduces

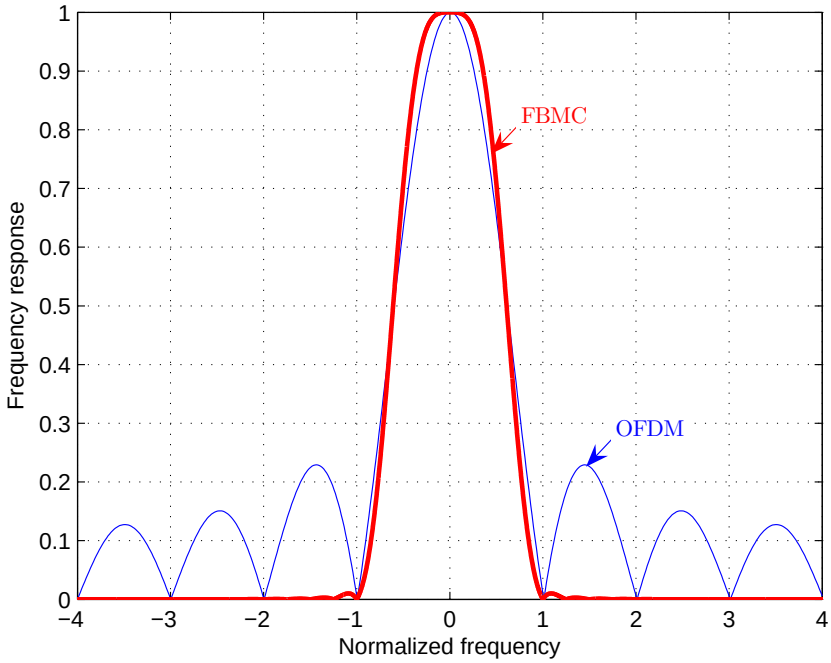

Figure 1.1: Frequency responses of OFDM and FBMC

the complexity of the equalization to a single complex coefficient per subcarrier equalizer

- its high spectral efficiency using closely spaced orthogonal subcarriers.

Unfortunately, OFDM has some weakness points. The redundancy, caused by the insertion of the cyclic prefix which is a part of the transmitted OFDM symbol, reduces the useful data rate. Furthermore, the leakage effect of the IFFT is illustrated in Fig. 1.1, which shows the frequency response of a subchannel in an OFDM system. The poor spectral localization of the OFDM subcarriers due to the large sidelobes gives rise to an additional spectral loss and interference problems with unsynchronized signals [23]. These shortcomings have stimulated the research of an alternative scheme that can overcome these problems. An enhanced physical layer based on the filter bank processing is proposed as an interesting alternative in PHYDYAS project. Increased spectral efficiency can be achieved using filter bank-based multicarrier (FBMC) techniques compared to OFDM. This is due to the reduced out-of-band leakage such that a higher number of subcarriers can be used within the allocated frequency band. Additionally in contrast to OFDM systems using a cyclic prefix to deal with the frequency selectivity of the propagation channels, there is no need of cyclic prefix in FBMC systems which increases again the effective throughput.

In the literature, it is often assumed that the users or base stations, coexisting in the same geographical area, are perfectly synchronized. However in reality, this hypothesis

cannot always be valid. Various scenarios, in which the asynchronism inherently exists, can be found such as:

OFDMA-based cellular networks orthogonal frequency division multiple access (OFDMA) represents the extension of the OFDM concept to multiuser communication scenarios. In OFDMA systems, the available frequency band is shared between distinct users for simultaneous transmission. However, timing synchronization is considered as a challenging task for which no efficient solution exists in the open literature [17].

OFDMA Ad-hoc networks In OFDMA networks, most of the synchronization techniques are based on closed-loop time correction techniques [17]. In contrast to these networks, the dynamism of the topology of ad-hoc networks makes expensive the implementation of these synchronization techniques.

Cognitive radio systems The problem of synchronization is worse in cognitive radio networks where both primary and secondary users transmit independently. The synchronization problem will be more detailed in the next chapter.

This asynchronism can cause a loss of orthogonality between subcarriers which harmfully affects the system performance. This loss of orthogonality gives rise to the asynchronous interference. Modeling this interference presents an important issue in the design of communication systems. Many approaches have been investigated to study this problem. The power spectral density (PSD) is commonly used to model the interference by measuring the out-of-band radiation [9], [10], [11]. Unfortunately, this model can lead to inaccurate results e.g. when the asynchronism is absorbed by the cyclic prefix in the CP-OFDM case, the orthogonality between subcarrier is indeed maintained, but the PSD modeling shows that the interference is independent of the timing asynchronism.

1.2 Thesis objectives

In this dissertation, the impact of timing asynchronism on the performance of OFDM and FBMC systems is addressed. As a matter of fact, we would like to:

- Properly estimate the interference part introduced by the timing asynchronism for OFDM systems.
- Propose an extension of this model to englobe the FBMC case, as it has, to our knowledge, never been considered in the literature.
- Based on the proposed interference model, derive closed-form expressions of the signal to interference plus noise ratio for both cases: OFDM and FBMC.
- Moreover investigate the impact of the interference on the system performance. Therefore, compute analytical expressions for the bit error rate as well as the spectral efficiency in OFDM and FBMC systems.

1.3 Thesis outline

Chapter 2 - Overview of Multicarrier techniques and Asynchronous Systems

Chapter 2 is devoted to introduce the background and the main state of the art related to the different concepts to be used throughout this thesis. First, the general concept of multicarrier transmissions is provided. The OFDM system and its implementation are briefly described. Next, we give the fundamental theory of FBMC techniques. Among FBMC schemes, we introduce staggered multitone (SMT), cosine modulated multitone (CMT) and filtered multitone (FMT). Furthermore, the polyphase implementation of the filter bank transceiver and the prototype filter design are reviewed. We finally discuss the timing asynchronism issue in multicarrier systems in the last part of this chapter.

Chapter 3 - Asynchronous Interference Modeling

In this chapter, the asynchronous OFDM and FBMC interference modeling is examined. We first give a literature review of the multicarrier interference analysis. Then, the general notion of interference tables is presented. We derive the PSD-based as well as instantaneous interference tables of CP-OFDM and FBMC considering PHYDYAS and IOTA prototype filters. The proposed instantaneous tables take into account the timing asynchronism. Next, we extend the interference analysis to the case of frequency selective environments. Finally, we propose a table-based estimation which can significantly reduce the complexity computation compared to the direct numerical evaluation.

Chapters 4 and 5 - Average Error Rates and Spectral Efficiency Analysis in Asynchronous Cellular Networks

In Chapters 4 and 5, we analyze the impact of timing asynchronism on OFDM and FBMC based multi-cellular networks. In fact, the average error rate performance and the spectral efficiency of the downlink are analyzed. The chapters start by presenting the state of the art related to the analysis of both the average error rate and the spectral efficiency in the presence of asynchronous interference. Then, we develop the analytical expression of the instantaneous SINR using the interference tables introduced in Chapter 3. Through the moment generating functions of the asynchronous interference power, we derive closed-form expressions of the average error rate and the spectral efficiency. These computations take into account the frequency correlation between adjacent interfering subcarriers. Analysis/derivations are done for various scenarios:

- several interfering BS in fully loaded networks.
- several interfering BS in partially loaded networks.

Some asymptotic analysis are also performed for the interference-free scenario and the noiseless case.

Chapter 6 - Conclusions and Perspectives

This chapter draws the final conclusions by highlighting the main contributions of this dissertation. Possible future research are provided at the end.

1.4 List of publications

The contributions presented in this thesis are published, submitted or under preparation:

Journal Papers

1. **Y. Medjahdi**, M. Terré, D. Le Ruyet, D. Roviras and A. Dziri "Performance Analysis in the Downlink of Asynchronous OFDM/FBMC based Multi-cellular Networks" *IEEE Transaction on wireless communications.* vol.10, no.8, pp.2630-2639, August 2011.

2. H.Zhang, D. Le Ruyet, D. Roviras, **Y. Medjahdi**, and H. Sun "Spectral Efficiency Comparison of OFDM/FBMC for Uplink Cognitive Radio Networks" *EURASIP Journal on Advances in Signal Processing*, vol. 2010.

3. **Y. Medjahdi**, D. Le Ruyet, D. Roviras "On the Accuracy of PSD-based Interference Modeling in Asynchronous MultiCarrier Transmissions" *in preparation*

Conference Papers

1. **Y. Medjahdi**, D. Le Ruyet, D. Roviras, H. Shaeik, R. Zakaria, "On the Impact of the Prototype Filter on FBMC Sensitivity to Time Asynchronism", *ISWCS 2012*, pp. 1-5, Paris, France, Aug. 2012.

2. R. Zakaria, D. Le Ruyet, **Y. Medjahdi**, "On ISI cancellation in MIMO-ML detection using FBMC/QAM modulation", *ISWCS 2012*, pp. 1-5, Paris, France, Aug. 2012.

3. **Y. Medjahdi**, M. Terré, D. Le Ruyet, D. Roviras, "On Spectral Efficiency of Asynchronous OFDM/FBMC based Cellular Networks", *IEEE PIMRC 2011*, pp. 1381-1385, Toronto, Canada, Sept. 2011.

4. **Y. Medjahdi**, M. Terré, D. Le Ruyet, D. Roviras, "The Impact of Timing Synchronization Errors on the Performance of OFDM/FBMC Systems", *IEEE international Conference on Communication (ICC'11)*, Kyoto, Japan, June 2011

5. M. Khodjet-Kesba, C. Saber, D. Roviras, **Y. Medjahdi**, "Multicarrier interference evaluation with jointly non-linear amplification and timing errors", *IEEE Vehicular Technology Conference (VTC'11-spring)*, Budapest, Hungary, May 2011.

6. **Y. Medjahdi**, M. Terré, D. Le Ruyet, D. Roviras," "Asynchronous OFDM/FBMC Interference Analysis in Selective Channels", *IEEE PIMRC 2010*, pp. 538- 542, Istanbul, Turkey, Sept. 2010.

7. **Y. Medjahdi**, M. Terré, D. Le Ruyet, D. Roviras, "Inter-Cell Interference Analysis for OFDM/ FBMC Systems", *IEEE Signal Processing Workshop (SPAWC 2009)*, Perugia, Italy, june 2009.

Project Technical Reports

1. **Y. Medjahdi**, M. Terré, "Interference Management", *technical contribution report in the deliverable D6.3* - European ICT-211887 FP7 PHYDYAS project, Oct. 2010

2. M. Terré , **Y. Medjahdi**, "Analysis of multiple access interference in the downlink OFDM/FBMC systems", *technical contribution report in the deliverable D6.1* - European ICT-211887 FP7 PHYDYAS project, Jan. 2009

Chapter 2

Overview of Multicarrier techniques and Asynchronous Systems

2.1 Introduction

In this chapter, we establish the theoretical framework of this dissertation by reviewing the appropriate background on multicarrier modulations (MCM). The theory presented here will provide a basis for the rest of this thesis. In Section 2.2, we succinctly explain the general concept of multicarrier transmissions. Section 2.3 presents a brief description of the most widely deployed MCM, namely, orthogonal frequency division multiplexing (OFDM). We then introduce the fundamental concepts of filter bank systems in Section 2.4. Next, the asynchronism issue in communication systems is discussed in Section 2.5, and finally, we conclude this chapter in Section 2.6.

2.2 The concept of multicarrier transmission

Let us consider a single carrier transmission scheme with linear modulation (e.g. M-QAM) and a symbol duration T. Let B the frequency bandwidth which is typically of the order of the inverse of the symbol duration (T^{-1}). For a propagation channel with a delay spread τ_{ds}, we can avoid the intersymbol interference (ISI) if

$$\tau_{\text{ds}} \ll T$$

On the other hand for $\tau_{\text{ds}} > T$, ISI remains but equalization at the receiver can deal with it. However when $\tau_{\text{ds}} \gg T$, the equalization complexity becomes too high and therefore MCM is preferred.

The key idea of multicarrier transmission to reduce the equalization complexity is to split the data stream into N parallel low-rate streams which are transmitted on N adjacent subcarriers. The bandwidth of each subcarrier is B/N, while the symbol duration T is multiplied by a factor of N. However, the choice of the number of subcarriers N must also avoid the sensitivity of the transmission to the time incoherence of the channel which is related to the maximum Doppler frequency ν_{max} by fulfilling the following condition

$$\nu_{max} T \ll 1$$

Therefore to obtain the best possible transmission for a given propagation channel characterized by parameters (τ_{ds},ν_{max}), we have to choose the optimal symbol duration that satisfies both conditions together.

2.3 Orthogonal Frequency Division Multiplexing

OFDM is the most well documented MCM scheme. It has also been adopted by various practical and commercial systems such as, digital audio broadcasting (DAB) [24], [25] terrestrial digital video broadcasting (DVB-T) [26], and the IEEE 802.11a wireless local area network (WLAN) [27], etc. This success comes from a number of advantages that it offers :

- Orthogonality of subcarrier signals that allows
  - trivial generation of transmit signal through an inverse fast Fourier transform (IFFT) block
  - simple equalization through a scalar gain per subcarrier.
- Closely spaced orthogonal subcarriers that divide the available bandwidth into a maximum collection of narrow subchannels.
- Adaptive modulation schemes that can be applied to maximize the spectral efficiency.

The block diagram of an OFDM transmission system is depicted in Fig. 2.1. The OFDM continuous-time baseband transmitted signal is defined as,

$$\begin{aligned} s(t) &= \sum_{m=0}^{N-1} \sum_{n=-\infty}^{+\infty} x_{m,n} f(t-nT) e^{j\frac{2\pi}{T}m(t-nT)} \\ &= \sum_{m=0}^{N-1} \sum_{n=-\infty}^{+\infty} x_{m,n} f(t-nT) e^{j\frac{2\pi}{T}mt} \end{aligned} \tag{2.1}$$

where, $x_{m,n}$ is the n-th complex input symbol of the m-th subcarrier and $f(t)$ is a rectangular pulse shape, that is,

$$f(t) = \begin{cases} \frac{1}{\sqrt{T}} & t \in [0,T] \\ 0 & elsewhere \end{cases} \tag{2.2}$$

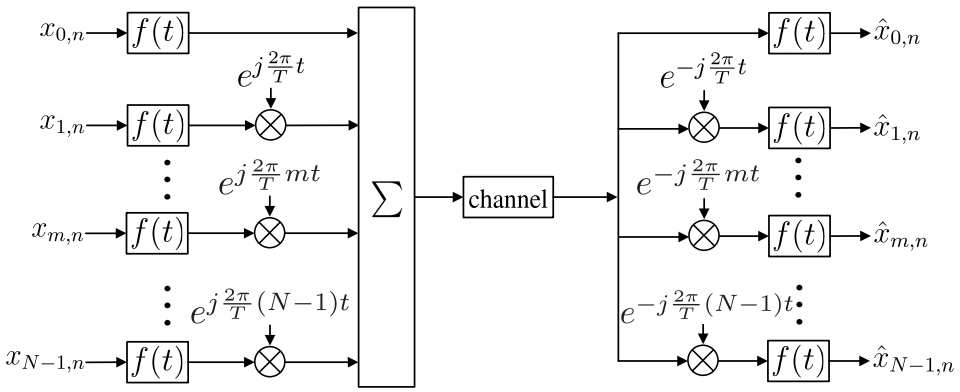

Figure 2.1: The block diagram of an OFDM system.

The received symbol $\hat{x}_{m_0,n_0}$ can be found at the output of the corresponding receive filter $f(t)$ and expressed as,

$$\begin{aligned}\hat{x}_{m_0,n_0} &= \langle s(t), f(t-n_0T)e^{j\frac{2\pi}{T}m_0(t-n_0T)}\rangle \\ &= \langle s(t), f(t-n_0T)e^{j\frac{2\pi}{T}m_0t}\rangle \\ &= \sum_{m=0}^{N-1}\sum_{n=-\infty}^{+\infty}\int_{-\infty}^{+\infty} x_{m,n}f(t-nT)f(t-n_0T)e^{j\frac{2\pi}{T}(m-m_0)t}dt \end{aligned} \tag{2.3}$$

where, $\langle .,. \rangle$ stands for the inner product.
In a distortion-free channel, the received symbol $\hat{x}_{m_0,n_0}$ equals the input one x_{m_0,n_0}. According to (2.2), one can find that,

$$\int_{-\infty}^{+\infty} f(t-nT)f(t-n_0T)e^{j\frac{2\pi}{T}(m-m_0)t}dt = \delta_{m,m_0}\delta_{n,n_0} \tag{2.4}$$

where $\delta_{m,m0}$ is the Kronecker delta function. δ_{m,m_0} is one if and only if $m = m_0$ and it is zero otherwise.
It is worth mentioning that (2.4) represents the orthogonality condition of the OFDM system when the subcarrier spacing is equal to $1/T$.

2.3.1 FFT Implementation of OFDM System

It is very simple to implement the OFDM system shown in Fig. 2.1 using the Fourier base. According to (2.1), the OFDM transmitted signal is just the inverse Fourier transform of the input signal, and besides, the receiver performs the Fourier transform to recover the data symbols $\hat{x}_{m,n}$ [see (2.3)]. Also when N is a power of 2, it is known that the Fourier analysis/synthesis can be efficiently implemented using the fast Fourier transform (FFT) and the inverse fast Fourier transform (IFFT), respectively. Such an implementation leads to the scheme depicted in Fig. 2.2.

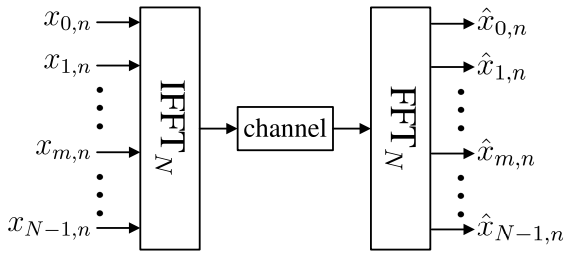

Figure 2.2: OFDM implementation using IFFT/FFT.

2.3.2 Cyclic Prefix based OFDM

In a classical OFDM transmission, the cyclic prefix (CP) is usually employed to eliminate the need for a complex equalizer on dispersive channels and furthermore it is used for synchronization purposes. This is required to maintain orthogonality between the subcarriers after demodulation [2]. The insertion of the cyclic prefix is illustrated in Fig. 2.3; this means that we copy a part of length Δ from the end of the original OFDM block and introduce it in the front of this block. The length of the cyclic prefix Δ is commonly set to accommodate the longest delay spread expected on the channel, therefore eliminating the inter-symbol interference (ISI). In such a case, the CP transforms the linear convolution channel to a cyclic convolution channel. Therefore, after the FFT operation, the equalization becomes trivial through a scalar gain per subcarrier as noted earlier.

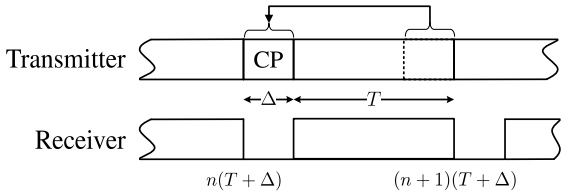

Figure 2.3: Cyclic Prefix insertion/suppression at the transmitter/receiver resp.

The following analysis demonstrates how a cyclic prefix can easily eliminate the interference caused by a multipath propagation channel
In the presence of the cyclic prefix, the OFDM transmitted signal becomes,

$$s(t) = \sum_{n=-\infty}^{+\infty} \sum_{m=0}^{N-1} x_{m,n} f_T(t - n(T+\Delta)) e^{j\frac{2\pi}{T} m(t-n(T+\Delta))} \tag{2.5}$$

Here, the duration of the transmit pulse $f_T(t)$ is $(T + \Delta)$ due to the insertion of the cyclic prefix with a duration Δ.
The signal $s(t)$ propagates through a frequency selective multipath channel, where its equiv-

alent sample-spaced impulse response [28] is given by

$$h(t) = \sum_{i=0}^{L-1} h_i \delta(t - \frac{n_i}{N}T) \tag{2.6}$$

where $n_0 < n_1 < ... < n_{L-1} < C$ and C is the maximum delay spread of the channel normalized by the sampling period (T/N), and h_i are the complex channel path gains, which are assumed mutually independent, where $\mathbb{E}[h_i h_i^*] = \gamma_i$, and $\mathbb{E}[h_i h_j^*] = 0$ when $i \neq j$. We further assume that the power is normalized such that $\sum_{i=0}^{L-1} \gamma_i = 1$.

We also assume that the propagation channel is stationary over one OFDM symbol. This is the case for time-invariant or slowly time-varying channels. This assumption is valid in most of wireless applications. In these application, the channel coherence time is much larger than the block duration and the assumption of a static channel is reasonable [17].

The baseband version of the received signal can thus be written as follows,

$$\begin{aligned}
r(t) &= h(t) \star s(t) \\
&= \left(\sum_{i=0}^{L-1} h_i \delta(t - \frac{n_i}{N}T) \right) \star \left(\sum_{n=-\infty}^{+\infty} \sum_{m=0}^{N-1} x_{m,n} f_T(t - n(T+\Delta)) e^{j\frac{2\pi}{T}m(t-n(T+\Delta))} \right) \\
&= \sum_{i=0}^{L-1} \sum_{n=-\infty}^{+\infty} \sum_{m=0}^{N-1} h_i x_{m,n} f_T(t - n(T+\Delta) - \frac{n_i}{N}T) e^{j\frac{2\pi}{T}m(t-n(T+\Delta)-\frac{n_i}{N}T)} \\
&= \sum_{n=-\infty}^{+\infty} \sum_{m=0}^{N-1} x_{m,n} e^{j\frac{2\pi}{T}m(t-n(T+\Delta))} \sum_{i=0}^{L-1} h_i f_T(t - n(T+\Delta) - \frac{n_i}{N}T) e^{-j\frac{2\pi}{N}mn_i}
\end{aligned} \tag{2.7}$$

where $(\star)$ denotes the convolutional product.

Consider the decoding of the m_0-th subcarrier on the n_0-th signalling interval. We obtain then,

$$\begin{aligned}
y_{m_0,n_0} &= \langle r(t), f_R(t - n_0(T+\Delta)) e^{j\frac{2\pi}{T}m_0(t-n_0(T+\Delta))} \rangle \\
&= \int_{-\infty}^{+\infty} r(t) f_R(t - n_0(T+\Delta)) e^{-j\frac{2\pi}{T}m_0(t-n_0(T+\Delta))} dt \\
&= \sum_{n=-\infty}^{+\infty} \sum_{m=0}^{N-1} x_{m,n} \sum_{i=0}^{L-1} h_i e^{-j\frac{2\pi}{N}mn_i} \\
&\times \int_{-\infty}^{+\infty} f_T(t - n(T+\Delta) - \frac{n_i}{N}T) f_R(t - n_0(T+\Delta)) e^{j\frac{2\pi}{T}m(t-n(T+\Delta))} e^{-j\frac{2\pi}{T}m_0(t-n_0(T+\Delta))} dt
\end{aligned} \tag{2.8}$$

Here, the duration of the receive pulse $f_R(t)$ remains T because the cyclic prefix is eliminated at the receiver. Hence,

$$f_T(t - n(T+\Delta) - \frac{n_i}{N}T) = \begin{cases} \frac{1}{\sqrt{T}} & t \in [n(T+\Delta) + \frac{n_i}{N}T, (n+1)(T+\Delta) + \frac{n_i}{N}T] \\ 0 & elsewhere \end{cases} \tag{2.9}$$

$$f_R(t - n_0(T+\Delta)) = \begin{cases} \frac{1}{\sqrt{T}} & t \in [n_0(T+\Delta)+\Delta, (n_0+1)(T+\Delta)] \\ 0 & elsewhere \end{cases} \tag{2.10}$$

Accordingly, the product $f_T(t - n(T+\Delta) - \frac{n_i}{N}T) f_R(t - n_0(T+\Delta))$ is non zero only when $t \in [\max\{n_0(T+\Delta) + \frac{n_i}{N}T, n_0(T+\Delta)+\Delta\}, \min\{(n_0+1)(T+\Delta), (n_0+1)(T+\Delta) + \frac{n_i}{N}T\}]$. As previously mentioned, the cyclic prefix duration Δ is set to be longer than the maximum delay spread of the channel τ_{ds},

$$\Delta > \tau_{\text{ds}} > \frac{n_i}{N}T, i = 0, ..., L-1.$$

Hence, the signal y_{m_0,n_0} becomes

$$\begin{aligned} y_{m_0,n_0} &= \sum_{m=0}^{N-1} \sum_{i=0}^{L-1} x_{m,n_0} h_i e^{-j\frac{2\pi}{N}mn_i} \int_{n_0(T+\Delta)+\Delta}^{(n_0+1)(T+\Delta)} \frac{1}{T} e^{j\frac{2\pi}{T}(m-m_0)(t-n_0(T+\Delta))} dt \\ &= \sum_{m=0}^{N-1} \sum_{i=0}^{L-1} x_{m,n_0} h_i e^{-j\frac{2\pi}{N}mn_i} \int_{\Delta}^{T+\Delta} \frac{1}{T} e^{j\frac{2\pi}{T}(m-m_0)t} dt \end{aligned} \tag{2.11}$$

Since,

$$\frac{1}{T} \int_{\Delta}^{T+\Delta} e^{j\frac{2\pi}{T}(m-m_0)t} dt = \begin{cases} 1 & m = m_0 \\ 0 & m \neq m_0 \end{cases} \tag{2.12}$$

we obtain,

$$y_{m_0,n_0} = H(m_0) x_{m_0,n_0} \tag{2.13}$$

where, $H(m_0) = \sum_{i=0}^{L-1} h_i e^{-j\frac{2\pi}{N}m_0 n_i}$ is the m_0-th component of the Fourier transform of the channel impulse response $h(t)$ which is also called the complex channel gain at subcarrier m_0.

The time-frequency phase-space lattice is a very useful tool that can be used to compare the different multicarrier schemes [29], [30], [31], [32]. A lattice associated to a given system is defined by the symbol period and the subcarrier spacing of this system [30].

According to (2.5), the data symbols are transmitted every $T_{\text{ofdm}} = T + \Delta$ seconds and are uniformly spread along the frequency axis at the spacing $F = 1/T$ as illustrated in Fig. 2.4. In each area $T_{\text{ofdm}} \times F$, there is one complex symbol. Therefore, the data symbol density [29] of the CP-OFDM system is

$$\frac{1}{T_{\text{ofdm}} F} = \frac{T}{T+\Delta} \leq 1 \tag{2.14}$$

Since we always need a cyclic prefix to avoid the interference in the presence of a propagation channel, the CP-OFDM can only achieve a symbol density of less than one.

2.4 Filter Bank based Multicarrier Systems

The pioneering work of Chang [33] in 1960s, has presented the conditions required for signaling a parallel set of pulse amplitude modulated (PAM) symbols sequences through a bank

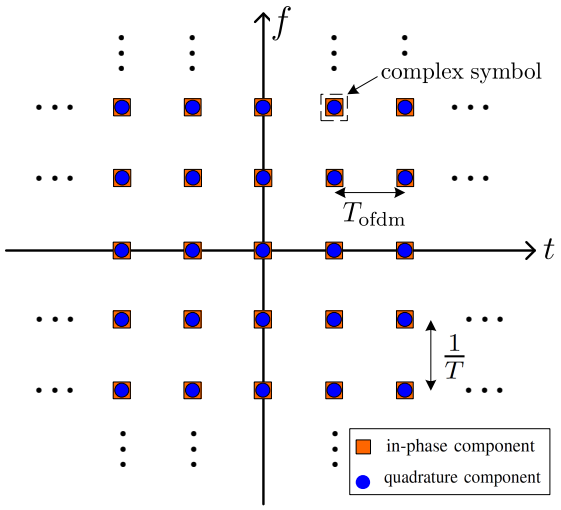

Figure 2.4: Time-frequency phase-space lattice representation of an OFDM system

of overlapping vestigial side-band (VSB) modulated filters. This idea has been extended by Saltzberg in [34], where he showed that the Chang's method could be adapted for the transmission of quadrature amplitude modulated symbols. Efficient digital implementation of Saltzberg technique through polyphase networks was first introduced by Bellanger [35] and later studied by Hirosaki in [36].
The advancements in digital subscriber line (DSL) technology motivated more activity beyond discrete multitone (DMT) (the equivalent terminology used in DSL literature instead of OFDM) and led to two classes of FBMC systems, namely, filtered multitone (FMT) modulation [37–39] and discrete wavelet multitone (DWMT) [40], which was later renamed to cosine modulated multitone (CMT) [41].

In the literature, there are mainly three classes of filter bank based multicarrier systems (FBMC) that have been studied. We give here a brief presentation of these FBMC classes:

FBMC-OQAM (SMT, staggered multitone)

Offset quadrature amplitude modulation (OQAM) is a modified version of quadrature amplitude modulation (QAM). Saltzberg showed that by choosing a root-Nyquist filter with symmetric impulse response for pulse-shaping at the transmitter and using the same for match filtering at the receiver in a multichannel QAM system, and by introducing a half symbol space delay between the in-phase and quadrature components of QAM symbols, it is possible to achieve baud-rate spacing between adjacent subcarrier channels and still recover the information symbols, free of intersymbol interference (ISI) and intercarrier interference (ICI). This method provides a higher spectral efficiency compared to conventional OFDM due to the non-use of any cyclic prefix.

FMT

In this class of filter bank systems, the subcarrier bands do not overlap. In order to avoid this overlapping, guard-band has to be reserved to allow for a transition band for each subcarrier. Hence, there is some bandwidth loss due to the guard-bands in FMT communication systems.

CMT

As noted earlier, the CMT multicarrier system is fundamentally the same as the discrete wavelet multitone (DWMT) where parallel streams of pulse amplitude modulated (PAM) data symbols are transmitted using a set of vestigial side-band (VSB) subcarrier channels. This scheme also has the maximum possible bandwidth efficiency. In a CMT system, in order to transmit N complex symbols on each multicarrier symbol, a system with $2N$ subcarrier is implemented where each carrier conveys a real symbol, while, in a FBMC-OQAM system the transceiver would have N subcarriers that convey N complex symbols. If FBMC-OQAM symbols are transmitted at the rate of $1/T$ complex symbols on each subcarrier with a bandwidth of $1/T$, an equivalent CMT system with the same data rate, would have a rate of $1/T$ real symbols on each subcarrier with the bandwidth of $1/2T$. Therefore, the same bandwidth is divided into twice as many subcarriers in case of CMT to achieve the same data rate.

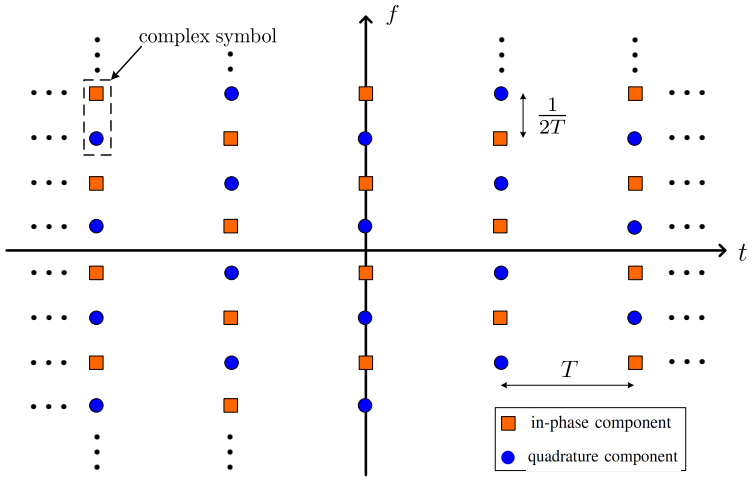

Figure 2.5: Time-frequency phase-space lattice representation of a CMT system

Among these different FBMC classes, FBMC-OQAM is preferred to be a suitable choice for various applications such as cognitive radio (CR) systems [42], where the performance of FMT, CMT and OQAM for CR networks are compared, and the conclusion reveals that OQAM presents highest stop-band attenuation among the three schemes for a fixed filter length and number of subcarriers.

In this dissertation, we mainly focus on FBMC-OQAM scheme where we use the terminology "filter bank based multicarrier (FBMC)" to refer to FBMC system that uses OQAM modulation.

2.4.1 Filter Bank Transceivers

The FBMC transmitter system is depicted in Fig. 2.6. The high-rate data stream is split into N parallel low-rate data streams and transmitted on N subcarriers that are closely spaced at a regular frequency spacing $\Delta f = 1/T$ (T is the symbol period). The main idea in this scheme is to transmit OQAM data symbols instead of conventional QAM ones [43], [44], where the in-phase and the quadrature components are time staggered by half a symbol period, $T/2$ [45–47]. The second specificity of this scheme is that considering two successive subcarriers, the time delay $T/2$ is introduced into the imaginary part of the QAM symbols on one of the subcarriers, whereas it is introduced into the real part of the symbols on the other one as shown in Fig. 2.7.

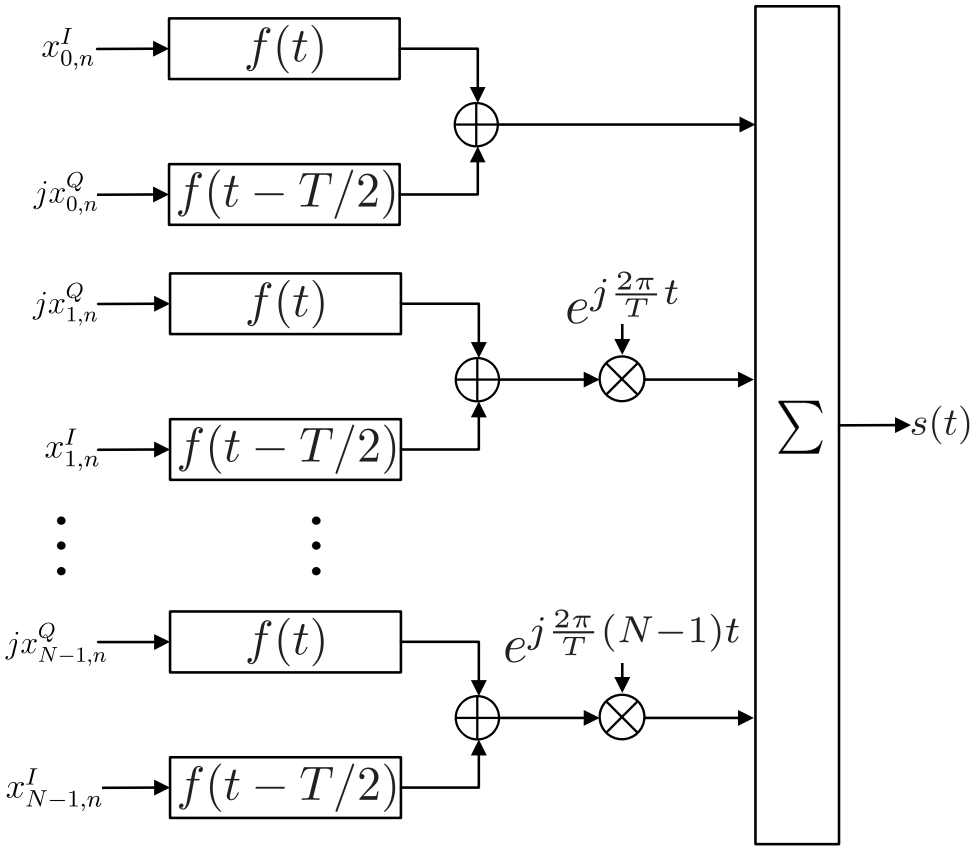

Figure 2.6: The structure of the continuous time FBMC transmitter

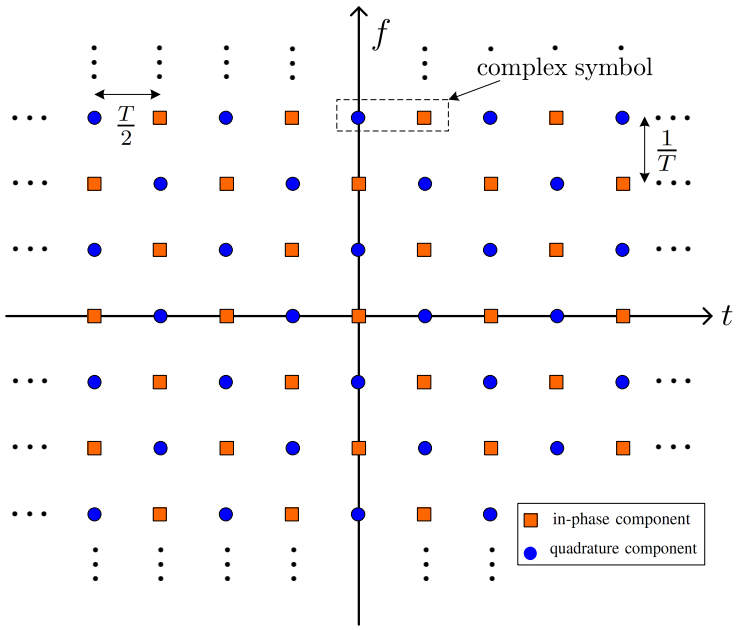

Figure 2.7: Time-frequency phase-space lattice representation of an FBMC-OQAM system

Suppose that we have the following complex input symbols,

$$x_{m,n} = x^I_{m,n} + jx^Q_{m,n} \tag{2.15}$$

where $x^I_{m,n}$ and $x^Q_{m,n}$ are the real and the imaginary parts of the n-th symbol of the m-th subcarrier, respectively.
The continuous-time baseband transmitted signal is defined as,

$$\begin{aligned} s(t) = \sum_{m=0}^{M-1} \sum_{n=-\infty}^{+\infty} & (x^I_{2m,n} f(t-nT) + jx^Q_{2m,n} f(t-nT-T/2)) e^{j\frac{2\pi}{T}(2m)t} \\ & + (x^I_{2m+1,n} f(t-nT-T/2) + jx^Q_{2m+1,n} f(t-nT)) e^{j\frac{2\pi}{T}(2m+1)t} \end{aligned} \tag{2.16}$$

where $f(t)$ is the impulse response of the prototype filter and the number of subcarriers $N = 2M$.
Let us introduce the following notations,

$$\begin{aligned} a_{2m,2n} &= x^I_{2m,n}, & a_{2m,2n+1} &= x^Q_{2m,n} \\ a_{2m+1,2n} &= x^Q_{2m+1,n}, & a_{2m+1,2n+1} &= x^I_{2m+1,n} \end{aligned} \tag{2.17}$$

Hence, we rewrite the transmitted signal $s(t)$ as follows,

$$\begin{aligned} s(t) &= \sum_{m=0}^{N-1} \sum_{n=-\infty}^{+\infty} a_{m,n} f(t - nT/2) e^{j\frac{2\pi}{T}mt} e^{j\varphi_{m,n}} \\ &= \sum_{m=0}^{N-1} \sum_{n=-\infty}^{+\infty} a_{m,n} \gamma_{m,n}(t) \end{aligned} \tag{2.18}$$

where

$$\varphi_{m,n} = \frac{\pi}{2}(m+n) - \pi mn \tag{2.19}$$

and

$$\gamma_{m,n}(t) = f(t - nT/2) e^{j\frac{2\pi}{T}mt} e^{j\varphi_{m,n}} \tag{2.20}$$

Assuming an ideal transmission system, the output of the receiver, $\hat{x}_{m,n}$, consists of the real and the imaginary parts $\hat{x}^I_{m,n}$, $\hat{x}^Q_{m,n}$.

$$\hat{x}_{m,n} = \hat{x}^I_{m,n} + j\hat{x}^Q_{m,n} \tag{2.21}$$

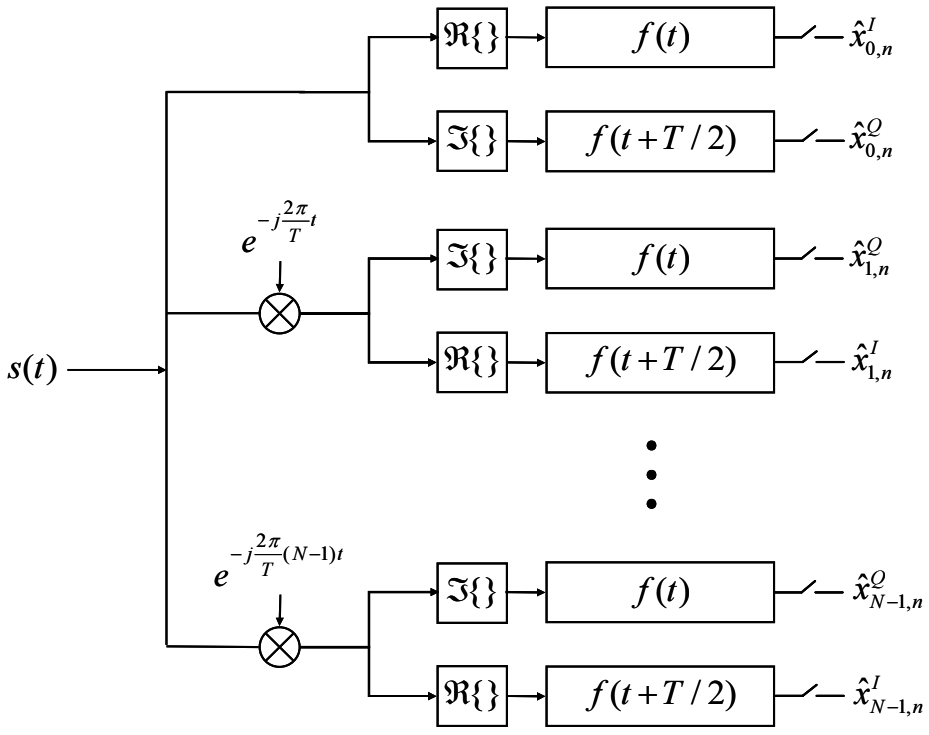

Figure 2.8: The structure of the continuous time FBMC receiver

We also denote,

$$\begin{aligned} \hat{a}_{2m,2n} &= \hat{x}^I_{2m,n} \qquad \hat{a}_{2m,2n+1} = \hat{x}^Q_{2m,n} \\ \hat{a}_{2m+1,2n} &= \hat{x}^Q_{2m+1,n} \quad \hat{a}_{2m+1,2n+1} = \hat{x}^I_{2m+1,n} \end{aligned} \tag{2.22}$$

Therefore, $\hat{a}_{m,n}$ can be found as the real part of the signal at the output of the corresponding receive filter with response $f(t)$ and expressed as,

$$\hat{a}_{m,n} = \mathrm{Re}\left[\langle s(t), \gamma_{m,n}(t)\rangle\right] = \mathrm{Re}\left[\int_{-\infty}^{+\infty} \gamma^*_{m,n}(t)s(t)dt\right] \tag{2.23}$$

Substituting (2.18) and (2.20) in (2.23), we obtain

$$\hat{a}_{m,n} = \sum_{m'=0}^{N-1}\sum_{n'=-\infty}^{+\infty}\int_{-\infty}^{+\infty} \mathrm{Re}\left[a_{m',n'}f(t-nT/2)f(t-n'T/2)e^{j\frac{2\pi}{T}(m'-m)t}e^{j(\varphi_{m',n'}-\varphi_{m,n})}dt\right] \tag{2.24}$$

We now proceed to discuss the design of the receive filter $f(t)$. In a distortion-free channel, the received signal equals the transmitted one

$$\hat{a}_{m,n} = a_{m,n} \tag{2.25}$$

For convenience of the design, it is common to constrain $f(t)$ to be real and symmetric (i.e $f(t) = f(-t)$). Therefore, (2.25) can be met, if $f(t)$ is chosen such that the following identity is satisfied,

$$\int_{-\infty}^{+\infty} f(t-nT/2)f(t-n'T/2)\cos\left(\frac{2\pi}{T}(m'-m)t + \varphi_{m',n'} - \varphi_{m,n}\right)dt = \delta_{m,m'}\delta_{n,n'} \tag{2.26}$$

In the presence of a multi-path channel with the impulse response $h(t)$ given in (2.6), the baseband version of the received signal can be written in continuous time as follows

$$r(t) = h(t) \star s(t) \tag{2.27}$$

Substituting (2.18) and (2.6) in (2.27), we obtain

$$\begin{aligned} r(t) &= \sum_{i=0}^{L-1} h_i\delta(t-\frac{n_i}{N}T) \star \sum_{m=0}^{N-1}\sum_{n=-\infty}^{+\infty} a_{m,n}f(t-nT/2)e^{j\frac{2\pi}{T}mt}e^{j\varphi_{m,n}} \\ &= \sum_{m=0}^{N-1}\sum_{n=-\infty}^{+\infty} a_{m,n}e^{j\varphi_{m,n}}\sum_{i=0}^{L-1} h_i f(t-nT/2-\frac{n_i}{N}T)e^{j\frac{2\pi}{T}m(t-\frac{n_i}{N}T)} \end{aligned} \tag{2.28}$$

Without loss of generality, let KT be the duration of the prototype filter $f(t)$, where K is an integer greater or equal to 1 (ie. $K \geq 1$). Thus, we can say that the bandwidth occupied by the filter is smaller than the coherence bandwidth B_c of the channel $B_c = 1/(2\tau_{\mathrm{ds}})$ [1], [13]. We recall that τ_{ds} denotes the maximum delay spread of the channel.

Looking at the integral in (2.28), we can notice that $f(t - nT/2 - \tau)$ may have relatively slow variations when $\tau \in [0, \tau_{\text{ds}}]$ [48], [49]. Indeed, compared to the coherence bandwidth B_c, the filter bandwidth is very small, which also means that the time variations of the prototype filter $f(t)$ are necessarily limited.
Consequently, (2.28) becomes,

$$\begin{aligned} r(t) &= \sum_{m=0}^{N-1} \sum_{n=-\infty}^{+\infty} a_{m,n} e^{j\varphi_{m,n}} f(t - nT/2) e^{j\frac{2\pi}{T}mt} \sum_{i=0}^{L-1} h_i e^{-j\frac{2\pi}{N}mn_i} \\ &= \sum_{m=0}^{N-1} \sum_{n=-\infty}^{+\infty} a_{m,n} e^{j\varphi_{m,n}} f(t - nT/2) e^{j\frac{2\pi}{T}mt} H(m) \end{aligned} \tag{2.29}$$

where, $H(m) = \sum_{i=0}^{L-1} h_i e^{-j\frac{2\pi}{N}mn_i}$ is the complex channel gain at subcarrier m.
The demodulated signal y_{m_0,n_0} at time instant n_0 and subcarrier m_0 is given by

$$\begin{aligned} y_{m_0,n_0} &= \int_{-\infty}^{+\infty} \gamma^*_{m,n}(t) r(t) dt \\ &= \sum_{m=0}^{N-1} \sum_{n=-\infty}^{+\infty} a_{m,n} e^{j(\varphi_{m,n} - \varphi_{m_0,n_0})} H(m) \int_{-\infty}^{+\infty} f(t - nT/2) f(t - n_0 T/2) e^{j\frac{2\pi}{T}(m-m_0)t} dt \end{aligned} \tag{2.30}$$

Now, let $\Omega_{\Delta m}$ be the neighborhood area around the subchannel m_0 where the channel can be considered to be constant,

$$\Omega_{\Delta m} = \{l, |l| \leq \Delta m \mid H(m_0 + l) \approx H(m_0)\}$$

It should be noticed that $\Omega_{\Delta m}$ depends on the coherence bandwidth B_c, i.e. on τ_{ds} [1], [13]. If we consider that the prototype filter is well localized in both time and frequency domains [43], [14] meaning that, $\int_{-\infty}^{+\infty} f(t - nT/2) f(t - n_0 T/2) e^{j\frac{2\pi}{T}(m-m_0)t} dt$ immediately tends to zero when $|n - n_0|$ and $|m - m_0|$ increase. We can write

$$y_{m_0,n_0} = H(m_0) \sum_{l \in \Omega_{\Delta m}} \sum_{n=-\infty}^{+\infty} a_{m,n} e^{j(\varphi_{m_0+l,n} - \varphi_{m_0,n_0})} \int_{-\infty}^{+\infty} f(t - nT/2) f(t - n_0 T/2) e^{j\frac{2\pi}{T}lt} dt \tag{2.31}$$

Assuming a perfect channel equalization, we obtain the resulting signal $y^{eq}_{m_0,n_0}$

$$y^{eq}_{m_0,n_0} = \sum_{l \in \Omega_{\Delta m}} \sum_{n=-\infty}^{+\infty} a_{m,n} e^{j(\varphi_{m_0+l,n} - \varphi_{m_0,n_0})} \int_{-\infty}^{+\infty} f(t - nT/2) f(t - n_0 T/2) e^{j\frac{2\pi}{T}lt} dt \tag{2.32}$$

After the OQAM decision, we write the recovered symbol $\hat{a}_{m_0,n_0}$ as follows,

$$\begin{aligned}\hat{a}_{m_0,n_0} &= \mathrm{Re}\left\{y^{eq}_{m_0,n_0}\right\} \\ &= \sum_{l\in\Omega_{\Delta m}} \sum_{n=-\infty}^{+\infty} a_{m,n} \int_{-\infty}^{+\infty} f(t-nT/2) f(t-n_0T/2) \cos\left(\frac{2\pi}{T} lt + \varphi_{m_0+l,n} - \varphi_{m_0,n_0}\right) dt\end{aligned} \tag{2.33}$$

According to the orthogonality condition of the prototype filter given by (2.26), we obtain

$$\hat{a}_{m_0,n_0} = \sum_{l\in\Omega_{\Delta m}} \sum_{n=-\infty}^{+\infty} a_{m,n}\delta_{m_0+l,m_0}\delta_{n,n_0} = a_{m_0,n_0} \tag{2.34}$$

In the case of highly frequency selective channels, the assumption that $f(t-\tau) \approx f(t)$ when $\tau \in [0, \tau_{\mathrm{ds}}]$ is no longer valid. In the following paragraph, we give a brief review of the different techniques of equalization of frequency selective channels.

2.4.2 Equalization techniques in FBMC

Three main approaches have been proposed in the literature to deal with frequency selective fading. The first one uses well localized waveforms that is, the pulse energy both in time and frequency domains are well contained to limit the effect on the neighborhood of a given symbol [14], [50], [43]. In this case, a basic equalizer structure of a single complex coefficient per subcarrier is considered.
The second approach uses FIR (finite impulse response) filters as subcarrier equalizers with cross connections between the adjacent subchannels to cancel the inter-carrier interference [51], [40].
The third approach applies a receiver filter bank structure providing over-sampled subcarrier signals to avoid the cross connections between the subchannels, and performs subcarrier equalization using FIR filters [52], [53], [54]. Recently, Waldhauser et al. have proposed MMSE (minimum mean square error) and decision feedback equalizer per subcarrier designed for FBMC/OQAM [55], [56]. Based on the same approach but using frequency sampling method, Ihalainen et al. have presented a multi-tap per-subcarrier equalizer in such a manner that the frequency response of the designed filter is forced to take the given target values at a set of considered frequency points within a subchannel [57].
Another interesting work has proposed a scheme of equalization with interference cancelation [49]. The basic principle of this method rests on an accurate computation of the interference term taking into account the channel and the prototype filter coefficients.
In this dissertation, we adopt the first approach of equalization which is efficient in the case of weakly and mildly frequency selective channels.

2.4.3 Polyphase Implementation of Filter Bank for Multicarrier Transmission

Filter bank based multicarrier (FBMC) systems are implemented using an efficient technique that is called polyphase implementation. The polyphase representation, invented by Bellanger over thirty five years ago [58], is a pivotal tool in multirate digital signal processing. This form provides great simplification of theoretical analysis and computationally efficient implementations for several filtering applications. The concept of this implementation is outlined in this section.

Polyphase Representation

Consider a finite impulse response (FIR) filter $F(z)$ of $L = KN$ coefficients,

$$F(z) = \sum_{l=0}^{L-1} f[l] z^{-l} \tag{2.35}$$

This filter can be decomposed into N elementary filters, in the following way,

$$\begin{aligned} F(z) &= \sum_{l=0}^{L-1} f[l] z^{-l} = \sum_{n=0}^{N-1} \sum_{k=0}^{K-1} f[kN+n] z^{-(kN+n)} \\ &= \sum_{n=0}^{N-1} \left[\sum_{k=0}^{K-1} f[kN+n] z^{-kN} \right] z^{-n} \end{aligned} \tag{2.36}$$

Consequently, the polyphase network (PPN) of the filter $F(z)$ (see Fig. 2.9) is given by,

$$F(z) = \sum_{n=0}^{N-1} E_n[z^N] z^{-n} \tag{2.37}$$

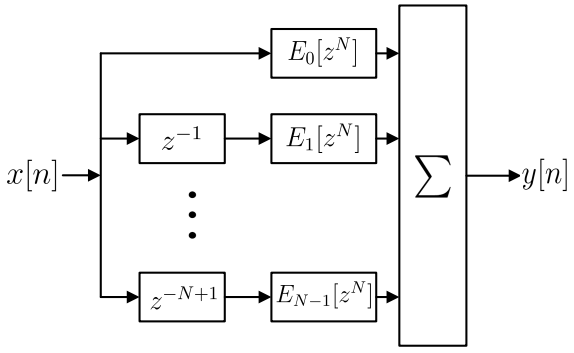

Figure 2.9: The polyphase implementation of the filter $F[z]$

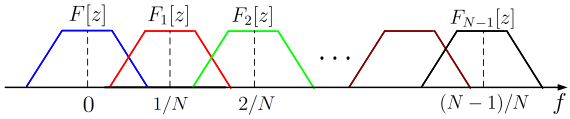

Figure 2.10: A general response for an N-filter uniform DFT filter bank

where $E_n[z^N] = \sum_{k=0}^{K-1} f[kN+n]z^{-kN}$ are called the polyphase components.
Now, let $F_i(z)$ be a replica of the filter $F(z)$ shifted by i/N in the frequency domain,

$$F_i(z) = \sum_{l=0}^{L-1} f[l]e^{j\frac{2\pi}{N}il}z^{-l} \tag{2.38}$$

Using the polyphase representation, $F_i(z)$ becomes,

$$\begin{aligned} F_i(z) &= \sum_{n=0}^{N-1}\sum_{k=0}^{K-1} f[kN+n]e^{j\frac{2\pi}{N}i(kN+n)}z^{-(KN+n)} \\ &= \sum_{n=0}^{N-1} e^{j\frac{2\pi}{N}ni}E_n[z^N]z^{-n} \end{aligned} \tag{2.39}$$

A uniform filter bank is obtained by shifting the response of $F(z)$ which is called the "*prototype filter*" on the frequency axis. Considering all shifts multiples of $1/N$ as shown in Fig. 2.10, we obtain

$$\begin{bmatrix} F_0(z) \\ F_1(z) \\ \vdots \\ F_{N-1}(z) \end{bmatrix} = \underbrace{\begin{bmatrix} 1 & 1 & \cdots & 1 \\ 1 & w^{-1} & \cdots & w^{-(N-1)} \\ \vdots & \vdots & \ddots & \vdots \\ 1 & w^{-(N-1)} & \cdots & w^{-(N-1)^2} \end{bmatrix}}_{IDFT_N} \underbrace{\begin{bmatrix} E_0[z^N] \\ z^{-1}E_1[z^N] \\ \vdots \\ z^{-(N-1)}E_{N-1}[z^N] \end{bmatrix}}_{PPN} \tag{2.40}$$

where $w = e^{-j\frac{2\pi}{N}}$ and the square matrix is the inverse discrete Fourier transform matrix of order N.

Multirate identities

Before discussing the digital implementation of the FBMC transceiver, it is worth recalling the multirate identities also called "noble identities" [59], [60]. In fact, using these identities the filtering operation can be performed at the lower rate with decimated filters, making the implementation more efficient.

First identity: the up-sampled filtering $E[z^N]$ followed by down-sampling ($\downarrow N$) is equivalent to down-sampling ($\downarrow N$) followed by filtering $E[z]$ (see Fig. 2.11.a).

Second identity: up-sampling ($\uparrow N$) followed by up-sampled filtering $E[z^N]$ is equivalent to filtering $E[z]$ followed by up-sampling ($\uparrow N$) (see Fig. 2.11.b).

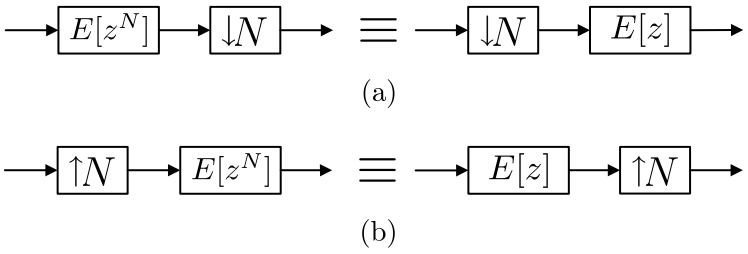

Figure 2.11: (a) the first noble identity, (b) the second noble identity

Polyphase Synthesis Filter Bank

The digital implementation of a synthesis filter bank (SFB) is presented in Fig. 2.12. The output signal $y[n]$ is synthesized by the transmission of a set of parallel data symbols $x_k[n]$ through a bank of modulated filters. According to (2.40), one can design the structure presented in Fig. 2.13. Since IDFT is a constant matrix multiplication, it can be switched with the up-sampling. Moreover, according to the second noble identity, we can commute the up-sampling with the polyphase components by replacing $E_n[z^N]$ with $E_n[z]$ and consequently the polyphase implementation of the synthesis filter bank simplifies to the scheme depicted in Fig. 2.14.

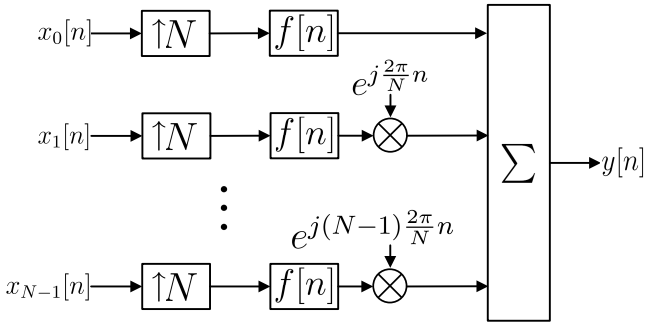

Figure 2.12: The general structure of a synthesis filter bank

Polyphase Analysis Filter Bank

The analysis filter bank (AFB), as indicated by its name, performs a frequency decomposition of the input signal. The polyphase implementation of the AFB represents a structure which is the dual of the previously considered synthesis filter bank, and is derived in a similar manner. The starting point of this is the general structure of N-channel analysis filter bank shown in Fig. 2.15.

Consider $F_{-i}(z)$ the demodulated version of $F(z)$ (a replica which is shifted in frequency

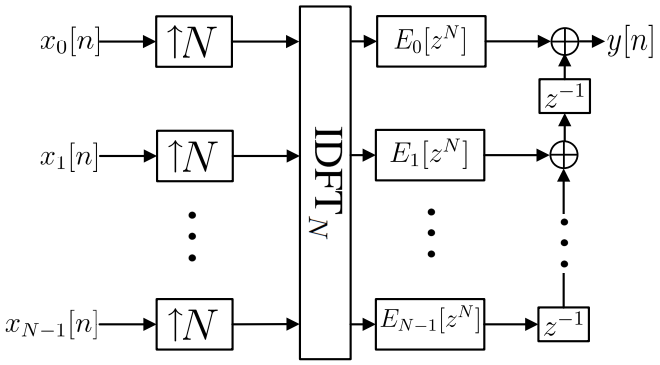

Figure 2.13: A polyphase implementation of a synthesis filter bank

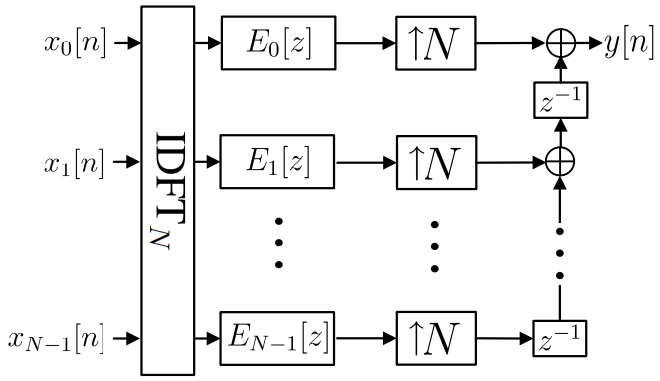

Figure 2.14: The simplified polyphase implementation of a synthesis filter bank

by $-i/N$),

$$F_{-i}(z) = \sum_{l=0}^{L-1} f[l] e^{-j\frac{2\pi}{N}il} z^{-l} \tag{2.41}$$

Using the polyphase representation, $F_{-i}(z)$ becomes,

$$\begin{aligned} F_{-i}(z) &= \sum_{n=0}^{N-1} \sum_{k=0}^{K-1} f[kN+n] e^{-j\frac{2\pi}{N}i(kN+n)} z^{-(KN+n)} \\ &= \sum_{n=0}^{N-1} e^{-j\frac{2\pi}{N}ni} E_n[z^N] z^{-n} \end{aligned} \tag{2.42}$$

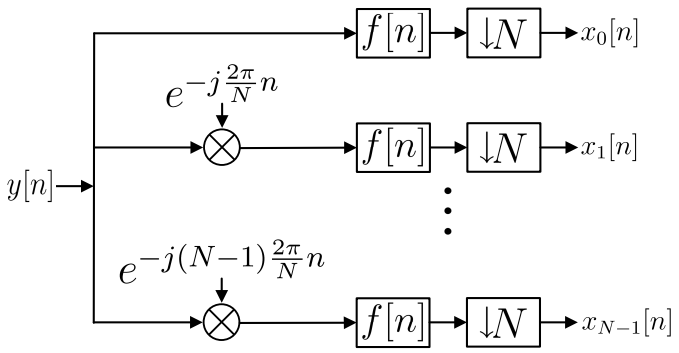

Figure 2.15: The general structure of an analysis filter bank

Thus, we can write

$$\begin{bmatrix} F_0(z) \\ F_{-1}(z) \\ \vdots \\ F_{-(N-1)}(z) \end{bmatrix} = \underbrace{\begin{bmatrix} 1 & 1 & \cdots & 1 \\ 1 & w & \cdots & w^{(N-1)} \\ \vdots & \vdots & \ddots & \vdots \\ 1 & w^{(N-1)} & \cdots & w^{(N-1)^2} \end{bmatrix}}_{DFT_N} \underbrace{\begin{bmatrix} E_0[z^N] \\ z^{-1}E_1[z^N] \\ \vdots \\ z^{-(N-1)}E_N[z^N] \end{bmatrix}}_{PPN} \tag{2.43}$$

where $w = e^{-j\frac{2\pi}{N}}$ and the square matrix is the discrete Fourier transform matrix of order N.

Therefore, the polyphase implementation of the analysis filter bank is depicted in Fig. 2.16, where the incoming signal is passed through a delay chain, and filtered by the polyphase components $E_n[z^N]$. This filtering operation is followed by IDFT operation. Similarly to the synthesis filter banks, the IDFT can be commutated with down-sampling and using the first noble identity the polyphase components are switched with down-sampling as presented in Fig. 2.17.

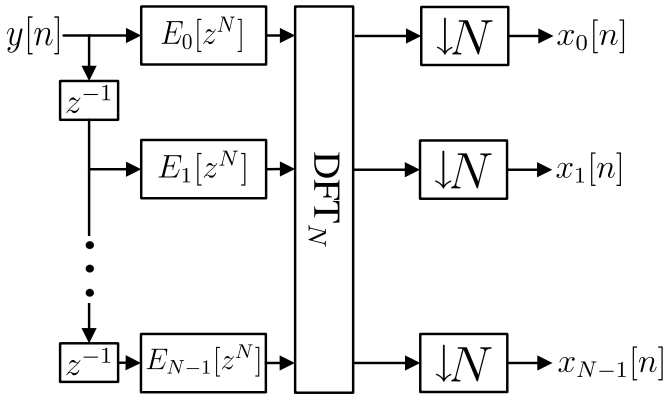

Figure 2.16: Polyphase implementation of an analysis filter bank

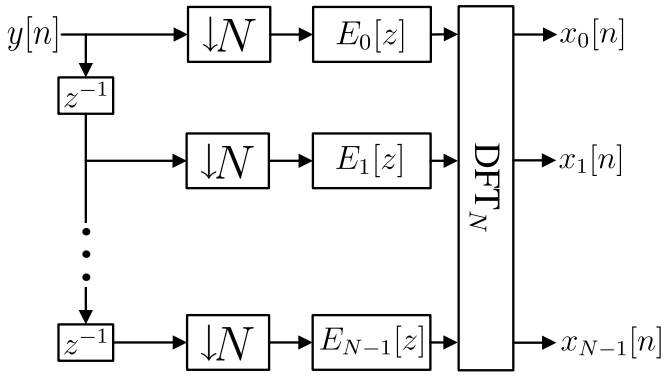

Figure 2.17: The simplified polyphase implementation of an analysis filter bank

FBMC Polyphase structure

The structure of the FBMC transmitter filter bank shown in Fig. 2.6 can be split into two subsystems: the first one with prototype filter $f(t)$ and the second one with prototype filter $f(t - T/2)$. Consequently, the structure of FBMC transmitter can be presented as in Fig. 2.18.
It is worth mentioning that we can move the delay of $N/2$ (which is equivalent to half a symbol period, T/2) from $f(n - N/2)$ to outside the second subsystem. Therefore, by replacing each subsystem in Fig. 2.18 with its polyphase implementation, we obtain the FBMC transmitter polyphase structure (see Fig. 2.19).

Similarly to the modifications performed on the FBMC transmitter,we can rearrange the FBMC receiver structure presented in Fig. 2.8 into two subsystems with prototype filters $f(t)$ and $f(t + T/2)$. Also, the delay -T/2 can be displaced to the input of the second subsystem. Doing these changes and using the polyphase implementation of the analysis filter bank of Fig. 2.17, the polyphase structure of the FBMC receiver can be obtained in Fig. 2.21. This type of structures are used in [61] and [60].
It should be pointed out that other polyphase implementations of the FBMC system has been proposed in the literature e.g [36], [43], [62]and [63].

2.4.4 Review of prototype filter design

The study of prototype filters is of a particular interest for FBMC systems because it offers an important degree of freedom compared to what is possible with conventional OFDM. A prototype filter has to meet orthogonality constraint that is given in continuous-time for the prototype function, cf. (2.26) or can be related to the polyphase components of the prototype filter in discrete-time as shown in [43]. Furthermore these prototypes can be built to satisfy some target objective, e.g. frequency selectivity or time-frequency localization, regularity, etc [64].

A basic constraint of data transmission is that the filter must satisfy the Nyquist crite-

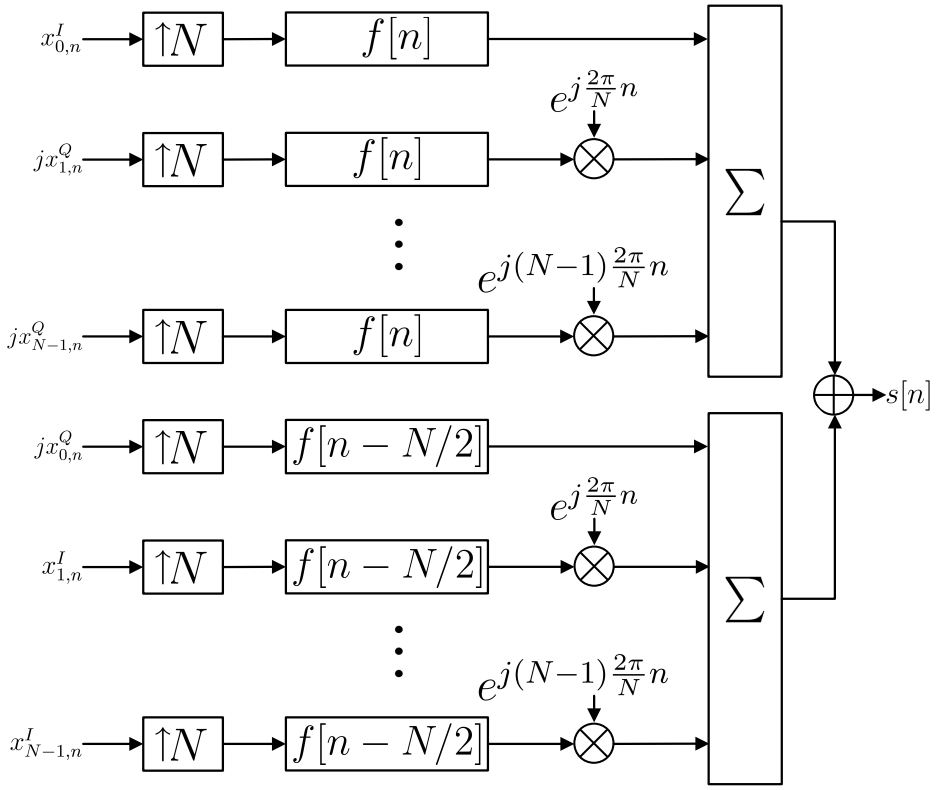

Figure 2.18: A discrete time FBMC transmitter

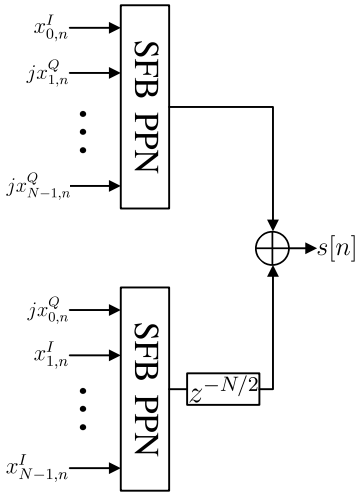

Figure 2.19: The block diagram of the polyphase implementation of an FBMC transmitter

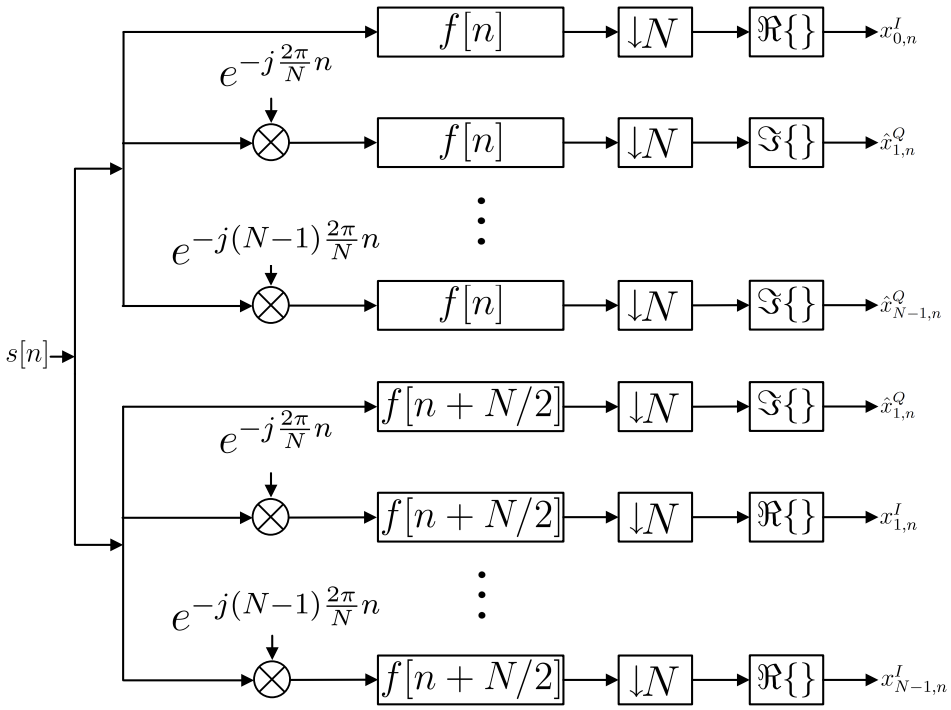

Figure 2.20: A discrete time FBMC receiver

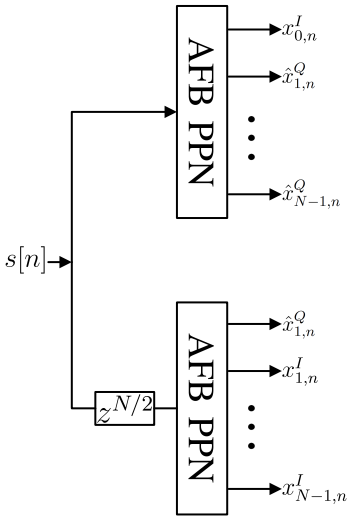

Figure 2.21: The block diagram of the polyphase implementation of an FBMC receiver

rion, to avoid inter-symbol interference (ISI). If the symbol period is T_{symb} and the symbol rate is $f_{symb} = 1/T_{symb}$, the channel frequency response must be symmetrical around the frequency $f_{symb}/2$. Accordingly, in FBMC, the prototype filter for the synthesis and analysis filter banks must be half-Nyquist, which means that the square of its frequency response must satisfy the Nyquist criterion.

So-called perfect-reconstruction (PR) filter banks implement the Nyquist criterion exactly, and also without introducing any cross-talk between subchannels in the back-to-back connection of SFB and AFB (so-called transmultiplexer). In wireless communications, the transmission channel introduces inevitably some distortion to the received subchannel signals. Therefore, the PR condition is not essential, and it is sufficient that the cross-talk between subchannels is small enough to be ignored in comparison to the residual interference, e.g., due to imperfect channel equalization. From the filter bank design point of view, this means that the so-called nearly perfect-reconstruction (NPR) designs are sufficient. Since NPR designs are more efficient than PR designs, e.g., in providing higher frequency selectivity with given prototype filter length, NPR filters are the favored choice in various applications [65].

In the following, we give a brief overview of some examples of prototype functions. The time and frequency representation are given in normalized scales, i.e. by the ratio $\frac{t}{T}$ and $\frac{f}{F}$.

Rectangular Window Function

The impulse response of the Rectangular Window (RW) function is defined by

$$f_{\Pi}(t) = \begin{cases} \frac{1}{\sqrt{T}} & t \in [0, T] \\ 0 & elsewhere \end{cases} \tag{2.44}$$

The frequency response of of this filter is given by

$$F_{\Pi}(f) = \sqrt{T} \times sinc(\pi f T) \tag{2.45}$$

where, $sinc(x) = \sin(x)/x$
It is the same function as the one used in the conventional OFDM. Its time and frequency representations are given in Fig. 2.22 and Fig. 2.23, respectively.

The Square Root of Raised Cosine (SRRC)

The SRRC pulse response is defined by [66], [67]

$$f_{srrc}(t) = \frac{\sin\left[\pi t(1-\beta)/T\right] + 4\beta t \cos\left[(\pi t/T)(1+\beta)/T\right]/T}{\pi t\left[1-(4\beta t/T)^2\right]} \tag{2.46}$$

Here, β is called the *roll-off factor* and takes values in the range $0 \leq \beta \leq 1$.
The frequency response of the SRRC filter is given by [66], [67]

$$F_{srrc}(f) = \begin{cases} \sqrt{T} & |f| \in [0, \frac{1-\beta}{2T}] \\ \sqrt{\frac{T}{2}}\left\{1 + \cos\left[\frac{\pi T}{\beta}\left(|f| - \frac{1-\beta}{2T}\right)\right]\right\}^{1/2} & |f| \in [\frac{1-\beta}{2T}, \frac{1+\beta}{2T}] \\ 0 & |f| > \frac{1+\beta}{2T} \end{cases} \tag{2.47}$$

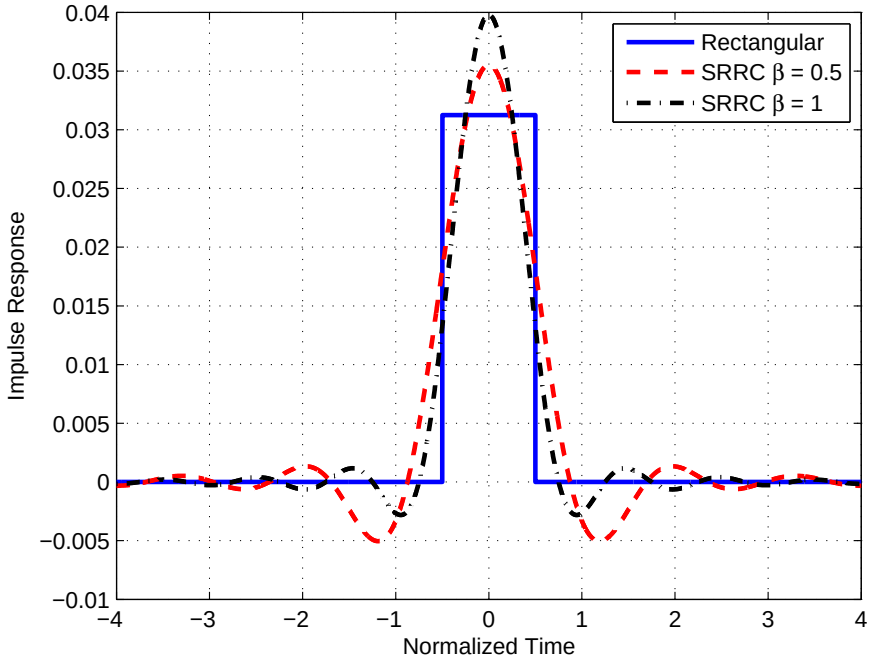

Figure 2.22: The impulse responses of the rectangular window and the SRRC filter, respectively

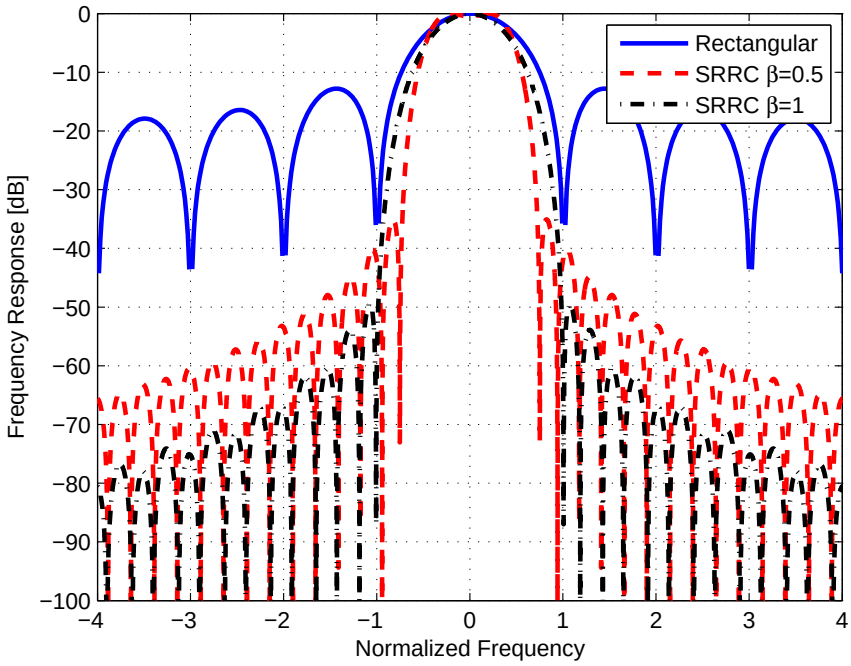

Figure 2.23: The frequency responses of the rectangular window and the SRRC filter, respectively

The time and the frequency responses of the SRRC filter are plotted in Fig. 2.22 and 2.23, respectively. Comparing the SRRC responses to the rectangular ones, one can see that the SRRC prototype filter presents a significant improvement in terms of frequency localization.

Extended Gaussian Function (EGF)

This class of prototype filter results from a two-step orthogonalization algorithm that is applied on the Gaussian function [14], [15]. The EGF is defined in time in [64]

$$f_{\alpha,\nu_0,\tau_0}(t) = \frac{1}{2}\sum_{k=0}^{\infty} d_{k,\alpha,\nu_0}\left[g_\alpha\left(t+\frac{k}{\nu_0}\right)+g_\alpha\left(t-\frac{k}{\nu_0}\right)\right]\sum_{l=0}^{\infty} d_{l,1/\alpha,\tau_0}\cos\left(2\pi l\frac{t}{\tau_0}\right) \quad (2.48)$$

where, $g_\alpha(t) = (2\alpha)^{1/4}\exp -\pi\alpha t^2$ and α is the spreading factor. The computation of the real coefficients d_{k,α,ν_0} is detailed in [64].
Originally the EGFs have been derived in closed form by Le Floch et al. [14] using the Isotropic Orthogonal Transform Algorithm (IOTA). Therefore, the IOTA prototype filter is obtained by setting $\nu_0 = \tau_0 = 1/\sqrt{2}$ and $\alpha = 1$. Note that the IOTA prototype function is identical to its Fourier Transform [14]. Accordingly, IOTA is equally localized in time and frequency domains. Its excellent time localization implies that it is less sensitive than the SRRC to time truncation [43]. The IOTA time and frequency responses are displayed in Fig. 2.24 and Fig. 2.25, respectively.

PHYDYAS Prototype Filter

This filter designed by Bellanger in [16], [68] has been considered as the reference prototype filter of the European project PHYDYAS. The design of this prototype filter is based on the so-called frequency sampling technique. The analytical formulas for calculating the coefficients of this filter provide a wide choice of the main parameters: the number of subchannels (N), the overlapping factor K and roll-off parameter α. In the design of this filter $\alpha = 1$, which means that the transition bands of a subchannel end at the centers of the adjacent subchannels. This means that only immediately adjacent subchannels are significantly interacting with each other.
The design starts with the determination of $L = KN$ desired values $F(k/L); k = 0, ..., L-1$ in the frequency domain by

$$\begin{aligned} &F_0 = 1, F_1 = 0.971960, F_2 = 1/\sqrt{2} \\ &F_3 = \sqrt{1-F_1^2}, F_k = 0; 4 < k < L-1 \end{aligned} \quad (2.49)$$

Then, the prototype filter coefficients are obtained by IDFT as

$$f(t) = \begin{cases} \frac{1}{\sqrt{A}}\left[1+2\sum_{k=1}^{K-1}(-1)^k F_k\cos\left(\frac{2\pi}{KT}kt\right)\right] & t\in[0,KT] \\ 0 & elsewhere \end{cases} \quad (2.50)$$

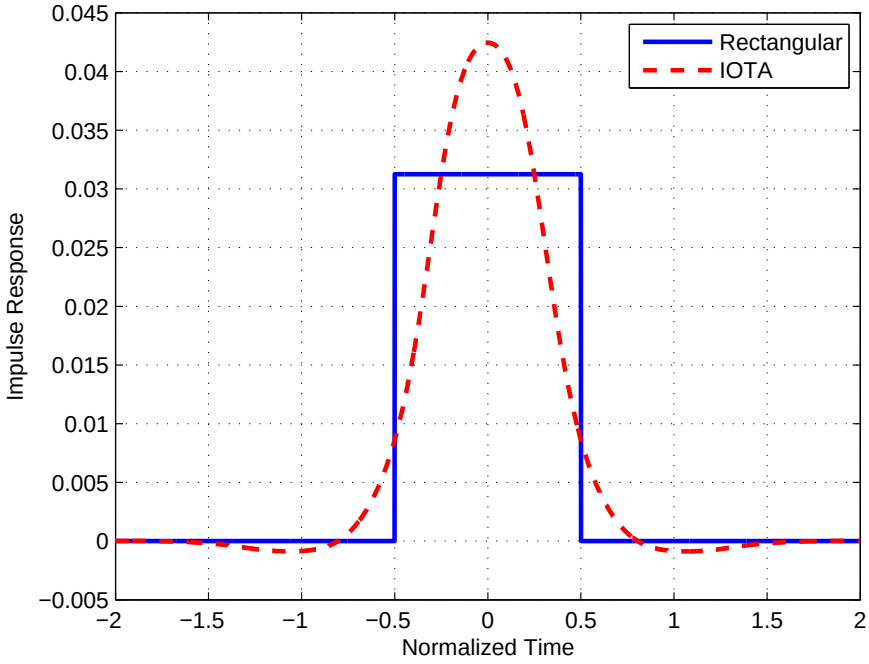

Figure 2.24: The impulse response of IOTA filter

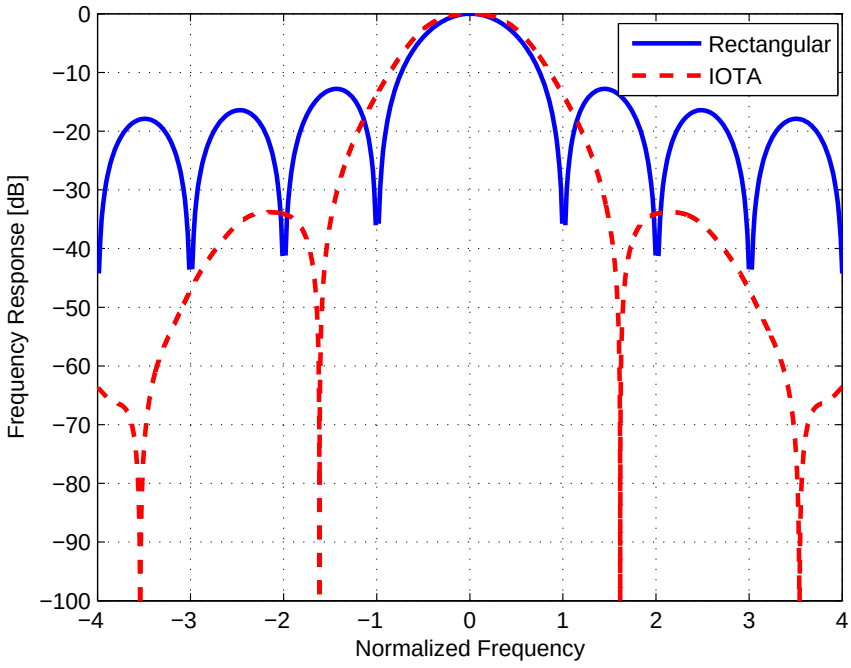

Figure 2.25: The frequency response of IOTA filter

where A is the normalization factor

$$A = \int_0^{KT} \left[1 + 2\sum_{k=1}^{K-1} (-1)^k F_k \cos\left(\frac{2\pi}{KT} kt\right)\right]^2 dt = KT\left[1 + 2\sum_{k=1}^{K-1} F_k^2\right] \tag{2.51}$$

The time and frequency responses of PHYDYAS prototype filter are shown in Fig. 2.26 and Fig. 2.27, respectively.

In the sequel of this dissertation, we consider PHYDYAS and IOTA prototype filters for FBMC systems. The PHYDYAS and IOTA transmultiplexer (transmitter and receiver connected back to back) impulse responses are given in Table. 2.1 and Table. 2.2, respectively. Each row of the table represents a sequence of the impulse response corresponding

Table 2.1: Transmultiplexer response of the FBMC system using PHYDYAS reference prototype filter

	n_0-4	n_0-3	n_0-2	n_0-1	n_0	n_0+1	n_0+2	n_0+3	n_0+4
k_0-3	0	0	0	0	0	0	0	0	0
k_0-2	0	0.0006	−0.0001	0	0	0	−0.0001	0.0006	0
k_0-1	0.0054	$0.0429j$	−0.1250	$-0.2058j$	0.2393	$0.2058j$	−0.1250	$-0.0429j$	0.0054
k_0	0	−0.0668	0.0002	0.5644	**1**	0.5644	0.0002	−0.0668	0
k_0+1	0.0054	$-0.0429j$	−0.1250	$0.2058j$	0.2393	$-0.2058j$	−0.1250	$0.0429j$	0.0054
k_0+2	0	0.0006	−0.0001	0	0	0	−0.0001	0.0006	0
k_0+3	0	0	0	0	0	0	0	0	0

Table 2.2: Transmultiplexer response of the FBMC system using IOTA prototype filter

	n_0-4	n_0-3	n_0-2	n_0-1	n_0	n_0+1	n_0+2	n_0+3	n_0+4
k_0-3	−0.0001	$0.0004j$	0.0016	$-0.0103j$	−0.0182	$0.0103j$	0.0016	$-0.0004j$	−0.0001
k_0-2	0	0.0016	0	−0.0381	0	−0.0381	0	0.0016	0
k_0-1	0.0013	$-0.0103j$	−0.0380	$0.2280j$	0.4411	$-0.2280j$	−0.0380	$0.0103j$	0.0013
k_0	−0.0007	−0.0183	0	0.4411	1	0.4411	0	−0.0183	−0.0007
k_0+1	0.0013	$0.0103j$	−0.0380	$-0.2280j$	0.4411	$0.2280j$	−0.0380	$-0.0103j$	0.0013
k_0+2	0	0.0016	0	−0.0381	0	−0.0381	0	0.0016	0
k_0+3	−0.0001	$-0.0004j$	0.0016	$0.0103j$	−0.0182	$-0.0103j$	0.0016	$0.0004j$	−0.0001

to a given subchannel. Row k_0 is the subchannel response that satisfies the Nyquist criteria. The other rows correspond to the impulse responses of the interference filters due to the overlapping of the neighboring subchannels $\{k_0-3, k_0-2, k_0-1, k_0+1, k_0+2, k_0+3\}$. From these tables, one can see that PHYDYAS-FBMC system offers better frequency localization compared to IOTA. On the other hand, IOTA is well localized in time domain compared to PHYDYAS. Looking at Table. 2.2, we can also see that the IOTA-FBMC response is isotropic in time-frequency domain.

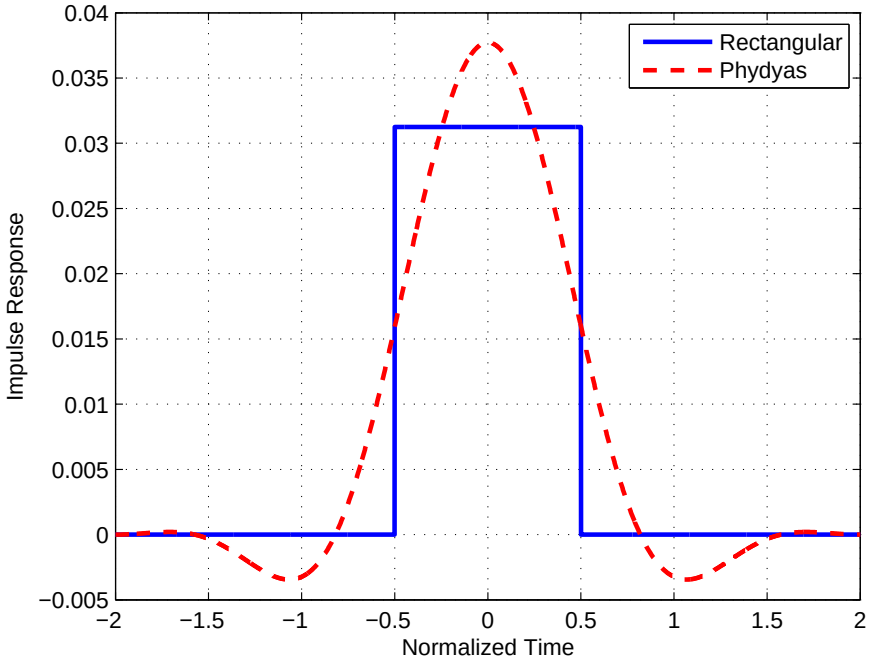

Figure 2.26: The impulse response of IOTA filter

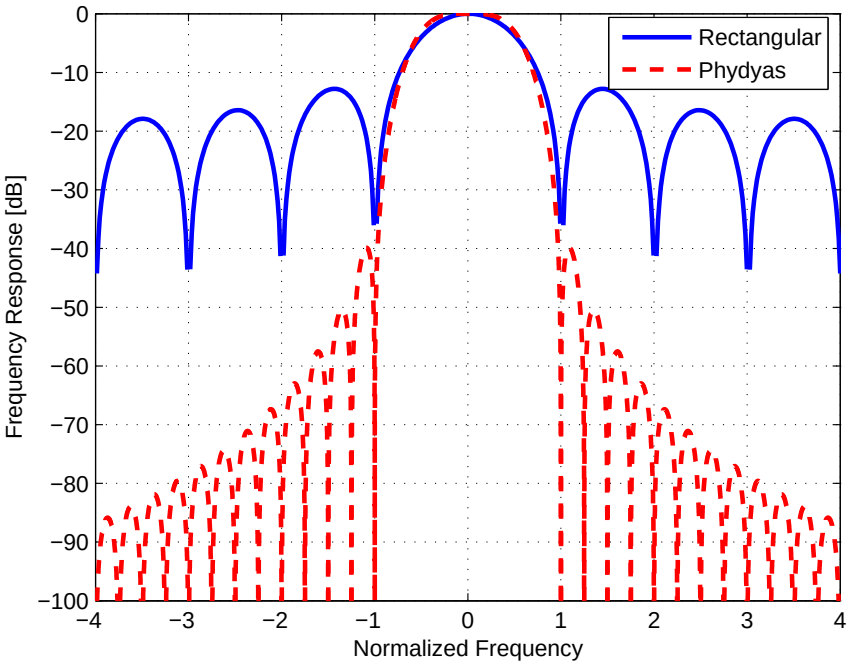

Figure 2.27: The frequency response of Phydyas filter

2.5 Asynchronous Multicarrier systems

In several communication systems, asynchronism inherently exists due to many factors e.g. the propagation delays and the spatial distribution of users. As one of the most challenging issue for communication systems design, the asynchronism can harmfully affect the system performance if it is ignored or not dealt with properly. In the literature, it is often assumed that the users are perfectly synchronized. However, this hypothesis cannot be valid in various scenarios. In what follows, we describe some of these scenarios.

2.5.1 OFDMA based cellular networks

There is currently a strong interest in extending the OFDM concept to multiuser communication scenarios. A prominent example of this trend is represented by the orthogonal frequency division multiple access (OFDMA) technology, which results from a combination of OFDM with the frequency division multiple access (FDMA) protocol. This scheme was originally suggested by Sari and Karam for cable TV (CATV) networks [69] and later adopted in the uplink of the Interaction Channel for Digital Terrestrial Television (DVB-RCT) [70]. More recently, it has become part of the emerging IEEE 802.16 standards for wireless metropolitan area networks (WMANs) [71], downlink LTE and is currently attracting vast research attention from both academia and industry.
In OFDMA systems, the available subcarriers are divided into several mutually exclusive clusters (subchannels or sub-bands) that are assigned to distinct users for simultaneous transmission.
The most challenging task consists in timing synchronization, for which no effective solution was available in the open literature [17], when this thesis was launched. Extending the length of the CP to comprehend both the channel delay spread and the two-way propagation delay results in a quasi-synchronous system and provides intrinsic protection against timing errors. Unfortunately, this approach cannot be used in recently standardized wireless metropolitan area networks. The reason is that in these applications, the propagation delay becomes comparable to the length of the OFDMA blocks, when the cell radius gets larger. As mentioned earlier, the multiple access channel model is based on the general assumption that signals belonging to distinct users propagate through distinct channels. At the receiver side synchronization can be achieved only for a given signal for a given time. After synchronization is established, the other arriving signal will inevitably be time misadjusted [72], [73]. Furthermore, in the uplink (UL), synchronization is made particularly difficult by the fact that each user's signal is characterized by different timing and frequency errors; the base station has thus to estimate a relatively large number of unknown parameters [17]. A second difficulty is related to how the estimated parameters are used to correct the uplink timing and frequency offsets.

2.5.2 OFDMA Ad-hoc networks

Generally, to preserve orthogonality between subcarriers in OFDMA, the users' signals must arrive at the input of receiver synchronously. Various multiuser synchronization techniques have been proposed in OFDMA based networks which ensure that all users' signals arriving to a given receiver are perfectly aligned. However, most of these techniques are based on closed-loop time correction techniques [17] which require the receiver to estimate all arrival times.
In contrast to classical cellular networks, it is known that, each user can communicate directly with other ones without passing through a central base station (BS) in OFDMA ad-hoc networks (ie. the topology of ad-hoc networks has dynamic characteristic parameters). Therefore it is expensive to implement these multiuser synchronization techniques at each receiver of the ad-hoc network. In this case, the most suited method consists in extending the cyclic prefix beyond what is required to eliminate the interference caused by the multipath effects [17]. Nevertheless, this solution increases redundancy and decreases the actual data rate of the system.

2.5.3 Cognitive radio systems

During the last decade, the scientific community witnessed the rise of a new paradigm in telecommunications: Cognitive radio [74], [75], [76]. It has emerged as a response to the problematic of the non-optimal management of the spectral resources in licensed bands [23]. The available communication channels are not being exploited in all locations and at all possible times. The cognitive radio is assumed to be able to sense the spectrum (SSA, spectrum sensing and awareness) and recognize the transmission opportunities, also named spectral white spaces which will be used dynamically (DSA, dynamic spectrum access).
Some particular forms of OFDMA have also been proposed for cognitive radio systems [77]. The problem of synchronization is worse in cognitive radio networks where both primary users and secondary users transmit independently.

2.6 Conclusion

In this chapter, we have presented the main framework of two multicarrier techniques: OFDM and FBMC. We have first given a brief review of the OFDM system and its implementation using the Fourier synthesis/analysis. We have shown that thanks to the introduction of a cyclic prefix in CP-OFDM, the interference caused by the multipath effects can be avoided and the equalization becomes very simple through a scalar coefficient per subcarrier. The second part of this chapter was devoted to describe the FBMC technique. The different schemes of FBMC : FBMC-OQAM, CMT and FMT were introduced. We have also reviewed the polyphase implementation of the filter bank transceivers and the choice of the prototype filters that can be used in FBMC has been discussed. In the last part of this chapter, we have presented an overview on the asynchronous multicarrier systems including

different scenarios e.g. ad-hoc and cognitive radio networks.
In the next chapter, the impact of the asynchronism on the multicarrier systems will be investigated and analyzed.

Chapter 3

Asynchronous Interference Modeling

3.1 Introduction

Interference at the radio receiver is a key source of degradation in quality of service in many wireless communication systems. In this chapter, we present a unified framework for multicarrier interference characterization and analysis in asynchronous environments. In Section 3.2,we present the state of the art of the interference modeling in multicarrier systems. In Section 3.3, we explain the general concept of the so-called interference tables. We develop then the theoretical derivation of the OFDM and FBMC interference tables in Section 3.4. Next, the extension of this model in the presence of frequency selective channels is investigated in Section 3.5. Simulation results are presented and discussed in Section 3.6. Section 3.7 concludes this chapter.

3.2 Literature review of interference modeling

In the previous chapter, we have seen that the multicarrier techniques consist in splitting up a wide band signal at a high symbol rate into several lower rate signals, each one occupying a narrower band. System performance improves because subcarriers experience flat fading channels and are orthogonal to each other, thus, minimizing the threat of interference. However, the multicarrier system performance tends to suffer from degradation because of possible episodes of imperfect time and frequency synchronization, since a loss in orthogonality can occur between subcarriers at the multicarrier receiver [78].

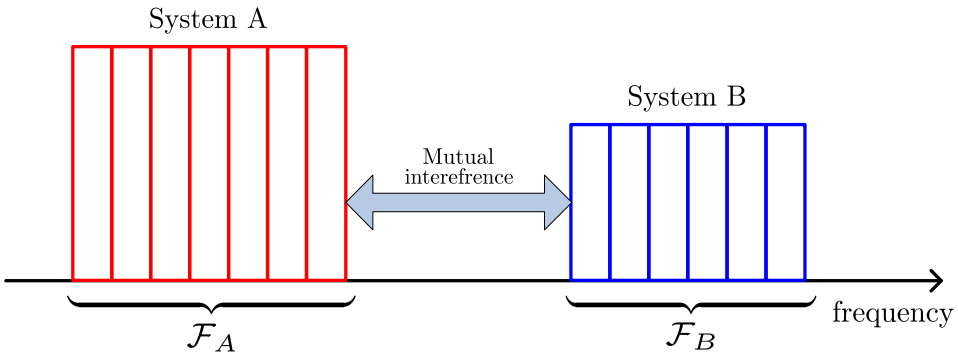

Figure 3.1: Frequency sub-bands of the asynchronous systems (A) and (B)

Interference modeling is an important problem, with numerous applications to the analysis and design of multiuser communication systems, as well as the development of interference mitigation techniques. This problem has been intensively investigated in the literature through numerous approaches. One of the most common approaches is the power spectral density (PSD) [9], [10], [11]. This model is based on the out-of band radiation which is determined by the PSD model of multicarrier signals. However, this model does not always give accurate results. For example, in multiuser CP-OFDM when the timing offset does not exceed the cyclic prefix duration, the interference comes only from the same subchannel and the other subchannels do not contribute to this interference. Unfortunately, in this case the PSD modeling still shows that the other carriers contribute in the resulting interference.

3.3 The general concept of interference tables

Let us consider two asynchronous systems (A) and (B) that coexist in the same geographical area. We assume that both systems share a given frequency band. As shown in Fig. 3.1, let $\mathcal{F}_A$ and $\mathcal{F}_B$ be the frequency sub-bands occupied by systems (A) and (B), respectively. Due to the non-orthogonality between their respective transmit signals, some amount of the power is spilled from a system to the other. In order to analyze this interaction, the PSD is generally used to evaluate the mutual interference between both systems [9], [10]. According to [10], the normalized mutual interference between the co-located systems is defined as

$$I(l) = \int_{(l-1/2)\Delta f}^{(l+1/2)\Delta f} \Phi(f)df \tag{3.1}$$

where:

- l is the spectral distance between the two interacting subcarriers
- Δf is the subcarrier spacing
- $\Phi(f)$ is the PSD which depends on the considered multicarrier technique.

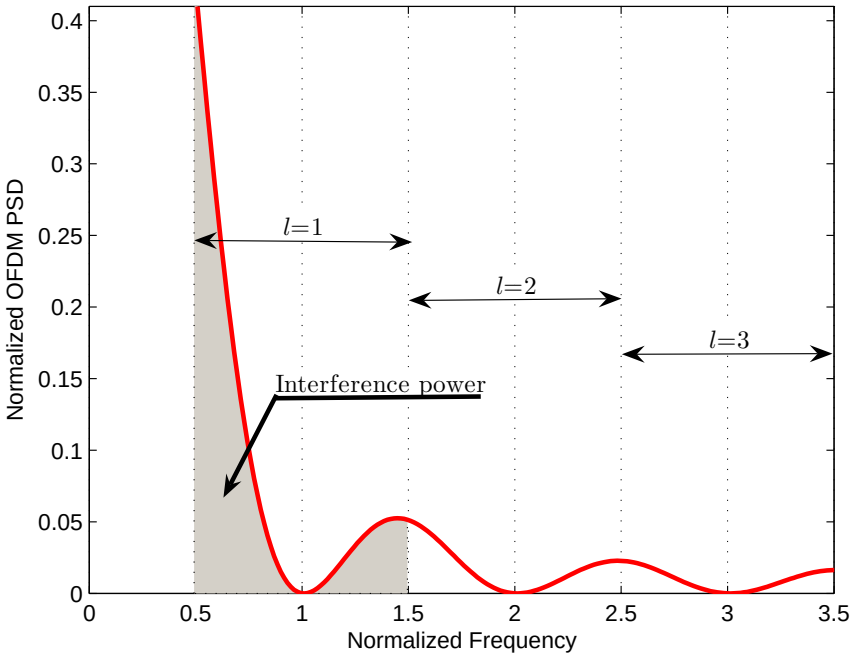

Figure 3.2: PSD of a single OFDM modulated carrier.

In the case of CP-OFDM system, the normalized PSD is given in [10] by

$$\Phi_{\text{OFDM}}(f) = T_{\text{OFDM}} \left(\frac{sin(\pi f T_{\text{OFDM}})}{\pi f T_{\text{OFDM}}} \right)^2 \tag{3.2}$$

where T_{OFDM} is the OFDM symbol duration given by the sum of the useful symbol duration T and the CP duration Δ.

The red curve of Fig. 3.2 depicts the normalized OFDM PSD. The mutual interference power when $l = 1$ corresponds to the gray-colored area.

The PSD of FBMC systems has been computed in [9], for two waveforms: IOTA and PHYDYAS. The respective expressions are

$$\Phi_{\text{IOTA}}(f) = (f_{1,\sqrt{2}/2,\sqrt{2}/2})^2 \tag{3.3}$$

$$\Phi_{\text{PHYDYAS}}(f) = (F(f))^2 \tag{3.4}$$

Here, $F(f)$ is the square root of the PHYDYAS filter frequency response which is given by,

$$F(f) = \sum_{k=-(K-1)}^{k=(K-1)} F_k \frac{\sin\left(\pi\left(f - \frac{k}{NK}\right)NK\right)}{NK \sin\left(\pi\left(f - \frac{k}{NK}\right)\right)} \tag{3.5}$$

We recall that $f_{1,\sqrt{2}/2,\sqrt{2}/2}$ and F_k are given in (2.48) and (2.49), respectively.

Based on equation (3.1), we can construct a table of mutual interference as a function of the

spectral distance l. The PSD-based interference tables for CP-OFDM are given in Table. 3.1 for different values of CP duration: $\Delta = 0, T/8$ and $T/4$. Moreover, we give in Table. 3.2 the PSD-based interference tables for FBMC considering PHYDYAS and IOTA waveforms. It is worth to point out that these tables are symmetrical as shown in Fig. 3.3.

In Fig. 3.4, we illustrate how to compute the interference caused by the different

l	$\Delta = 0$ [dB]	$\Delta = T/8$ [dB]	$\Delta = T/4$ [dB]
0	-01.11	-00.87	-00.70
1	-11.04	-12.00	-13.08
2	-18.52	-19.72	-20.72
3	-22.30	-23.55	-23.16
4	-24.88	-25.98	-25.14
5	-26.86	-27.62	-27.97
6	-28.46	-28.83	-30.34
7	-29.82	-29.92	-30.72
8	-31.00	-31.05	-31.24

Table 3.1: OFDM mutual interference tables based on the PSD for $\Delta = 0, T/8$ and $T/4$, respectively

subcarriers of $\mathcal{F}_A$ to a given subcarrier m of system (B). The total interference is the sum of the contribution of each interfering subcarrier m', and can thus be written as

$$I_{tot} = \sum_{m' \in \mathcal{F}_A} P(m') I(|m' - m|) \tag{3.6}$$

where $P(m')$ is the transmitted power on the m'-th interfering subcarrier and $I(m' - m)$ is the PSD-based interference table coefficient computed in Table. 3.1 and Table. 3.2.
Various analysis have been developed based on this interference estimation e.g. SINR, spectral efficiency analysis in [9], [10] and resource allocation algorithms [79].

According to (3.1), one can see that the interference remains the same for any timing misalignment between the transmitted signals of both systems, since the signals are considered to be non-orthogonal. However in CP-OFDM systems, the orthogonality between the different transmit signals is maintained as long as the timing misalignment does not exceed the cyclic prefix duration. This example highlights the overestimation of the asynchronous interference term. In fact, the real asynchronous interference is always a function of the timing offset between the considered asynchronous systems that is not taken into account in the PSD-based interference tables generation.
In the next section, we propose new interference tables that model the correlation between the interfering subcarrier and the victim one considering the timing offset between them in addition to the different parameters already considered by the PSD-based interference tables.

l	PHYDYAS [dB]	IOTA [dB]
0	-00.58	-00.70
1	-11.95	-09.27
2	-65.02	-35.56
3	-80.30	-42.55
4	-89.22	-65.17
5	-95.68	-71.72
6	-100.80	-87.31
7	-105.08	-90.53
8	-108.80	-91.45

Table 3.2: FBMC mutual interference tables based on the PSD for PHYDYAS and IOTA waveforms, respectively

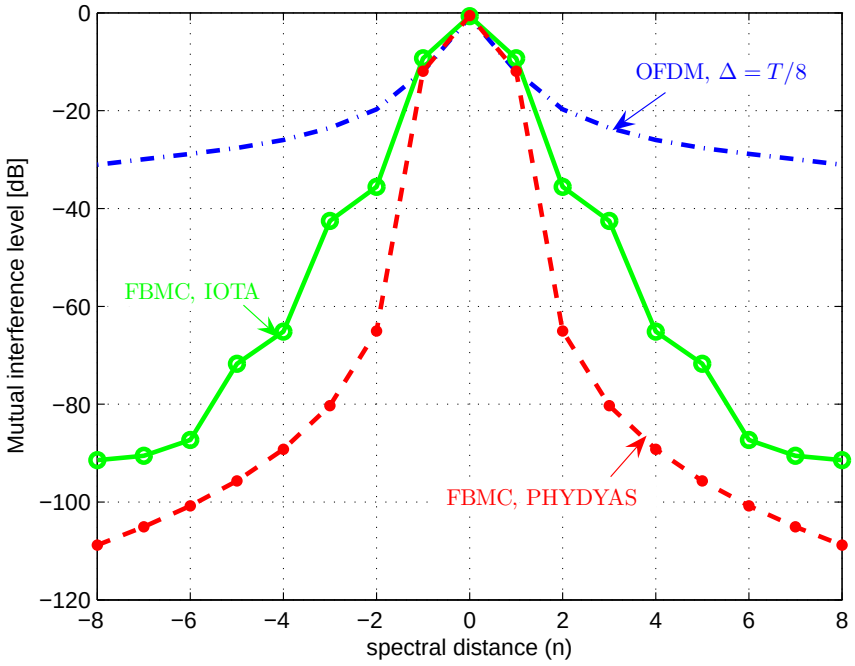

Figure 3.3: PSD-based interference tables of OFDM and FBMC.

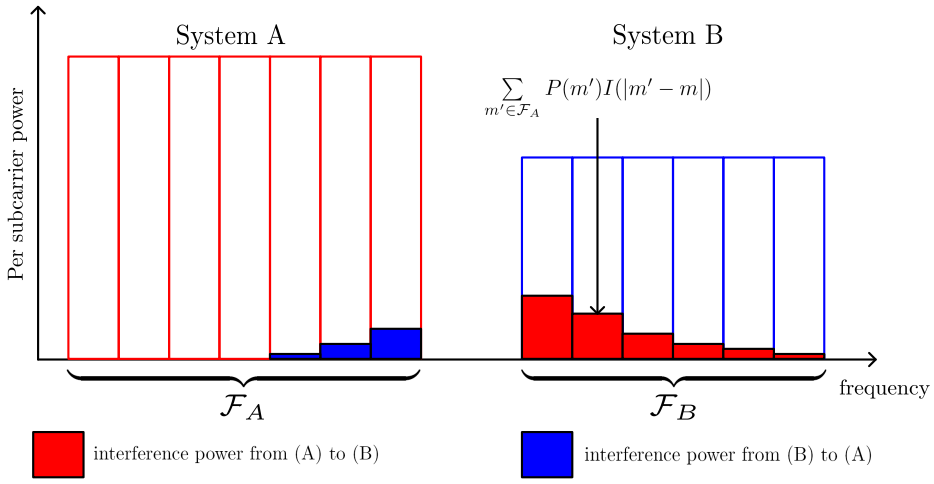

Figure 3.4: Illustration of how to compute the interference caused by a set of subcarriers.

3.4 OFDM/FBMC interference tables

[80] To take into account the detrimental effects of interference caused by the imperfect syn-

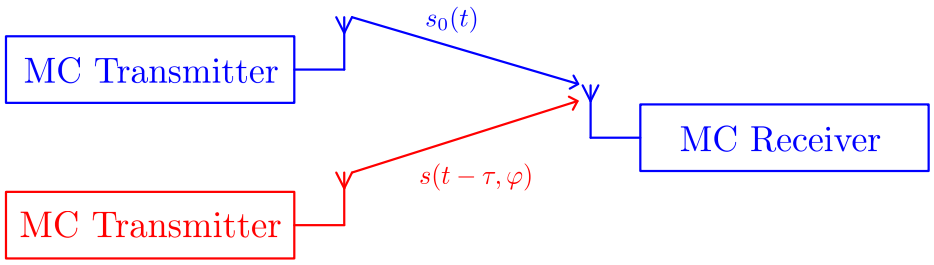

Figure 3.5: Asynchronous interference in multicarrier systems

chronization in multicarrier techniques, we consider the system model depicted in Fig. 3.5. We refer, here, to a receiver which suffers from the interference coming from an asynchronous transmitter. This receiver is assumed to be perfectly synchronized with its corresponding transmitter. Moreover, the timing offset τ and the phase offset φ are assumed to be uniform random variables that are distributed on $\tau \in [0, T]$ and $\varphi \in [0, 2\pi]$, respectively. In the following analysis, we will be interested in the impact of the interfering signal $s(t - \tau)$ on the reference receiver.

3.4.1 CP-OFDM case

Consider the following asynchronous signal coming from the interferer on the m-th subcarrier

$$s_m(t-\tau,\varphi) = \sum_{n=-\infty}^{n=+\infty} x_{m,n} f_T(t-n(T+\Delta)-\tau) e^{j\left[\frac{2\pi}{T}m(t-n(T+\Delta)-\tau)+\varphi\right]} \tag{3.7}$$

where

- $x_{m,n}$ are the complex data symbols transmitted by the interferer
- T and Δ are the useful OFDM symbol duration and the CP duration, respectively
- the timing offset and the phase offset between the reference receiver and the interferer are respectively denoted by τ and φ.

We recall also that $f_T(t)$ and $f_R(t)$ are respectively, the transmit and the receiver pulse shapes,

$$f_T(t) = \begin{cases} \frac{1}{\sqrt{T}} & t \in [0, T+\Delta] \\ 0 & elsewhere \end{cases} \qquad f_R(t) = \begin{cases} \frac{1}{\sqrt{T}} & t \in [\Delta, T+\Delta] \\ 0 & elsewhere \end{cases}$$

The m_0-th output of the receiver filter on the n_0-th signalling interval coming from $s_m(t-\tau,\varphi)$, will be

$$\begin{aligned} y_{m_0,n_0}(\tau,\varphi) &= \langle s_m(t-\tau,\varphi), f_R(t-n_0(T+\Delta)) e^{j\frac{2\pi}{T}m_0(t-n_0(T+\Delta))} \rangle \\ &= \int_{-\infty}^{+\infty} s_m(t-\tau,\varphi) f_R(t-n_0(T+\Delta)) e^{-j\frac{2\pi}{T}m_0(t-n_0(T+\Delta))} dt \\ &= \sum_{n=-\infty}^{+\infty} x_{m,n} e^{-j\left[\frac{2\pi}{T}m\tau-\varphi\right]} \\ &\times \int_{-\infty}^{+\infty} f_T(t-n(T+\Delta)-\tau) f_R(t-n_0(T+\Delta)) e^{j\frac{2\pi}{T}m(t-n(T+\Delta))} e^{-j\frac{2\pi}{T}m_0(t-n_0(T+\Delta))} dt \end{aligned} \tag{3.8}$$

In the general case, we see that the product $f_T(t-n(T+\Delta)-\tau) f_R(t-n_0(T+\Delta))$ and the choice of τ determine the limits of the integral appearing in (3.8), we have then two cases to analyze

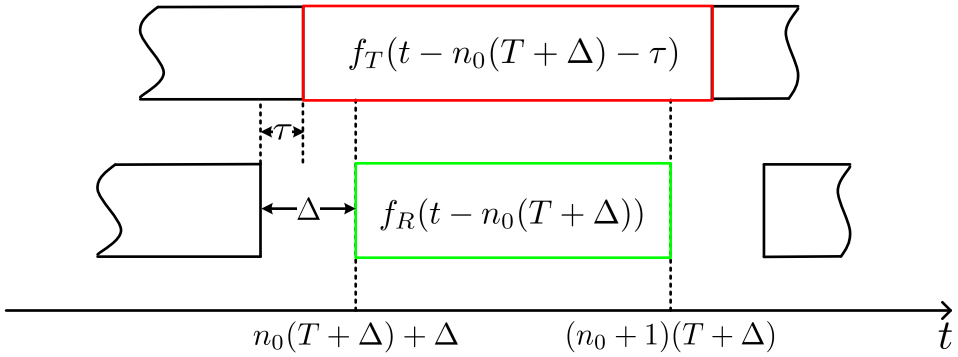

Figure 3.6: Respective positions of transmit and receiver pulses when $\tau \in [0, \Delta]$.

Case 1: $(0 < \tau < \Delta)$

In this case, the positions of the receiver window and the interferer window are depicted in Fig.3.6 and the signal $y_{m_0,n_0}(\tau)$ becomes,

$$y_{m_0,n_0}(\tau,\varphi) = x_{m,n_0} e^{-j\left[\frac{2\pi}{T}m\tau-\varphi\right]} \int_{n_0(T+\Delta)+\Delta}^{(n_0+1)(T+\Delta)} \frac{1}{T} e^{j\frac{2\pi}{T}(m-m_0)(t-n_0(T+\Delta))} dt$$
$$= \begin{cases} x_{m_0,n_0} e^{-j\left[\frac{2\pi}{T}m_0\tau-\varphi\right]} & m = m_0 \\ 0 & otherwise \end{cases} \tag{3.9}$$

Here, the timing offset τ is absorbed by the cyclic prefix Δ. The interference will only occur on the same subcarrier $m = m_0$, the other subcarriers are free of interference due to the orthogonality between them.

Case 2: $(\Delta < \tau < T + \Delta)$

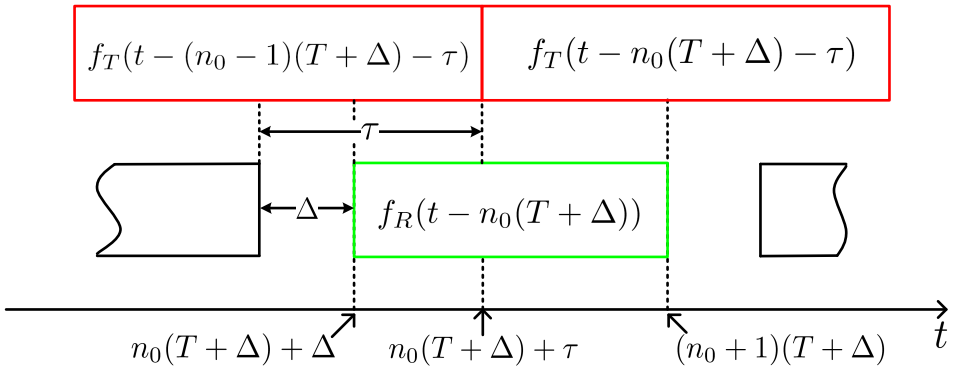

Figure 3.7: Respective positions of transmit and receiver pulses when $\tau \in [\Delta, T + \Delta]$.

As illustrated in Fig. 3.7, the product $f_T(t-n(T+\Delta)-\tau)f_R(t-n_0(T+\Delta))$ is non zero when $n=n_0-1$ and $n=n_0$, simultaneously. Consequently, the signal $y_{m_0,n_0}(\tau)$ can be written as follows

$$\begin{aligned}
y_{m_0,n_0}(\tau,\varphi) &= e^{-j\left[\frac{2\pi}{T}m\tau-\varphi\right]} \\
&\quad\times\left\{x_{m,n_0-1}\int_{n_0(T+\Delta)+\Delta}^{n_0(T+\Delta)+\tau}\frac{1}{T}e^{j\frac{2\pi}{T}m(t-(n_0-1)(T+\Delta))}e^{-j\frac{2\pi}{T}m_0(t-n_0(T+\Delta))}dt\right. \\
&\qquad\left.+\,x_{m,n_0}\int_{n_0(T+\Delta)+\tau}^{(n_0+1)(T+\Delta)}\frac{1}{T}e^{j\frac{2\pi}{T}(m-m_0)(t-n_0(T+\Delta))}dt\right\} \\
&= e^{-j\left[\frac{2\pi}{T}m\tau-\varphi\right]} \\
&\quad\times\left\{\frac{x_{m,n_0-1}}{T}e^{-j\frac{2\pi}{T}m(T+\Delta)}\int_{n_0(T+\Delta)+\Delta}^{n_0(T+\Delta)+\tau}e^{j\frac{2\pi}{T}(m-m_0)(t-n_0(T+\Delta))}dt\right. \\
&\qquad\left.+\,\frac{x_{m,n_0}}{T}\int_{n_0(T+\Delta)+\tau}^{(n_0+1)(T+\Delta)}e^{j\frac{2\pi}{T}(m-m_0)(t-n_0(T+\Delta))}dt\right\} \qquad (3.10)
\end{aligned}$$

When $m\neq m_0$ equation (3.10) is reduced, upon the change of variables $t=t'-n_0(T+\Delta)$, to

$$\begin{aligned}
y_{m_0,n_0}(\tau,\varphi) &= e^{-j\left[\frac{2\pi}{T}m\tau-\varphi\right]} \\
&\quad\times\left\{\frac{x_{m,n_0-1}}{T}e^{-j\frac{2\pi}{T}m(T+\Delta)}\int_{\Delta}^{\tau}e^{j\frac{2\pi}{T}(m-m_0)t}dt+\frac{x_{m,n_0}}{T}\int_{\tau}^{(T+\Delta)}e^{j\frac{2\pi}{T}(m-m_0)t}dt\right\} \\
&= e^{-j\left[\frac{2\pi}{T}m\tau-\varphi\right]} \\
&\quad\times\left\{\frac{x_{m,n_0-1}}{j2\pi(m-m_0)}e^{-j\frac{2\pi}{T}m(T+\Delta)}\left[e^{j\frac{2\pi}{T}(m-m_0)\tau}-e^{j\frac{2\pi}{T}(m-m_0)\Delta}\right]\right. \\
&\qquad\left.+\frac{x_{m,n_0}}{j2\pi(m-m_0)}\left[e^{j\frac{2\pi}{T}(m-m_0)(T+\Delta)}-e^{j\frac{2\pi}{T}(m-m_0)\tau}\right]\right\} \qquad (3.11)
\end{aligned}$$

Using some trigonometric transformations, the signal $y_{m_0,n_0}(\tau)$ can be written in the following form

$$\begin{aligned}
y_{m_0,n_0}(\tau,\varphi) &= e^{-j\left[\frac{2\pi}{T}m\tau-\varphi\right]} \\
&\quad\times\left\{\frac{x_{m,n_0-1}}{\pi(m-m_0)}e^{-j\frac{2\pi}{T}m(T+\Delta)}e^{j\frac{\pi}{T}(m-m_0)(\tau+\Delta)}\sin\left[\pi(m-m_0)(\tau-\Delta)/T\right]\right. \\
&\qquad\left.+\frac{x_{m,n_0}}{\pi(m-m_0)}e^{j\frac{\pi}{T}(m-m_0)(T+\Delta+\tau)}\sin\left[\pi(m-m_0)(T+\Delta-\tau)/T\right]\right\} \qquad (3.12)
\end{aligned}$$

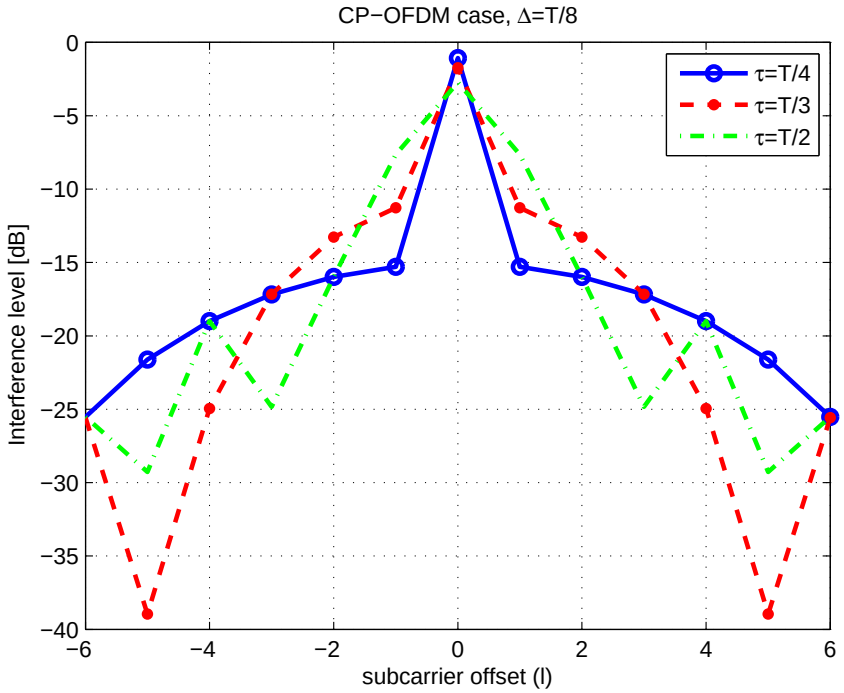

Figure 3.8: OFDM instantaneous interference tables for $\tau = \{T/4, T/3, T/2\}$.

when $m = m_0$, the signal $y_{m_0,n_0}(\tau)$ is given by

$$y_{m_0,n_0}(\tau,\varphi) = e^{-j\left[\frac{2\pi}{T}m_0\tau-\varphi\right]}\left\{x_{m_0,n_0-1}e^{-j\frac{2\pi}{T}m_0(T+\Delta)}\frac{\tau-\Delta}{T} + x_{m_0,n_0}\frac{T+\Delta-\tau}{T}\right\} \quad (3.13)$$

Accordingly when the timing offset τ is larger than the cyclic prefix duration Δ, the orthogonality between subcarriers is damaged. Thus, the interference is caused by all subcarriers.

As the communication symbols $x_{m,n}$ are zero mean uncorrelated variables, the corresponding interference power is the sum of the interference power coming respectively from two successive data symbols $(x_{m,n-1}, x_{m,n})$. Without loss of generality, we assume that $\mathbb{E}[|x_{m,n}|^2] = 1$, we can define the instantaneous interference tables by the following expression

$$\begin{aligned} I(\tau,l) &= \mathbb{E}_x\left[\left|y_{m_0,n_0}(\tau,\varphi)\right|^2\right] \\ &= \begin{cases} \delta(l) & \tau \in [0,\Delta] \\ \left[(T+\Delta-\tau)^2 + (\tau-\Delta)^2\right]/T^2 & \tau \in [\Delta, T+\Delta], l = 0 \\ \left|\frac{\sin(\pi l(T+\Delta-\tau)/T)}{\pi l}\right|^2 + \left|\frac{\sin(\pi l(\tau-\Delta)/T)}{\pi l}\right|^2 & \tau \in [\Delta, T+\Delta], l \neq 0 \end{cases} \end{aligned} \quad (3.14)$$

where $\delta(l)$ is the Kronecker delta and $l = |m - m_0|$ is the spectral distance between the interfering subcarrier and the victim one.

According to (3.14), the OFDM interference power tables do not depend on the phase offset φ. In Table. 3.3, we give some examples of the instantaneous interference tables for $\tau = T/4, T/3$ and $T/2$. These examples are also depicted in Fig. 3.8 where we see that the interference level vary with respect to the timing offset τ and the spectral distance l.

l	$\tau = T/4$ [dB]	$\tau = T/3$ [dB]	$\tau = T/2$ [dB]
0	-01.06	-01.72	-02.73
1	-15.29	-11.27	-07.63
2	-15.98	-13.28	-15.98
3	-17.18	-17.17	-24.83
4	-19.00	-24.95	-19.00
5	-21.62	-38.96	-29.27
6	-25.52	-25.58	-25.52

Table 3.3: OFDM instantaneous interference tables for $\tau = \{T/4, T/3, T/2\}$

OFDM mean interference Table

In order to calculate the mean interference table $\overline{I}(l)$, we assume a timing offset τ uniformly distributed in $[0, T + \Delta]$,

$$\overline{I}(l) = \int_{\tau} I(\tau, l) p(\tau) d\tau \tag{3.15}$$

where $p(\tau)$ is the probability density function of the random variable τ,

$$p(\tau) = \begin{cases} 1/(T+\Delta) & \tau \in [0, T+\Delta] \\ 0 & elsewhere \end{cases} \tag{3.16}$$

Substituting (3.14) and (3.16) into (3.15), we obtain

case 1 ($l = 0$)

$$\begin{aligned} \overline{I}(0) &= \frac{1}{T+\Delta} \left[\int_0^{\Delta} d\tau + \int_{\Delta}^{T+\Delta} \frac{(T+\Delta-\tau)^2 + (\tau-\Delta)^2}{T^2} d\tau \right] \\ &= \frac{2T+3\Delta}{3(T+\Delta)} \end{aligned} \tag{3.17}$$

case 2 ($l \neq 0$)

$$\begin{aligned} \overline{I}(l) &= \frac{1}{T+\Delta} \int_{\Delta}^{T+\Delta} \left| \frac{\sin\left(\pi l (T+\Delta-\tau)/T\right)}{\pi l} \right|^2 + \left| \frac{\sin\left(\pi l (\tau-\Delta)/T\right)}{\pi l} \right|^2 d\tau \\ &= \frac{T}{(\pi l)^2 (T+\Delta)} \end{aligned} \tag{3.18}$$

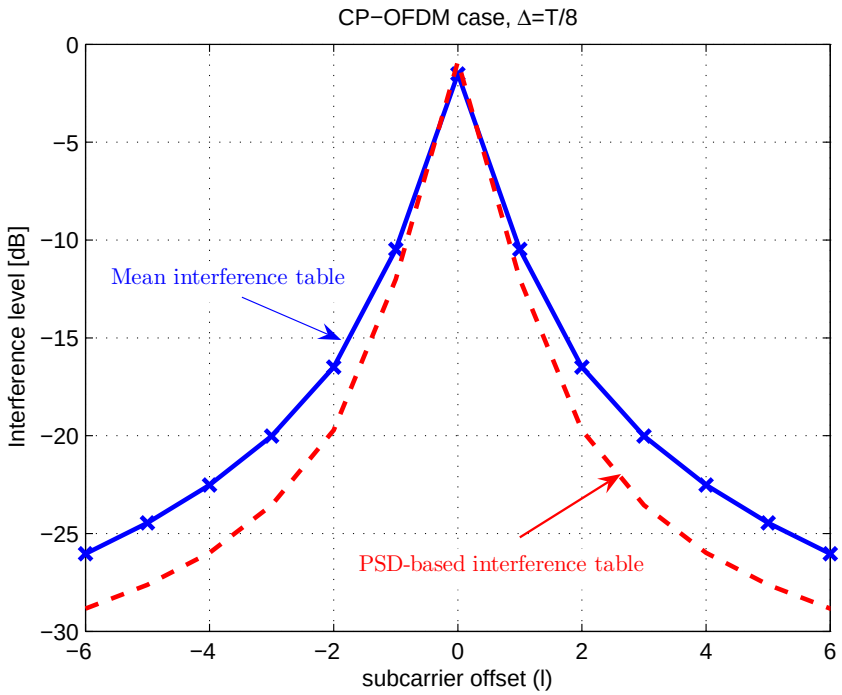

Figure 3.9: OFDM mean interference table vs. PSD-based OFDM interference Table.

The OFDM mean interference table is compared to the PSD-based OFDM interference table in Fig. 3.9 and Table. 3.4. We can see that the two interference levels computed by the PSD and the proposed interference tables are quite different. In fact, the bigger the spectral distance is, the greater the gap in interference level becomes. It must be noted that, except for $l = 0$, the interference levels presented by the proposed model is higher than the PSD-based one.

3.4.2 FBMC case

In this case, we consider that the asynchronous signal $s(t-\tau,\varphi)$ is an FBMC signal. According to (2.18), we define the asynchronous signal coming from the interferer on the m-th subcarrier $s_m(t-\tau,\varphi)$ as follows

$$s_m(t-\tau,\varphi) = \sum_{m=0}^{N-1}\sum_{n=-\infty}^{+\infty} a_{m,n}\gamma_{m,n}(t-\tau)e^{j\varphi} \tag{3.19}$$

we recall that,

$$\gamma_{m,n}(t) = f(t-nT/2)e^{j\frac{2\pi}{T}mt}e^{j\varphi_{m,n}} \tag{3.20}$$

and

$$\varphi_{m,n} = \frac{\pi}{2}(m+n) - \pi mn$$

l	Mean interf. table [dB]	PSD interf. table [dB]
0	-01.51	-00.87
1	-10.48	-12.00
2	-16.50	-19.72
3	-20.02	-23.55
4	-22.52	-25.98
5	-24.45	-27.62
6	-26.04	-28.83

Table 3.4: OFDM mean interference table vs. PSD-based OFDM interference Table.

The m_0-th output of the receiver filter on the n_0-th signalling interval (ie. $t = n_0 T/2$) coming from $s_m(t-\tau,\varphi)$, will be

$$\begin{aligned} y_{m_0,n_0}(\tau,\varphi) &= \langle s_m(t-\tau,\varphi), \gamma_{m_0,n_0}(t)\rangle \\ &= \int_{-\infty}^{+\infty} s_m(t-\tau,\varphi)\gamma^*_{m_0,n_0}(t)dt \end{aligned} \tag{3.21}$$

Substituting (3.19) and (3.20) in (3.21), the signal $y_{m_0,n_0}(\tau)$ becomes

$$\begin{aligned} y_{m_0,n_0}(\tau,\varphi) = \sum_{m=0}^{N-1}\sum_{n=-\infty}^{+\infty} a_{m,n} e^{j(\varphi+\varphi_{m,n}-\varphi_{m_0,n_0})} e^{-j\frac{2\pi}{T}m\tau} \\ \times \int_{-\infty}^{+\infty} f(t-nT/2-\tau) f(t-n_0T/2) e^{j\frac{2\pi}{T}(m-m_0)t} dt \end{aligned} \tag{3.22}$$

In order to get simplified, easier-to-manipulate expressions, let us define the following integral

$$\Psi(t,\tau,l)\Big|_{t=t_1}^{t_2} = \int_{t_1}^{t_2} f(t-\tau) f(t) e^{j\frac{2\pi}{T}lt} dt \tag{3.23}$$

If we consider the PHYDYAS prototype filter, the explicit form expressions of this integral are given in (3.24) and (3.25) respectively for $l = 0$ and $l \neq 0$. The details of calculus are

given in Appendix A.

$$\begin{aligned}\Psi(t,\tau,0)\Big|_{t=t_1}^{t_2} &= \int_{t_1}^{t_2} f(t-\tau)f(t)dt \\ &= \frac{t}{A}\left[1+2\sum_{k=1}^{K-1}F_k^2\cos\left(\frac{2\pi}{KT}k\tau\right)\right] \\ &\quad + \frac{KT}{\pi A}\left\{\sum_{k=1}^{K-1}\sum_{k'=1}^{K-1}(-1)^{k+k'}\frac{F_kF_{k'}}{k+k'}\sin\left(\frac{2\pi}{KT}((k+k')t-k\tau)\right)\right. \\ &\quad + \sum_{k=1}^{K-1}\sum_{\substack{k'=1\\k\neq k'}}^{K-1}(-1)^{k+k'}\frac{F_kF_{k'}}{k-k'}\sin\left(\frac{2\pi}{KT}((k-k')t-k\tau)\right) \\ &\quad \left. + \sum_{k=1}^{K-1}(-1)^k\frac{F_k}{k}\left[\sin\left(\frac{2\pi}{KT}k\tau\right)+\sin\left(\frac{2\pi}{KT}k(t-\tau)\right)\right]\right\}\Big|_{t=t_1}^{t_2}\end{aligned} \tag{3.24}$$

$$\begin{aligned}\Psi(t,\tau,l)\Big|_{t=t_1}^{t_2} &= \frac{T}{j2\pi lA}e^{j\frac{2\pi}{T}lt} \\ &+ \frac{KT}{j2\pi A}\sum_{k=1}^{K-1}(-1)^kF_k\left[\frac{1+e^{-j\frac{2\pi}{KT}k\tau}}{k+Kl}e^{j\frac{2\pi}{KT}(k+Kl)t}-\frac{1+e^{j\frac{2\pi}{KT}k\tau}}{k-Kl}e^{-j\frac{2\pi}{KT}(k-Kl)t}\right] \\ &+ \frac{KT}{j2\pi A}\sum_{k=1}^{K-1}\sum_{k'=1}^{K-1}(-1)^{k+k'}F_kF_{k'}\left[e^{-j\frac{2\pi}{KT}k\tau}\left(\frac{e^{j\frac{2\pi}{KT}(k+k'+Kl)t}}{k+k'+Kl}+\frac{e^{j\frac{2\pi}{KT}(k-k'+Kl)t}}{k-k'+Kl}\right)\right. \\ &\quad \left. - e^{j\frac{2\pi}{KT}k\tau}\left(\frac{e^{-j\frac{2\pi}{KT}(k+k'-Kl)t}}{k+k'-Kl}+\frac{e^{-j\frac{2\pi}{KT}(k-k'-Kl)t}}{k-k'-Kl}\right)\right]\Big|_{t=t_1}^{t_2}\end{aligned} \tag{3.25}$$

Without loss of generality, let us assume that the prototype filter $f(t)$ can be non zero only when $t \in [0, KT]$ where K represents its overlapping factor. Accordingly, the product $f(t)f(t-\tau)$ can be non zero only when the timing offset $\tau \in [-KT, +KT]$. Therefore in order to compute $y_{m_0,n_0}(\tau)$, we have to consider two cases:

Case 1 : $((n_0-n)\frac{T}{2} < \tau)$

In this case, (3.22) and (3.23) yield

$$y_{m_0,n_0}(\tau,\varphi) = \sum_{n=\lfloor\frac{-\tau}{T/2}\rfloor+n_0+1}^{2K+n_0-1} a_{m,n}e^{j(\varphi+\varphi_{m,n}-\varphi_{m_0,n_0})}e^{-j\frac{2\pi}{T}m\tau}\Psi(t,\tau,l)\Big|_{t=\tau}^{KT+(n_0-n)\frac{T}{2}} \tag{3.26}$$

where $\lfloor\alpha\rfloor$ denotes the floor function (the largest integer less than or equal to α).

Case 2 : ($\tau < (n_0 - n)\frac{T}{2}$)

According also to (3.22) and (3.23), we obtain

$$y_{m_0,n_0}(\tau,\varphi) = \sum_{n=-2K+n_0+1}^{n_0+\lceil \frac{-\tau}{T/2} \rceil - 1} a_{m,n} e^{j(\varphi+\varphi_{m,n}-\varphi_{m_0,n_0})} e^{-j\frac{2\pi}{T}m\tau} \Psi(t,\tau,l)\Big|_{t=(n_0-n)\frac{T}{2}}^{KT+\tau} \tag{3.27}$$

where $\lceil \alpha \rceil$ is the ceil function (the smallest integer greater than or equal to α).
After the OQAM decision, we can write the total complex symbol $y_{tot}(\tau,\varphi)$ as follows

$$y_{tot}(\tau,\varphi) = \mathrm{Re}\left\{y_{m_0,n_0}(\tau,\varphi)\right\} + j\mathrm{Re}\left\{y_{m_0,n_0+1}(\tau,\varphi)\right\} \tag{3.28}$$

and the corresponding interference power table $I(\tau,l)$ can thus be given by the following expression

$$I(\tau,l) = \mathbb{E}_{a_{m,n},\varphi}\left[\left|y_{tot}(\tau,\varphi)\right|^2\right] \tag{3.29}$$

In Fig. 3.10 and Fig. 3.11, PHYDYAS and IOTA interference tables $I(\tau,l)$ are plotted for different values of the timing offset $\tau = T/4, T/3, T/2$. We also see that the interference varies with respect to the timing offset τ and the spectral distance l between the interfering subcarrier and the victim one. Furthermore, PHYDYAS and IOTA mean interference tables are compared to the respective PSD-based interference tables in Fig. 3.12 and Fig. 3.13, respectively. Looking at these figures, we find that the two models lead to different results. However, this difference is negligible when the interference level is high.

3.5 Asynchronous interference in frequency selective channels

[81] In this section, we refer to the system model shown in Fig. 3.14. In this case, the interference signal received at the input of the multicarrier demodulator $r(t-\tau,\varphi)$ is given by

$$r(t-\tau,\varphi) = h(t) * s(t-\tau,\varphi) \tag{3.30}$$

we recall that $h(t)$ is the channel impulse response which is given in (2.6). In the following analysis, we investigate the effects of the propagation channel on the asynchronous interference signal coming from the m-th subcarrier $s_m(t-\tau,\varphi)$. In the following analysis, two cases will be investigated : CP-OFDM case and FBMC one.

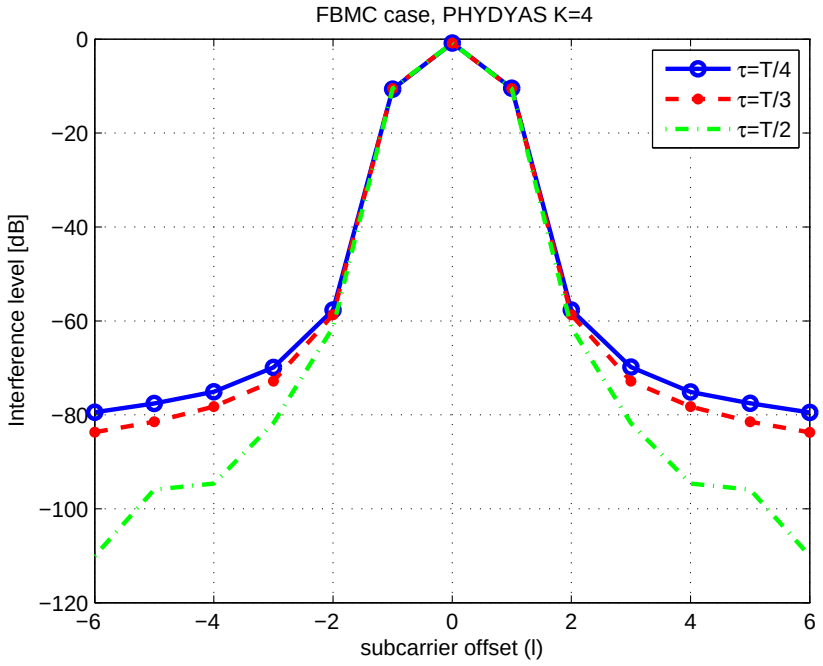

Figure 3.10: FBMC instantaneous interference tables for $\tau = \{T/4, T/3, T/2\}$: PHYDYAS case.

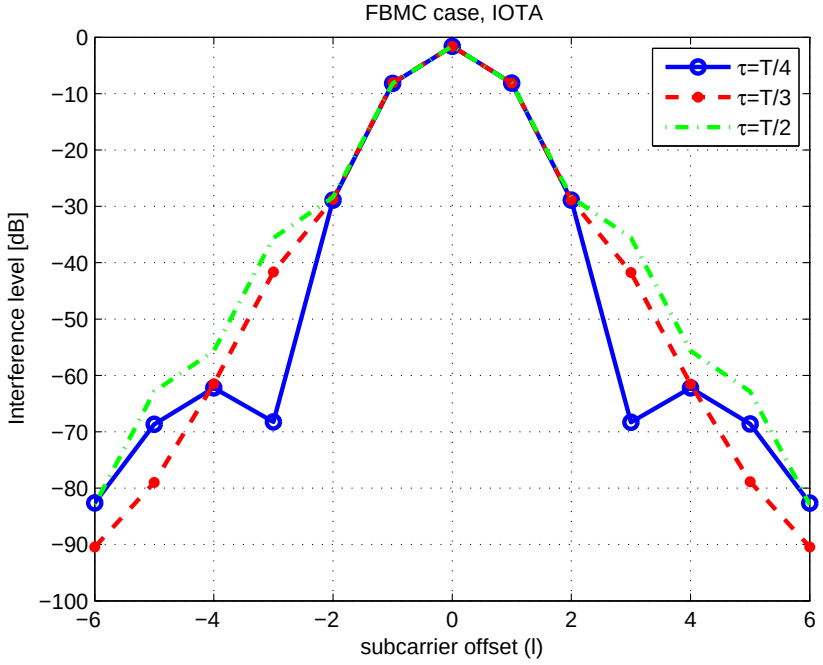

Figure 3.11: FBMC instantaneous interference tables for $\tau = \{T/4, T/3, T/2\}$: IOTA case.

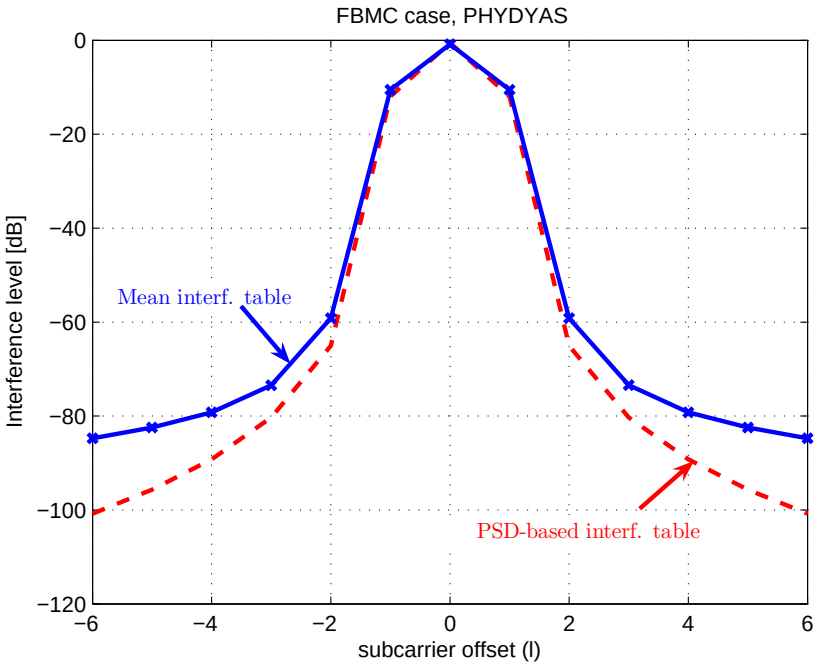

Figure 3.12: FBMC mean interference table vs. PSD-based FBMC interference Table : PHYDYAS case.

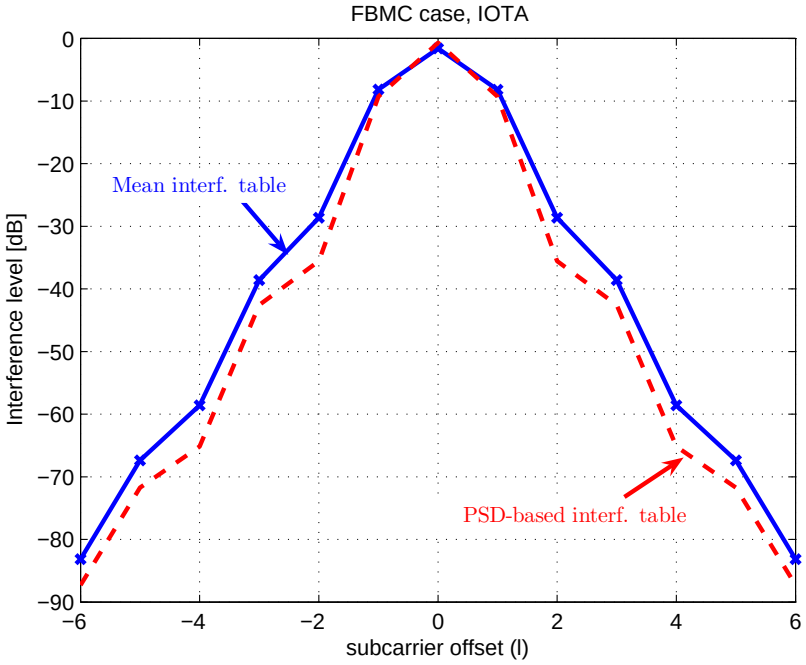

Figure 3.13: FBMC mean interference table vs. PSD-based FBMC interference Table : IOTA case.

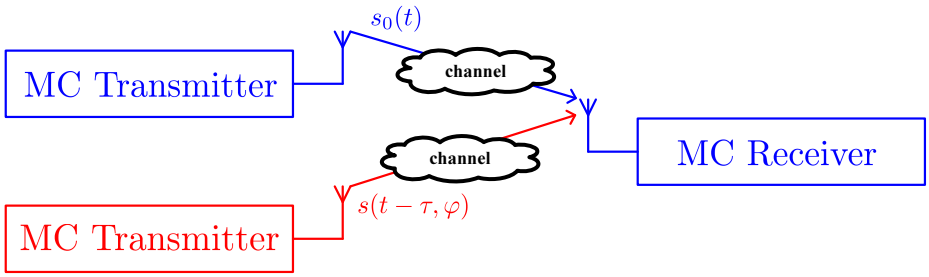

Figure 3.14: Asynchronous interference in the presence of multi-path effects

3.5.1 CP-OFDM case

According to (3.7) and (3.30), the interference signal at the input of the OFDM receiver can be written as follows

$$\begin{aligned} r(t-\tau,\varphi) &= h(t) * s_m(t-\tau,\varphi) \\ &= \left(\sum_{i=0}^{L-1} h_i \delta(t-\frac{n_i}{N}T)\right) \star \left(\sum_{n=-\infty}^{n=+\infty} x_{m,n} f_T(t-n(T+\Delta)-\tau) e^{j\left[\frac{2\pi}{T}m(t-n(T+\Delta)-\tau)+\varphi\right]}\right) \\ &= \sum_{i=0}^{L-1}\sum_{n=-\infty}^{+\infty} h_i x_{m,n} f_T(t-n(T+\Delta)-\tau-\frac{n_i}{N}T) e^{j\left[\frac{2\pi}{T}m(t-n(T+\Delta)-\tau-\frac{n_i}{N}T)+\varphi\right]} \end{aligned} \tag{3.31}$$

In weakly and mildly frequency selective channels, $\frac{n_i}{N}T$ is small enough. We can thus consider that $f_T(t-n(T+\Delta)-\tau-\frac{n_i}{N}T) = f_T(t-n(T+\Delta)-\tau)$. Hence, the signal $r(t-\tau,\varphi)$ becomes

$$\begin{aligned} r(t-\tau,\varphi) &= \sum_{i=0}^{L-1} h_i e^{j\frac{2\pi n_i}{N}m} \sum_{n=-\infty}^{+\infty} x_{m,n} f_T(t-n(T+\Delta)-\tau) e^{j\left[\frac{2\pi}{T}m(t-n(T+\Delta)-\tau)+\varphi\right]} \\ &= H(m) \sum_{n=-\infty}^{+\infty} x_{m,n} f_T(t-n(T+\Delta)-\tau) e^{j\left[\frac{2\pi}{T}m(t-n(T+\Delta)-\tau)+\varphi\right]} \\ &= H(m) s_m(t-\tau,\varphi) \end{aligned} \tag{3.32}$$

where $H(m) = \sum_{i=0}^{L-1} h_i e^{j\frac{2\pi n_i}{N}m}$ representing the complex channel gain at the m-th subcarrier. Based on (3.32), (3.9) and (3.13), the m_0-th output of the receiver filter on the n_0-th signalling interval resulting from the received interference signal $r(t-\tau,\varphi)$ is expressed for both cases $0<\tau<\Delta$ and $\Delta<\tau<T+\Delta$ as follows

Case 1: $(0 < \tau < \Delta)$

$$y_{m_0,n_0}(\tau,\varphi) = \begin{cases} H(m_0)x_{m_0,n_0}e^{-j\left[\frac{2\pi}{T}m_0\tau-\varphi\right]} & m = m_0 \\ 0 & otherwise \end{cases} \tag{3.33}$$

Case 2: $(\Delta < \tau < T + \Delta)$

when $m \neq m_0$

$$\begin{aligned} y_{m_0,n_0}(\tau,\varphi) &= H(m)e^{-j\left[\frac{2\pi}{T}m\tau-\varphi\right]} \\ &\times \left\{ \frac{x_{m,n_0-1}}{\pi(m-m_0)}e^{-j\frac{2\pi}{T}m(T+\Delta)}e^{j\frac{\pi}{T}(m-m_0)(\tau+\Delta)}\sin\left[\pi(m-m_0)(\tau-\Delta)/T\right] \right. \\ &\left. + \frac{x_{m,n_0}}{\pi(m-m_0)}e^{j\frac{\pi}{T}(m-m_0)(T+\Delta+\tau)}\sin\left[\pi(m-m_0)(T+\Delta-\tau)/T\right] \right\} \end{aligned} \tag{3.34}$$

when $m = m_0$, the signal $y_{m_0,n_0}(\tau)$ is given by

$$y_{m_0,n_0}(\tau,\varphi) = H(m_0)e^{-j\left[\frac{2\pi}{T}m_0\tau-\varphi\right]}\left\{ x_{m_0,n_0-1}e^{-j\frac{2\pi}{T}m_0(T+\Delta)}\frac{\tau-\Delta}{T} + x_{m_0,n_0}\frac{T+\Delta-\tau}{T} \right\} \tag{3.35}$$

Consequently, the resulting interference power P_{interf} will be the product of the channel power gain of the interfering subchannel and the corresponding interference table coefficient given in (3.3). Then, we write the interference power in m_0-th subchannel as

$$P_{\text{interf}}(m_0,\tau) = P_{\text{trans}}(m)I(\tau,|m-m_0|)|H(m)|^2 \tag{3.36}$$

where,

- $P_{\text{trans}}(m)$ is the transmitted power on the subchannel m
- $I(\tau,|m-m_0|)$ represents the interference table coefficient for the timing offset τ and the spectral distance $|m-m_0|$
- $|H(m)|^2$ is the channel power gain for subchannel m.

3.5.2 FBMC case

Similarly, we express the interference signal received at the input of the FBMC receiver $r(t-\tau,\varphi)$. According to (3.19) and (3.30), we write

$$\begin{aligned} r(t-\tau,\varphi) &= h(t) * s_m(t-\tau,\varphi) \\ &= \left(\sum_{i=0}^{L-1} h_i\delta(t-\frac{n_i}{N}T)\right) \star \left(\sum_{m=0}^{N-1}\sum_{n=-\infty}^{+\infty} a_{m,n}\gamma_{m,n}(t-\tau)e^{j\varphi}\right) \\ &= \sum_{i=0}^{L-1}\sum_{n=-\infty}^{+\infty} h_i a_{m,n}\gamma_{m,n}(t-\tau-\frac{n_i}{N}T)e^{j\varphi} \end{aligned} \tag{3.37}$$

Substituting (3.20) in (3.37), we obtain

$$\begin{aligned} r(t-\tau,\varphi) &= \sum_{i=0}^{L-1}\sum_{n=-\infty}^{+\infty} h_i a_{m,n} f(t-nT/2-\tau-\frac{n_i}{N}T)e^{j\frac{2\pi}{T}m(t-\tau-\frac{n_i}{N}T)}e^{j\varphi} \\ &= \sum_{i=0}^{L-1} h_i e^{-j\frac{2\pi}{N}mn_i}\sum_{n=-\infty}^{+\infty} a_{m,n} f(t-nT/2-\tau-\frac{n_i}{N}T)e^{j\frac{2\pi}{T}m(t-\tau)}e^{j\varphi} \end{aligned} \tag{3.38}$$

we can notice that $f(t-nT/2-\tau-\frac{n_i}{N}T)$ may have relatively slow variations when $\frac{n_i}{N}T \in [0,\tau_{\text{ds}}]$ (τ_{ds} is the maximum delay spread of the channel) [48], [49]. Indeed, compared to the coherence bandwidth B_c, the filter bandwidth is very small, which also means that the time variations of the prototype filter $f(t)$ are necessarily limited.
Consequently, the signal $r(t-\tau,\varphi)$ becomes

$$\begin{aligned} r(t-\tau,\varphi) &= \sum_{i=0}^{L-1} h_i e^{-j\frac{2\pi}{N}mn_i}\sum_{n=-\infty}^{+\infty} a_{m,n} f(t-nT/2-\tau)e^{j\frac{2\pi}{T}m(t-\tau)}e^{j\varphi} \\ &= H(m)s_m(t-\tau,\varphi) \end{aligned} \tag{3.39}$$

Now, let $\varphi_{H(m)}$ be the phase angle of the complex channel gain $H(m)$, i.e.

$$H(m) = |H(m)|e^{j\varphi_{H(m)}}$$

Hence, we can write $r(t-\tau,\varphi)$ as follows

$$r(t-\tau,\varphi) = |H(m)|s_m(t-\tau,\varphi+\varphi_{H(m)}) \tag{3.40}$$

According (3.28) and (3.40), the output signal after the OQAM decision is given by

$$y'_{tot}(\tau,\varphi) = |H(m)|y_{tot}(\tau,\varphi+\varphi_{H(m)}) \tag{3.41}$$

where, $y_{tot}(\tau,\varphi)$ is given in (3.28).
Now, let φ and φ' be two uniform random variables defined in the following intervals $\varphi \in [0,2\pi]$ and $\varphi' \in [\alpha,\alpha+2\pi]$, respectively. We notice that,

$$\mathbb{E}_{a_{m,n},\varphi}\left[|y_{tot}(\tau,\varphi)|^2\right] = \mathbb{E}_{a_{m,n},\varphi'}\left[|y_{tot}(\tau,\varphi')|^2\right]$$

Therefore, the corresponding interference power P_{interf} is also the product of the channel power gain of the interfering subcarrier $|H(m)|^2$ and the corresponding interference table coefficient given in (3.29). Thus, the interference power at the m_0-th subchannel is given by

$$P_{\text{interf}}(m_0,\tau) = P_{\text{trans}}(m)I(\tau,|m-m_0|)|H(m)|^2 \tag{3.42}$$

In general, the asynchronous interference power arriving through a frequency selective channel can be calculated using the following expression

$$P_{\text{interf}}(m_0,\tau) = d^{-\beta}P_{\text{trans}}(m)I(\tau,|m-m_0|)|H(m)|^2 \tag{3.43}$$

where,

- d is the distance between the interferer and the victim user
- β is the path loss exponent
- $P_{\text{trans}}(m)$ is the transmitted power on the interfering subchannel m
- $I(\tau, |m-m_0|)$ is the interference table coefficient for the timing offset τ and the spectral distance $|m - m_0|$
- $|H(m)|^2$ is the channel power gain between the interfering transmitter and the victim receiver on subchannel m.

In the next section, we investigate the accuracy of the proposed interference modeling expressed by Equation (3.43). Several applications and scenarios can be studied using this interference model.

3.6 Simulation results

In this section, we consider the uplink transmission in OFDM/FBMC based network depicted in Fig. 3.15.a. The reference mobile user MU_0 and the interfering one MU_1 communicating respectively with BS_0 and BS_1. Moreover, MU_0 and MU_1 are respectively located at distances d_0 and d from the reference base station BS_0. It is assumed that, the transmitted power of each user must guarantee a target signal to noise ration $\text{SNR}_\text{t} = 20\text{dB}$ at its base station (BS_0 for MU_0 and BS_1 for MU_1).

Concerning the frequency scheme, the subcarriers are allocated according to the scheme described in Fig. 3.15.b. Here, the size of each subcarrier block is set at 18 subcarriers. Here, we have chosen the practical size of subcarrier block in WiMax 802.16 [4].

All signals propagate through different multipath channels using a similar propagation model, where the impulse responses of the multipath channel between MU_0, MU_1 and the reference base station BS_0 are denoted by h_0 and h_1, respectively. The considered model is the Pedestrian-A model whose parameters are given in Table. 3.5. The choice of this model is based on the assumption that the subcarriers of interest experience flat fading. Therefore, the interference caused by the multipath effects are negligible, in the FBMC case.

Parameter	value
Pedestrian-A Relative Delay	[0 110 190 410] ns
Pedestrian-A Average Power	[0 -9.7 -19.2 -22.8] dB

Table 3.5: Channel parameters used in simulations

Furthermore, the underlying channel model includes path loss effects which takes into account the position of the mobile user with respect to the reference base station BS_0. The path loss of a received signal at distance d is governed by the following expression [82]

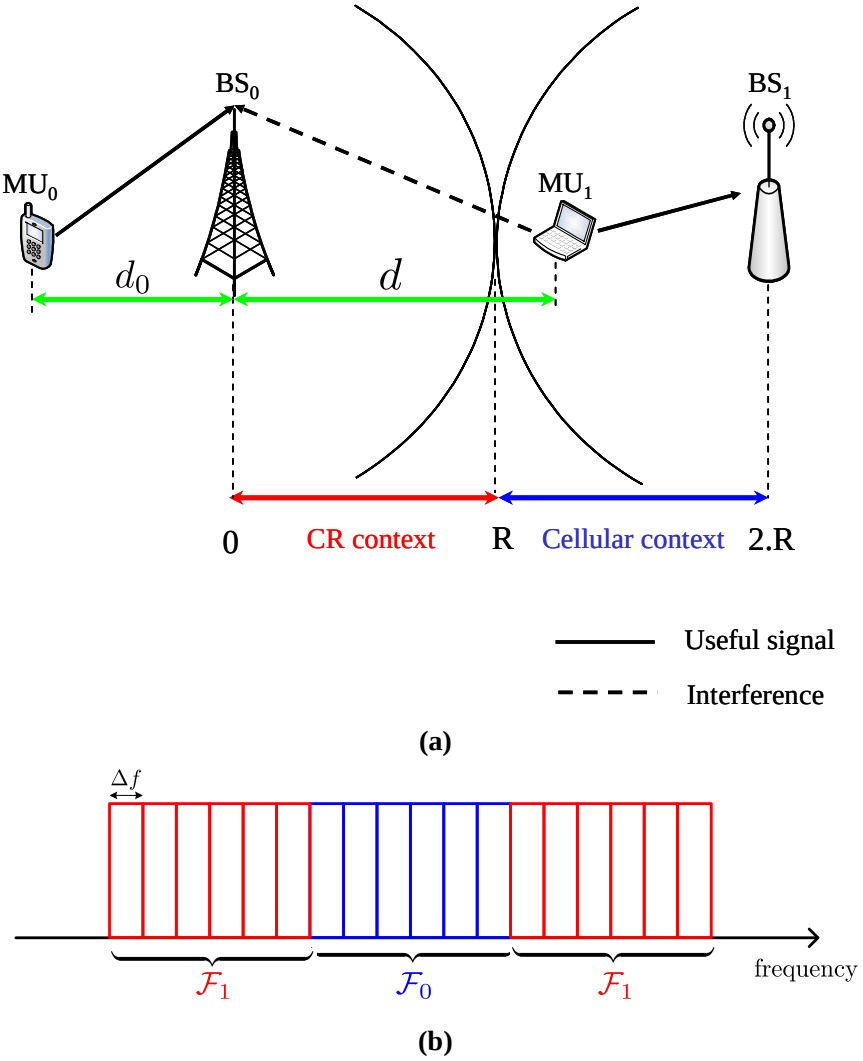

Figure 3.15: Interference model: the reference user coexists with an asynchronous interferer.

corresponding to a path loss exponent $\beta = 3.76$ and a carrier frequency of 2 GHZ

$$\Gamma_{\text{loss}}(d) = 128.1 + 37.6 \log_{10}(d[km])[dB]$$

On the other hand, we consider a system with $N = 1024$ subcarriers and a sampling frequency of 10 MHz. The noise term is considered as a thermal noise with spectral density $N_0 = -174$ dBm/Hz.

Each mobile user is assumed to be perfectly synchronized with its corresponding base station but it is not synchronized with the other base station. Because of the timing misalignment between MU_1 and BS_0, the signal arriving from MU_1 at BS_0 appears non-orthogonal to the desired signal arriving from MU_0. This non-orthogonality generates interference and

degrades the signal to interference plus noise ratio SINR. Using the interference tables introduced previously, the instantaneous SINR on a given subcarrieer $m \in \mathcal{F}_0$ can be expressed as

$$\mathrm{SINR}(m) = \frac{d_0^{-\beta} P_{\mathrm{trans}}(m) \left|H_0(m)\right|^2}{\sum\limits_{m' \in \mathcal{F}_1} d^{-\beta} P_{\mathrm{trans}}(m') I(\tau, |m'-m|) \left|H_1(m')\right|^2 + N_0 \Delta f} \tag{3.44}$$

where Δf is the subcarrier spacing.
Here, it is worth mentioning that the interference table coefficient I is computed by two methods : PSD-based interference tables and our proposed interference tables.

The objective of this section is to evaluate the average SINR and the spectral efficiency expressed, respectively by,

$$\mathrm{SINR}_{\mathrm{average}}(m) = \mathbb{E}\left[\mathrm{SINR}(m)\right] \tag{3.45}$$

$$C_{\mathrm{average}}(m) = \mathbb{E}\left[\log_2\left(1 + \mathrm{SINR}(m)\right)\right] \tag{3.46}$$

where $\mathbb{E}[.]$ stands for the statistical expectation which is computed over all channel realizations $(H_0(m), \{H_1(m'), m' \in \mathcal{F}_1\})$ and all values of the timing offset τ which is uniformly distributed over $[0, T]$.

Two different contexts will be analyzed as depicted in Fig. 3.15:

- **The classical multi-cellular context**: when d varies from R to $2R$, i.e. MU_1 can move from the edge to the center of cell 1
- **The cognitive radio context**: when d varies from 0 to $2R$, i.e. MU_1 can be very close to BS_0 while transmitting to BS_1.

In Fig. 3.16, Fig. 3.17 and Fig. 3.18, we investigate, respectively, the accuracy of the SINR expression in the CP-OFDM, FBMC-PHYDYAS and FBMC-IOTA cases. The averaged SINRs over all subcarriers $m \in \mathcal{F}_0$ are plotted against the distance d, using the instantaneous tables (line), the PSD-based table (point markers) and numerical simulation (cross markers). The instantaneous tables results depicted in these figures show a perfect match to the corresponding simulation results. However, the PSD-based method exhibits a strong inaccuracy especially in the cognitive radio context.

In the cognitive radio context, we observe a significant degradation of the OFDM SINR with respect to the target SNR ($20dB$). Such a result can be explained by the high level of OFDM asynchronous interference caused by the timing misalignment which damages the orthogonality between the subcarriers. On the other hand, we notice a slight loss of the FBMC SINR with respect also to the target SNR of $20dB$. The better performance of PHYDYAS-FBMC compared to IOTA-FBMC and CP-OFDM can be justified by the fact that only the two subcarriers on the edge of the cluster (subcarrier block) $\mathcal{F}_0$ suffer from the interference caused by their immediate adjacent subcarriers in $\mathcal{F}_1$ as depicted in Fig.

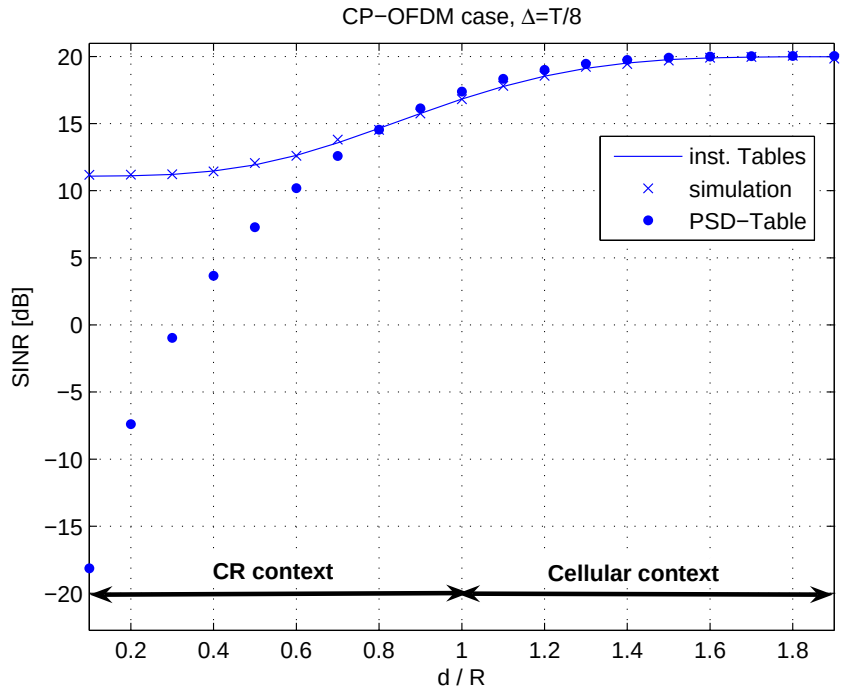

Figure 3.16: CP-OFDM average SINR *vs.* distance between MU_1 and BS_0, $\tau \in [0, T]$

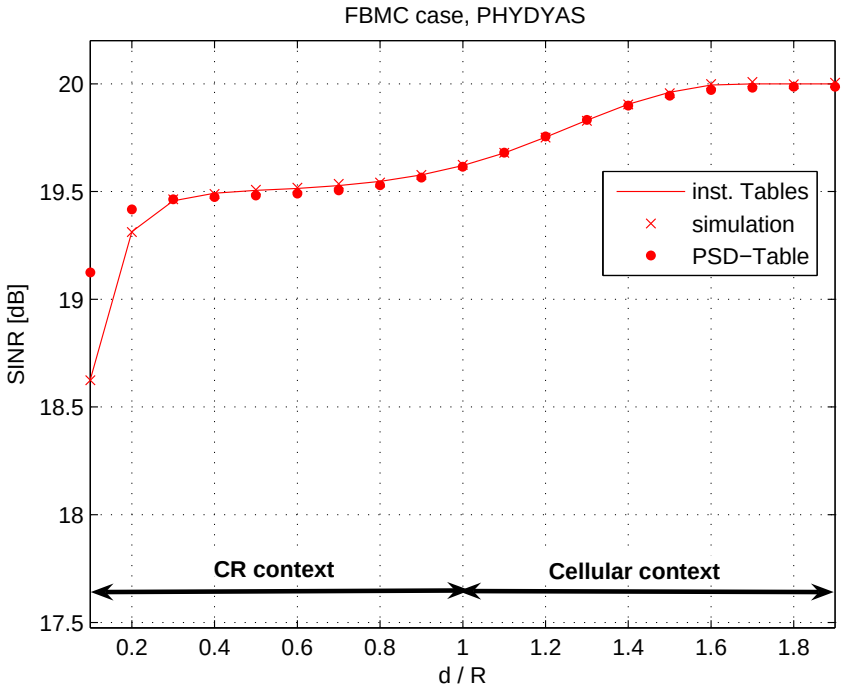

Figure 3.17: PHYDYAS-FBMC average SINR *vs.* distance between MU_1 and BS_0, $\tau \in [0, T]$

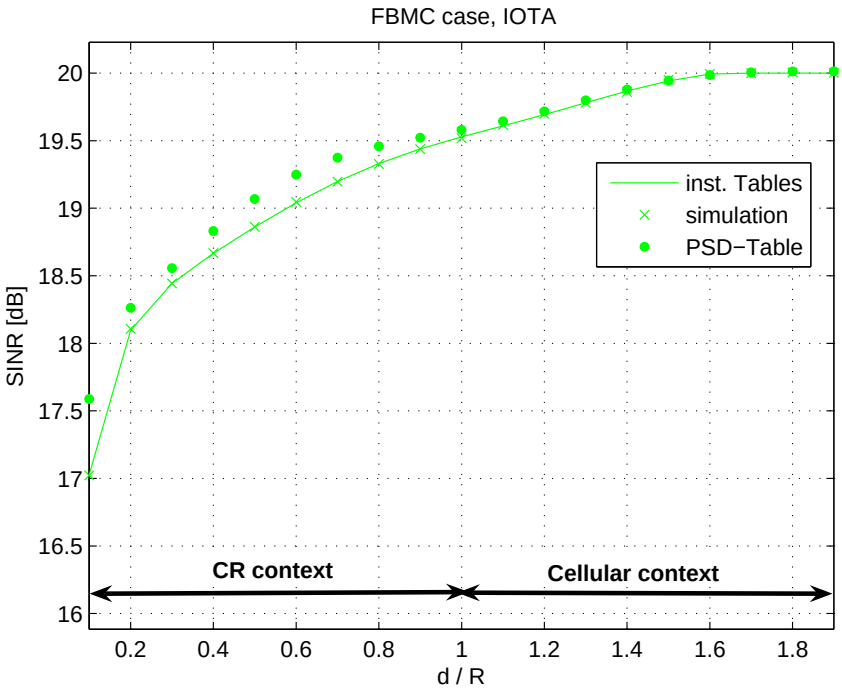

Figure 3.18: IOTA-FBMC average SINR *vs.* distance between MU_1 and BS_0, $\tau \in [0, T]$

3.12; whereas in IOTA-FBMC, two subcarriers at each edge are affected by the asynchronous interference coming from the two neighboring subcarriers at each edge as shown in Fig. 3.13. Furthermore, the entire cluster $\mathcal{F}_0$ suffers, in the CP-OFDM case, from the asynchronous interference caused by all subcarriers of $\mathcal{F}_1$ (see Fig. 3.9).

In the cellular context, the asynchronous interferer MU_1 is quite far from the reference base station BS_0 and, at the same time, it is close to its base station BS_1. This means that its transmitted power is reduced and consequently the interference power received by BS_0 will be much lower due to the path-loss effect (d is quite large). Therefore, the impact of the asynchronous interference is less significant in the cellular context for all waveforms. Also, it is worth mentioning that SINRs of OFDM and FBMC converge to the target SNR ($20dB$) when MU_1 is very far from BS_0 as the interference becomes negligible compared to the noise level.

The impact of the asynchronous interference on the average spectral efficiency has also been investigated. Fig. 3.19, shows the average spectral efficiency over all subcarriers $m \in \mathcal{F}_0$ against the distance d, for CP-OFDM (solid line $-$), FBMC-PHYDYAS (dashed-dotted line $-.$) and FBMC-IOTA (dashed line $--$). Also, the accuracy of instantaneous and PSD-based tables is examined. Fig. 3.19 shows that timing synchronization errors cause a degradation of the spectral efficiency. The same remarks can be formulated, here, where the FBMC system still outperforms the OFDM system. Furthermore, simulation

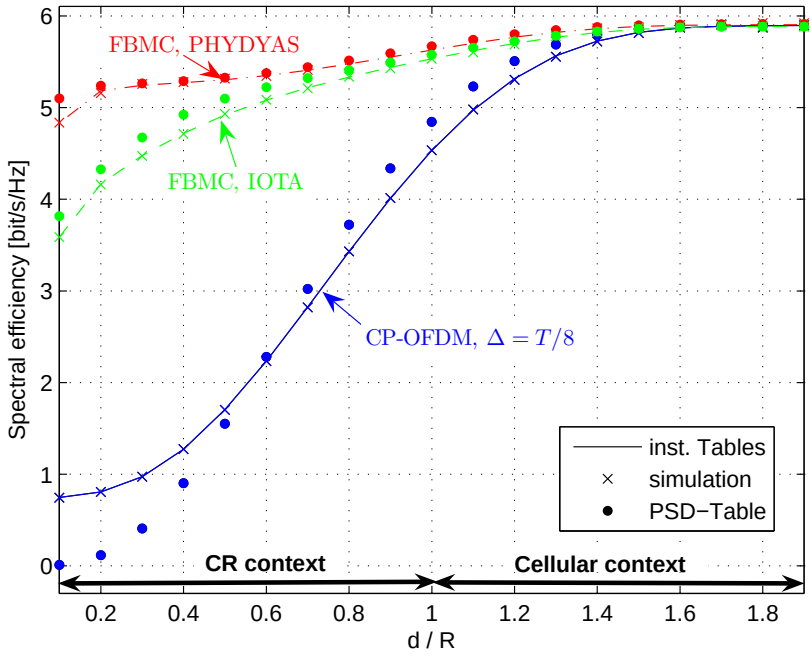

Figure 3.19: Spectral efficiency *vs.* distance between MU_1 and BS_0, $\tau \in [0, T]$

and instantaneous tables results shown in Fig. 3.19 validate the accuracy of the proposed interference model while the PSD-based tables still present a strong inaccuracy with respect to simulation results especially in the cognitive radio context where the noise level becomes negligible compared to the asynchronous interference caused by MU_1. We see that both modulation schemes (OFDM and FBMC) lead to identical spectral efficiency floor when MU_1 is close to its base station because of the predominance of the noise term. We have to remind that the actual bit rate is lower for CP-OFDM because of the redundancy introduced by the cyclic prefix in each OFDM block.

3.7 Conclusion

In this chapter, we have investigated the asynchronous interference modeling in OFDM and FBMC systems. We have first given a state-of-the-art review for the interference analysis in multicarrier techniques. Then, the general concept of interference tables has been introduced where we have derived the PSD-based interference tables of CP-OFDM and FBMC for two considered waveforms : PHYDYAS and IOTA. It has been noticed that the PSD-based tables do not consider the timing offset between the interferer and the victim user.

Next, we have proposed new interference tables that model the correlation between a given interfering subcarrier and the victim one, not only as a function of the spectral distance

separating both subcarriers but also with respect to the timing misalignment between the subcarrier holders. Theoretical expressions of these tables have been derived for CP-OFDM, PHYDYAS-FBMC and IOTA-FBMC systems.
The interference analysis has been extended to the case of frequency selective environments where we have proposed a table-based estimation method as a computationally simpler alternative to the numerical evaluation; as this latter requires huge computational efforts.
Finally, the accuracy of the proposed model has been validated through different simulation results, where the results based on the instantaneous tables method shows an excellent match with the corresponding simulation ones. In contrast to the instantaneous interference tables, we have shown through this evaluation that the PSD modeling exhibits a strong inaccuracy with respect to the numerical results.

However, it is worth pointing out that the proposed method is a semi-analytical method which means that we always need to simulate the different channel realizations (useful and interference channels). Hence, one can see that the complexity of the performance evaluation still remains significant, especially when the number of interferers is important.
In the next two chapters, we develop new analytical expressions that significantly reduce the computational complexity of the performance evaluation : error rate and spectral efficiency.

Chapter 4

Average Error Rates Analysis in Asynchronous Cellular Networks

4.1 Introduction

In the literature, the impact of asynchronous interference in OFDM systems has been intensively investigated. A performance analysis of OFDM in the presence of timing synchronization can be found in [78], [83], [80], [84]. Using the Gaussian approximation for interchannel interference, [85] gives approximate expressions of the symbol error rates. Moreover, the degradation of the signal to interference plus noise ratio is a common criterion to analyze the impact of timing desynchronization on the system performance [83], [86].

Although interference analysis in single user OFDM has become popular in the literature e.g [87], [88], [89], the extension of this analysis to a multi-cellular environment is not so straightforward. This problem is crucial for the following reasons. First, in a multi-cellular environment the interference stems from subcarriers distributed among several transmitters which require more than one random variable (RV) to properly model this interference, therefore, the analysis becomes more difficult.

In this chapter, we present an analytical interference analysis related to asynchronous downlink OFDM/FBMC in multi-cellular environment, providing exact expressions of average error rates in frequency selective fading channels.

The evaluation of the average error rate of a given transmission is considered as the most common criterion used in the investigation of the impact of interference on the system performance. Beaulieu [90], [91], based on the Fourier series and a Chernoff bound technique, was able to express the average of the Gaussian complementary distribution function which

is used for the evaluation of the average error rate. A recent study [78] has presented a theoretical analysis of the average error rate of an asynchronous OFDM system in the special case of interleaved subcarrier assignment scheme. However, to the best of our knowledge, there is no published works addressing the impact of the asynchronous interference on the bit error rate for FBMC systems.

Based on the interference table model introduced in the previous chapter, we derive in this chapter an explicit expression of the bit error rate of time-asynchronous OFDM and FBMC systems, taking into account the correlation between the subchannel gains belonging to a given block subcarrier. The computation of the average error rate is based on the moment generating function of the interference power.

The outline of this chapter is organized as follows. The SINR analysis is discussed in Section 4.2. We further derive explicit expressions of the average error rates of asynchronous OFDM/FBMC systems in Section 4.3. Section 4.4 is devoted to describing the system model of the downlink of OFDM and FBMC based multi-cellular networks. Simulation results are presented and discussed in Section 4.5. Section 4.6 concludes this chapter.

4.2 Interference and SINR Analysis

Let us consider a given receiver (receiver of interest) communicating synchronously with its corresponding transmitter. Other transmitters, that coexist in the same geographical area, are operating asynchronously in a wireless environment subject to path loss and multipath fading.

We can express the composite signal at the reference receiver by the sum of the desired signal coming from the reference transmitter and the interference signal coming from the other transmitters,

$$r(t) = \underbrace{d_0^{-\beta/2} s_0(t) * h_0(t)}_{\text{desired signal}} + \underbrace{\sum_{k=1}^{K} d_k^{-\beta/2} s_k(t-\tau_k) * h_k(t)}_{\text{interference signal}} + n(t) \tag{4.1}$$

where

- K is the total number of interfering transmitters
- d_0 is the distance between the reference receiver and its corresponding transmitter
- d_k represents the distance separating the reference receiver and the k-th interfering transmitter
- $s_0(t)$ denotes the useful transmitted signal coming from the transmitter of interest
- $s_k(t)$ is the interfering signal arriving from the k-th transmitter
- $h_k(t)$ represents the propagation channel between the receiver of interest and the transmitter k

- τ_k stands for the timing offset between the reference receiver and the k-th interferer
- $n(t)$ is the additive white Gaussian noise (AWGN)
- β denotes the path loss exponent

Because of the timing misalignment between the reference receiver and the other transmitters, the signals arriving from the latter will appear non-orthogonal to the desired signal. This non-orthogonality will generate interference and will degrade the SINR. This degradation will be investigated in the following analysis.

Based on (3.43) and (4.1), we can easily express the total interference power occurring at the m-th output filter of the reference receiver by

$$P_{\text{interf}}(m, \{\tau_k, k = 1, ..., K\}) = \sum_{k=1}^{K} \sum_{m' \in \mathcal{F}_k} d_k^{-\beta} P_{trans}(m') I(\tau_k, |m' - m|) \left|H_k(m')\right|^2 \quad (4.2)$$

where,

- $\mathcal{F}_k$ denotes the set of subcarriers that are assigned to the k-th transmitter
- $P_{trans}(m')$ is the transmitted power on the m'-th interfering subcarrier
- $\left|H_k(m')\right|^2$ is the channel power gain between the reference receiver and the k-th transmitter on subchannel m'

As previously mentioned, the reference receiver is assumed to be perfectly synchronized with its transmitter. Consequently, the power of the desired signal can be written as

$$P_{\text{desired}}(m) = d_0^{-\beta} P_{trans}(m) \left|H_0(m)\right|^2 \quad (4.3)$$

In the OFDM case, it is obvious that expression (4.3) is valid under the assumption that the cyclic prefix duration Δ is larger than the maximum delay spread of the channel. However in the FBMC case, the subcarrier channel gains cannot be assumed flat unless the number of subcarriers is very high. As we have said in Section 2.4.2, there are several approaches to deal with the frequency selective fading as in [43], [51], [57]. One interesting approach which is appropriate to our FBMC configuration, performs per-subcarrier equalization using finite impulse response (FIR) filters [57]. It is worth noticing that the use of multi-tap equalizers will be at the expense of a higher complexity. The purpose of this chapter being to focus on the sensibility of OFDM and FBMC to timing synchronization errors. For this reason, we assume that the subcarriers experience flat fading which is applicable in the case of weakly and mildly frequency selective channels.

According to (4.2) and (4.3), the instantaneous SINR is given by

$$\text{SINR}(m) = \frac{d_0^{-\beta} P_{trans}(m) \left|H_0(m)\right|^2}{\sum_{k=1}^{K} \sum_{m' \in \mathcal{F}_k} d_k^{-\beta} P_{trans}(m') I(\tau_k, |m' - m|) \left|H_k(m')\right|^2 + N_0 \Delta f} \quad (4.4)$$

where N_0 represents the noise power spectral density and Δf is the bandwidth of the m-th subcarrier.
From (4.4), we can rewrite the instantaneous SINR in the following form,

$$\mathrm{SINR}(m) = \frac{|H_0(m)|^2}{\sum_{k=1}^{K} \sum_{m' \in \mathcal{F}_k} A_{k,m,m'} |H_k(m')|^2 + b} \tag{4.5}$$

where

$$A_{k,m,m'} = \left[\frac{d_k}{d_0}\right]^{-\beta} \frac{P_{trans}(m')}{P_{trans}(m)} I(\tau_k, |m' - m|) \tag{4.6}$$

$$b = \frac{N_0 \Delta f}{d_0^{-\beta} P_{trans}(m)} \tag{4.7}$$

It should be noticed that we consider the transmitted power $P_{trans}(m)$, of each transmitter, as a constant. The coefficient $A_{k,m,m'}$ can thus be written as follows,

$$A_{k,m,m'} = \left[\frac{d_k}{d_0}\right]^{-\beta} I(\tau_k, |m' - m|) \tag{4.8}$$

4.3 Average Error Rates Analysis

This section is devoted to derive a closed-form expression of the average bit error rate considering the asynchronous interference caused by the surrounding asynchronous transmitters. The calculation of the bit error rate of any constellation is readily available in the literature when the decision variables are Gaussian random variables. [18] gives the BER of a square M-QAM in AWGN channel as

$$\mathrm{BER}(\mathrm{SNR}) = \sum_{i=0}^{\sqrt{M}-2} \lambda_i \mathrm{erfc}\left((2i+1)\sqrt{\frac{1}{2}\mathrm{SNR}}\right) \tag{4.9}$$

where λ_is are constants that depend on the constellation size M and $\sum_{i=0}^{\sqrt{M}-2} \lambda_i = 1/2$.
In the following derivation we analyze the QPSK constellation case, the extension to another M-QAM constellation is straightforward.
For a QPSK constellation, (4.9) becomes

$$\mathrm{BER}(\mathrm{SNR}) = \frac{1}{2}\mathrm{erfc}\left(\sqrt{\frac{1}{2}\mathrm{SNR}}\right) \tag{4.10}$$

Without loss of generality, we consider constant values of the timing offsets τ_k to compute the interference coefficients $A_{k,m,m'}$. In this case, by conditioning on the set of variables $\mathcal{H} = \{H_0(m), H_k(m'), k \in \{1, ..., K\}, m' \in \mathcal{F}_k\}$ and substituting (4.5) in (4.10), we can obtain

the exact closed form for the conditional error probabilities in the presence of interference

$$\mathrm{BER(SINR)}|_{\mathcal{H}} = \frac{1}{2}\mathrm{erfc}\left(\frac{1}{2}\frac{|H_0(m)|^2}{\sum\limits_{k=1}^{K}\sum\limits_{m'\in\mathcal{F}_k} A_{k,m,m'}\,|H_k(m')|^2 + b}\right)^{1/2} \tag{4.11}$$

It is worth mentioning that the BER expressed in (4.11) is obtained without any processing for optimal multiuser detection as done in [92].
According to (4.11), the average error rate is thus given by

$$\mathrm{BER_{average}} = \mathbb{E}_{\mathcal{H}}\left[\mathrm{BER(SINR)}|_{\mathcal{H}}\right] = \mathbb{E}_{\mathcal{H}}\left[\frac{1}{2}\mathrm{erfc}\left(\frac{1}{2}\frac{|H_0(m)|^2}{\sum\limits_{k=1}^{K}\sum\limits_{m'\in\mathcal{F}_k} A_{k,m,m'}\,|H_k(m')|^2 + b}\right)^{1/2}\right] \tag{4.12}$$

The direct approach to compute the average of this conditional error rate leads to a complex $(K \times |\mathcal{F}_k|)$-fold integration ($|\mathcal{F}_k|$ is the cardinality of $\mathcal{F}_k$) that is analytically intractable in most cases

$$\mathrm{BER_{average}} = \int\limits_{\mathcal{H}} \frac{1}{2}\mathrm{erfc}\left(\frac{1}{2}\frac{|H_0(m)|^2}{\sum\limits_{k=1}^{K}\sum\limits_{m'\in\mathcal{F}_k} A_{k,m,m'}\,|H_k(m')|^2 + b}\right)^{1/2} p(\mathcal{H})d\mathcal{H} \tag{4.13}$$

Here, $p(\mathcal{H})$ stands for the probability density function of the vector $\mathcal{H}$.
In order to reduce the complexity of computing the average bit error, we refer to the following lemma [19], which is based on the moment generating function of the interference power.

Lemma Let x be a unit-mean gamma random variable (RV) with parameter α and c is an arbitrary constant. Let g be an arbitrary non-negative random variable that is independent of x. Then

$$\mathbb{E}_{x,y}\left[\mathrm{erfc}\left(\frac{x}{g+c}\right)^{1/2}\right] = 1 - \frac{2}{\pi}\frac{\Gamma\left(\alpha+\frac{1}{2}\right)}{\Gamma(\alpha)}\int\limits_{0}^{+\infty}\frac{e^{-z}}{\sqrt{z}}{}_1F_1\left(1-\alpha;\frac{3}{2};z\right)\mathcal{M}_g(\alpha z)e^{-z\alpha c}dz \tag{4.14}$$

where

- $\Gamma(\alpha) = \int\limits_{0}^{+\infty} z^{\alpha-1}e^{-z}dz$ is the Gamma function (defined for $\alpha \in \mathbb{C}$ and $\mathrm{Re}(\alpha) > 0$) [20]
- ${}_1F_1(a;b;z) = \frac{\Gamma(b)}{\Gamma(b-a)\Gamma(a)}\int\limits_{0}^{1} e^{zu}u^{a-1}(1-z)^{b-a-1}du$ ($\mathrm{Re}(a) > 0$ and $\mathrm{Re}(b) > 0$) is the confluent hypergeometric function of the first kind [20]

- $\mathcal{M}_g(z) = \mathbb{E}_g\left[e^{-zg}\right]$ is the moment generating function (MGF) of g.

Let $x = |H_0(m)|^2$, since $|H_0(m)|$ is a Rayleigh random variable, x is an exponential RV with a probability density function (pdf) $f(x) = e^{-x}$, $x \geq 0$. In other words, x is a unit-mean gamma RV with $\alpha = 1$. This latter implies that ${}_1F_1(1-\alpha; 3/2; z) = {}_1F_1(0; 3/2; z) = 1$. Hence, (4.14) becomes

$$\mathbb{E}_{x,y}\left[\operatorname{erfc}\left(\frac{x}{g+c}\right)^{1/2}\right] = 1 - \frac{1}{\sqrt{\pi}}\int_0^{+\infty}\frac{e^{-z(1+c)}}{\sqrt{z}}\mathcal{M}_g(z)dz \tag{4.15}$$

Note that (4.15) could be obtained directly as shown in Appendix B.
For simplicity's sake, we will denote in the sequel of this chapter $|H_k(m')|^2$ by

$$g_{k,m'} = |H_k(m')|^2 \tag{4.16}$$

and the RV related to the total interference power by

$$g = 2\sum_{k=1}^{K}\sum_{m'\in\mathcal{F}_k} A_{k,m,m'}g_{k,m'} \tag{4.17}$$

4.3.1 The multi-interfering transmitters case

[93–95] In this case, the random variable related to the total interference power is

$$g = 2\sum_{k=1}^{K}\sum_{m'\in\mathcal{F}_k} A_{k,m,m'}g_{k,m'} \tag{4.18}$$

where $g_{k,m'} = |H_k(m')|^2$.
As the signals coming from the different interfering transmitters $\{\sum_{m'\in\mathcal{F}_k} A_{k,m,m'}g_{k,m'}, k \in \{1,...,K\}\}$ are independent, the moment generating function of g is given by

$$\begin{aligned}\mathcal{M}_g(z) &= \mathbb{E}_{\{g_{k,m'},\forall k,m'\}}\left[e^{-2z\sum_{k=1}^{K}\sum_{m'\in\mathcal{F}_k}A_{k,m,m'}g_{k,m'}}\right]\\ &= \prod_{k=1}^{K}\mathbb{E}_{\{g_{k,m'},\forall m'\}}\left[e^{-2z\sum_{m'\in\mathcal{F}_k}A_{k,m,m'}g_{k,m'}}\right]\end{aligned} \tag{4.19}$$

Consequently, the MGF of g is the product of the MGFs $\mathcal{M}_k(z)$ where

$$\mathcal{M}_k(z) = \mathbb{E}_{\{g_{k,m'},m'\in\mathcal{F}_k\}}\left[e^{-2z\sum_{m'\in\mathcal{F}_k}A_{k,m,m'}g_{k,m'}}\right] \tag{4.20}$$

However, the RVs $\{g_{k,m'} = |H_k(m')|^2, m' \in \mathcal{F}_k\}$ are correlated because they belong to the same cluster used by the k-th interfering transmitter. To deal with this problem, let $\mathbf{\Omega}_k$ defined by

$$\mathbf{\Omega}_k = \left[\rho_{i,j}\right]_{(i,j)\in\mathcal{F}_k\times\mathcal{F}_k}$$

where $\rho_{i,j} = \rho_{j,i}$, is the correlation matrix of the RVs $\{g_{k,m'}, m' \in \mathcal{F}_k\}$.

From [21], the MGF $\mathcal{M}_k(z)$ is obtained by

$$\mathcal{M}_k(z) = \left|\mathbf{I}_{L_k} + 2\mathbf{D}_k^A\,\mathbf{\Omega}_k\,z\right|^{-1} \tag{4.21}$$

where

- $\mathbf{I}_{L_k}$ is the $L_k \times L_k$ identity matrix and L_k denotes the cardinal of $\mathcal{F}_k$
- $\left|\mathbf{I}_{L_k} + 2\mathbf{D}_k^A\,\mathbf{\Omega}_k\,z\right|$ stands for the determinant of the matrix $\mathbf{I}_{L_k} + 2\mathbf{D}_k^A\,\mathbf{\Omega}_k\,z$
- $\mathbf{D}_k^A$ is a diagonal matrix with diagonal elements,

$$\mathbf{D}_k^A(i,i) = A_{k,m,i} \qquad i \in \mathcal{F}_k \tag{4.22}$$

Substituting (4.21) in expression (4.19), we obtain the MGF related to the total interference RV g defined in (4.18),

$$\mathcal{M}_g(z) = \prod_{k=1}^{K} \mathcal{M}_k(z) = \prod_{k=1}^{K} \left|\mathbf{I}_{L_k} + 2\mathbf{D}_k^A\,\mathbf{\Omega}_k\,z\right|^{-1} \tag{4.23}$$

Therefore, using expressions (4.15) and (4.23), the final expression of the average BER for K interfering transmitters is shown in (4.24).

$$\mathrm{BER}_{\mathrm{average}} = \frac{1}{2} - \frac{1}{2\sqrt{\pi}} \int_0^{+\infty} \frac{e^{-z(1+2b)}}{\sqrt{z}} \prod_{k=1}^{K} \left|\mathbf{I}_{L_k} + 2\mathbf{D}_k^A\,\mathbf{\Omega}_k\,z\right|^{-1} dz \tag{4.24}$$

We have derived the exact expression of the average error rate in the case of subcarrier block assignment considering the frequency fading correlation between the interfering subchannels belonging to a subcarrier block of a given interfering transmitter.

Now, let us examine the asymptotic performance of the average BER in (4.24) with respect to the correlation between the subcarriers belonging to a given interfering transmitter. Two cases will be analyzed: $\rho_{i,j\neq i} = 1$ and $\rho_{i,j\neq i} = 0$

Flat fading channels $\rho_{i,j\neq i} = 1$

In the case of flat fading channels, the interfering subcarriers of a given transmitter k experience the same power channel gain g_k,

$$g_{k,m'} = g_k \quad m' \in \mathcal{F}_k \tag{4.25}$$

Hence, the MGF $\mathcal{M}_k(z)$ becomes

$$\begin{aligned}\mathcal{M}_k(z) &= \left|\mathbf{I}_{L_k} + 2\mathbf{D}_k^A\,\mathbf{\Omega}_k\,z\right|^{-1} \\ &= \begin{vmatrix} 1+2A_{k,m,m'_1}z & 2A_{k,m,m'_1}z & \cdots & 2A_{k,m,m'_1}z \\ 2A_{k,m,m'_2}z & 1+2A_{k,m,m'_2}z & \cdots & 2A_{k,m,m'_2}z \\ \vdots & \vdots & \vdots & \\ 2A_{k,m,m'_{L_k}}z & 2A_{k,m,m'_{L_k}}z & \cdots & 1+2A_{k,m,m'_{L_k}}z \end{vmatrix}^{-1} \\ &= \left(1+2\sum_{m'\in\mathcal{F}_k} A_{k,m,m'}z\right)^{-1} \end{aligned} \tag{4.26}$$

The proof of this expression is provided in Appendix B.
Therefore, the average error rate $\mathrm{BER}_{\text{average}}$ in the case of flat fading channels is given by

$$\mathrm{BER}_{\text{average}} = \frac{1}{2} - \frac{1}{2\sqrt{\pi}}\int_0^{+\infty}\frac{e^{-z(1+2b)}}{\sqrt{z}}\prod_{k=1}^{K}\left(1+2\sum_{m'\in\mathcal{F}_k} A_{k,m,m'}z\right)^{-1} dz \tag{4.27}$$

Totally uncorrelated interfering subcarriers $\rho_{i,j\neq i} = 0$

In this case, the power gains of the interfering subcarriers of a given transmitter k are assumed to be independent, such a case could be found when we use the interleaved subcarrier scheme in frequency selective channels. Hence, the correlation matrix $\mathbf{\Omega}_k$ becomes the identity matrix

$$\mathbf{\Omega}_k = \mathbf{I}_{L_k} \tag{4.28}$$

and the MGF $\mathcal{M}_k(z)$ becomes

$$\begin{aligned}\mathcal{M}_k(z) &= \left|\mathbf{I}_{L_k} + 2\mathbf{D}_k^A\,z\right|^{-1} \\ &= \begin{vmatrix} 1+2A_{k,m,m'_1}z & 0 & \cdots & 0 \\ 0 & 1+2A_{k,m,m'_2}z & \cdots & 0 \\ \vdots & \vdots & \vdots & \\ 0 & 0 & \cdots & 1+2A_{k,m,m'_{L_k}}z \end{vmatrix}^{-1} \\ &= \prod_{m'\in\mathcal{F}_k}(1+2A_{k,m,m'}z)^{-1} \end{aligned} \tag{4.29}$$

Consequently, $\mathrm{BER}_{\text{average}}$ in this case is given by

$$\mathrm{BER}_{\text{average}} = \frac{1}{2} - \frac{1}{2\sqrt{\pi}}\int_0^{+\infty}\frac{e^{-z(1+2b)}}{\sqrt{z}}\prod_{k=1}^{K}\prod_{m'\in\mathcal{F}_k}(1+2A_{k,m,m'}z)^{-1}\,dz \tag{4.30}$$

4.3.2 The partially-loaded network

In the previous subsection, we have derived a closed-form expression of the average error rates for a fully-loaded network. However, a likely scenario would be that a given transmitter experiences silent periods. Consequently, the network becomes partially loaded. Let us

consider a Bernoulli RV $Q_k \in (0,1)$ that models the partial load for each interfering transmitter ($Q_k = 1$ when the transmitter k is active, and $Q_k = 0$ when it becomes inactive). We assume that the $Q_k, k = 1, ..., K$ are independent and with probability density function

$$p(Q_k) = \begin{cases} \alpha_k & Q_k = 1 \\ 1 - \alpha_k & Q_k = 0 \end{cases}, \quad k \in \{1, ..., K\} \tag{4.31}$$

Our aim in this subsection is to derive a new closed-form expression of the average error rate in the partially-loaded case. The total interference RV g can be written as follows

$$g = 2 \sum_{k=1}^{K} Q_k A_{k,m,m'} g_{k,m'} \tag{4.32}$$

According to (4.21) and (4.32), the MGF $\mathcal{M}_g(z)$ is expressed as follows

$$\begin{aligned} \mathcal{M}_g(z) &= \prod_{k=1}^{K} (1 - \alpha_k + \alpha_k \mathcal{M}_k(z)) \\ &= \prod_{k=1}^{K} \left(1 - \alpha_k + \alpha_k \left|\mathbf{I}_{L_k} + 2\,\mathbf{\Omega}_k\,\mathbf{D}_k^A z\right|^{-1}\right) \end{aligned} \tag{4.33}$$

Therefore, using expressions (4.15) and (4.33), the average error rate for a partially-loaded network of K interfering transmitters is shown in (4.34).

$$\mathrm{BER}_{\mathrm{average}} = \frac{1}{2} - \frac{1}{2\sqrt{\pi}} \int_0^{+\infty} \frac{e^{-z(1+2b)}}{\sqrt{z}} \prod_{k=1}^{K} \left(1 - \alpha_k + \alpha_k \left|\mathbf{I}_{L_k} + 2\,\mathbf{\Omega}_k\,\mathbf{D}_k^A z\right|^{-1}\right) dz \tag{4.34}$$

The obtained BER expressions have been derived in the general case. Nevertheless, in order to investigate the accuracy of these expressions, we are going to limit our simulations to the following system model.

4.4 System model

In this Section, we describe the system model which is considered in simulations performed in Chapters 4 and 5. We consider the downlink transmission in OFDM/FBMC based multi-cellular networks depicted in Fig. 4.1 (a). The reference mobile user is located at (u, v). The reference base station is assumed to be situated at the origin $(u_0, v_0) = (0, 0)$. In this analysis, we consider two tiers of the neighboring cells that are surrounding the reference mobile user. Let the k-th base station be located at (u_k, v_k), then, the distance between the reference mobile user and the k-th base station is given by

$$d_k = \sqrt{(u_k - u)^2 + (v_k - v)^2} \tag{4.35}$$

The cell radius is denoted by R in Fig. 4.1.

Concerning the frequency reuse scheme, the subcarriers are allocated according to the most common subcarrier assignment scheme, namely, the subcarrier block assignment scheme

[78] which is described in Fig. 4.1 (b). Each block k consists of the set of subcarriers assigned to base station k. We assume in this scheme that δ adjacent subcarriers to each block are free and serve as guard bands between the different blocks.

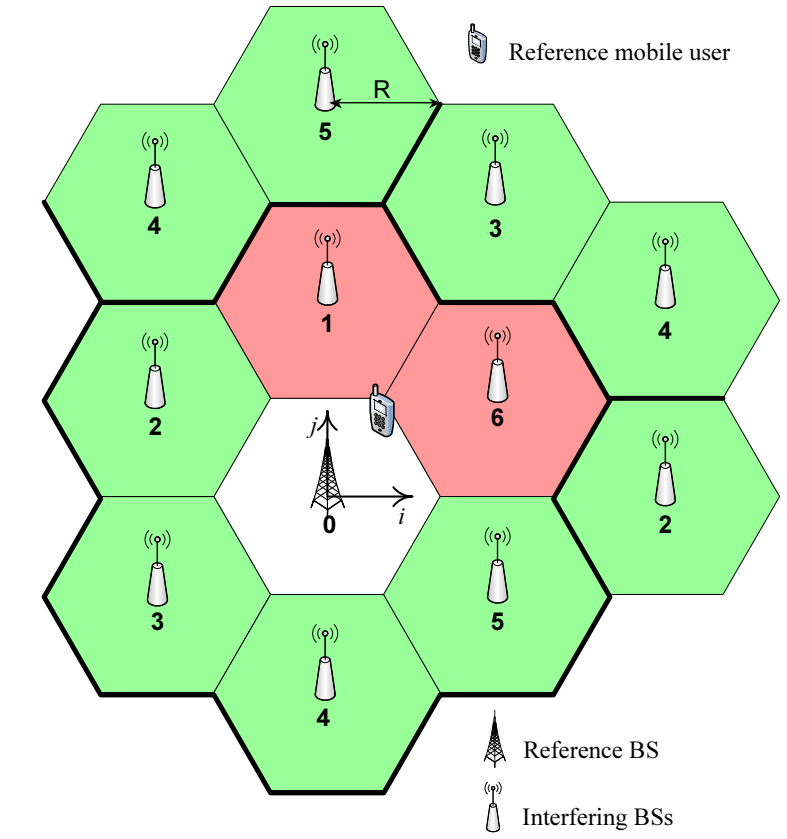

Figure 4.1: The geometry of the downlink of OFDM/FBMC based networks with a cluster size of 7

All signals propagate through different multipath channels using a similar propagation model, where the impulse response of the multipath channel between the k-th base station

and the reference mobile user is given by

$$h_k(t) = \sum_{i=0}^{L-1} h_{k,i}\delta(t - \frac{n_{k,i}}{N}T) \tag{4.36}$$

where $n_{k,0} < n_{k,1} < ... < n_{k,(L-1)} < C$. We recall that C is the maximum delay spread of the channel normalized by the sampling period (T/N), and $h_{k,i}$ are the complex channel path gains, which are assumed mutually independent, where $\mathbb{E}[h_{k,i}h_{k,i}^*] = \gamma_{k,i}$, and $\mathbb{E}[h_{k,i}h_{k,j}^*] = 0$ when $i \neq j$. We further assume that the power is normalized for each channel such that $\sum_{i=0}^{L-1} \gamma_{k,i} = 1, \forall k$. T and N denote respectively the OFDM symbol duration and the total number of subcarriers in the system.

We also assume that the propagation channels are stationary over one OFDM symbol. This is the case for time-invariant or slowly varying channels. Furthermore, the underlying channel model includes path-loss effects which take into account the positions of the base stations with respect to the reference mobile user. The reference mobile user is assumed to be perfectly synchronized with its base station but it is not necessarily synchronized with the other base stations.

Therefore, the composite signal at the reference mobile user can be expressed by the sum of the desired signal coming from the reference base station and the interference signal coming from the surrounding base stations. This corresponds to the signal expression previously given in (4.1).

4.5 Simulation Results

In the Section 4.3, we have derived closed-form expressions of the average error rates in the downlink of an asynchronous K-cell network. In contrast to direct complex analytical methods, these expressions present an efficient approach to compute the average BER with a significantly reduced computational complexity. In this section, we present numerical results for the downlink of OFDM and FBMC systems based on the subcarrier block scheme as described in Section 4.4. We consider $K = 11$ interfering base stations which correspond to two tiers of the neighboring cells surrounding the reference mobile user located at the vertex of the cell as shown in Fig. 4.1. The cell radius in our simulation is R= 1km. Finally, as the analytical expressions have been derived for a fixed value of τ, we need for these simulations results to perform a numerical average over the different values of τ.

We have considered the Pedestrian-A model as a Rayleigh fading propagation channel where the parameters are given in Table 3.5 [96]. The choice of this model is based on the assumption that the subcarriers of interest experience flat fading channels. Therefore, we can focus on the impact of the asynchronous inter-cell interference since the intra-cell interference in the FBMC case is negligible. The path loss of the received signal at a distance d, corresponding to a path loss exponent $\beta = 3.76$ and a carrier frequency of 2 GHz, is governed by the following expression [82]

$$\Gamma_{loss}(d) = 128.1 + 37.6\log_{10}(d[km])[dB]$$

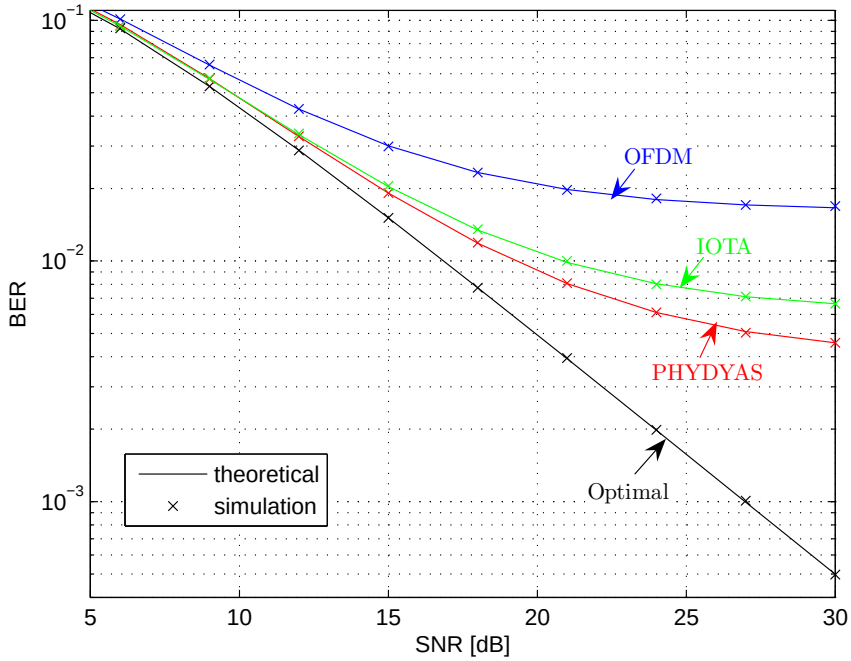

Figure 4.2: The OFDM/FBMC average BER against the SNR for $\tau \in [0, T]$, the guard band size $\delta = 0$

On the other hand, we consider a system with $N = 1024$ subcarriers. The data are QPSK modulated and the sampling frequency is 10 MHz. The noise term is characterized by a thermal noise density of -174 dBm/Hz. The cyclic prefix duration is fixed at $\Delta = T/8$, and the size of the subcarrier block is set at 18 subcarriers. For the FBMC system, we recall that we use the PHYDYAS and IOTA prototype filters with an overlapping factor of 4. It is worth mentioning that the following results are compared to the so-called optimal scenario in which the orthogonality between the different subchannels is assumed to be maintained.

In Fig. 4.2, we investigate the accuracy of the derived BER expressions corresponding to the fully loaded case. The average BERs of OFDM and FBMC modulations are plotted against the SNR, in absence of a guard band between the clusters of the different cells ($\delta = 0$). Both theoretical and simulation results are displayed in Fig. 4.2. The theoretical results are evaluated using (4.24). The exact theoretical results depicted in Fig. 4.2 show an excellent match with the corresponding simulation ones. In this case, we assume that the timing offset τ is a uniform RV in the interval [0,T]. Fig. 4.2 also shows that the timing synchronization errors cause a severe degradation in the average error rate. Moreover, this degradation becomes larger for increasing SNR levels. We can also see an error floor at high SNR values. This observation can be explained by the fact that the noise level is negligible compared to the asynchronous interference caused by the other BSs. Such a case is expected in the noise-less scenario.On the other hand, we observe a better performance

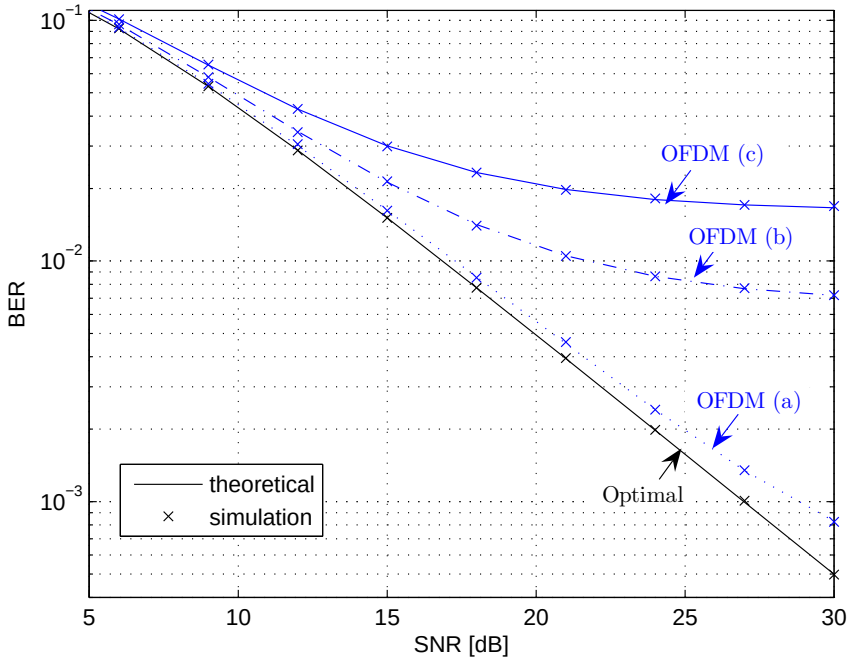

Figure 4.3: The OFDM average BER for different timing offset intervals : Optimal case (a). $\tau \in$[0,T/7] (b). $\tau \in$[0,T/4] (c). $\tau \in$[0,T], the guard-band size δ =0

of the asynchronous FBMC when compared to the asynchronous OFDM. Such a gain can be explained by the fact that only a single subcarrier (PHYDYAS case) or two subcarriers (IOTA case) on each edge suffer from the interference caused by their adjacent subcarriers in the FBMC case (see Fig. 3.10 and Fig. 3.11). However, in the OFDM case, the entire cluster suffers from the interference caused by all neighboring clusters (see Fig. 3.8). In the optimal case, both modulation schemes lead to identical results which means that the actual bit rate is higher for FBMC as it does not use CP.

In Fig. 4.3, we plot the OFDM average BER versus the SNR with different timing offset scenarios: [0,T/7] in scenario (a), [0,T/4] in scenario (b) and [0,T] in scenario (c). All scenarios are compared to the optimal case.
In the OFDM system, the degradation is severe and increases when the timing error interval gets larger. We can explain this result as follows: when the timing offset is lower than the cyclic prefix duration $\tau \in$[0,Δ], the orthogonality between the different clusters is maintained; otherwise the reference user will suffer from an asynchronous interference. Since the timing offset is a uniform random variable, the probability of obtaining the performance of the perfect synchronized case is given by the CP duration over the whole timing offset interval (Δ/τ_{max}). The probability of the orthogonality decreases as τ_{max} increases. Therefore, the average error probability becomes higher.

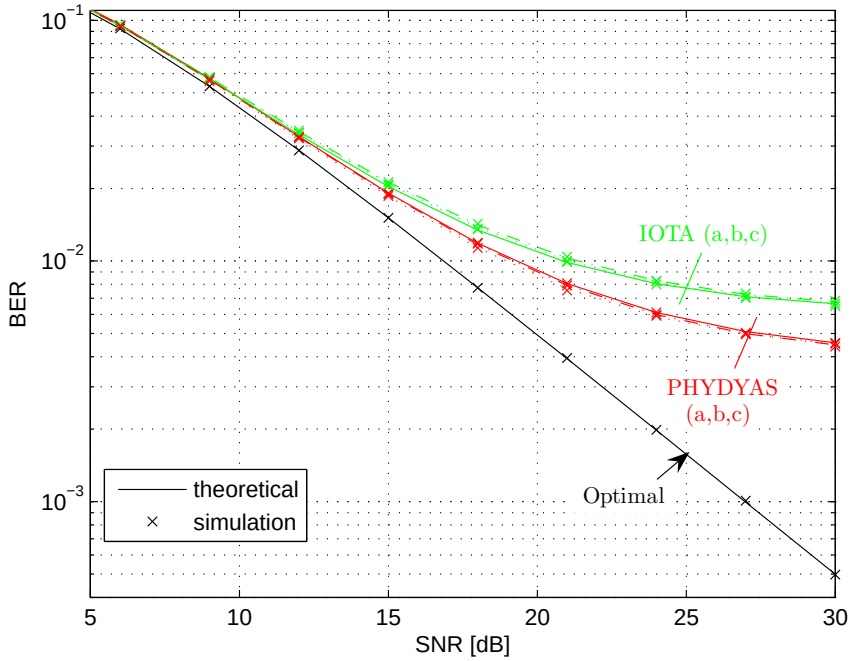

Figure 4.4: The FBMC average BER for different timing offset intervals : Optimal case (a). $\tau \in [0,T/7]$ (b). $\tau \in [0,T/4]$ (c). $\tau \in [0,T]$, the guard-band size $\delta = 0$

In Fig. 4.4, the same evaluation has been performed on PHYDYAS and IOTA FBMC systems. Through the results shown in Fig. 4.4, we find that the FBMC system is not sensitive to the timing offset interval length because the significant interference (with a power level higher than 30 dB) is roughly invariable with respect to the timing offset value (c.f Fig. 3.10 and Fig. 3.11).

The impact of the guard-band length δ on the system performance has also been investigated. Fig. 4.5 shows the OFDM average BER against the SNR for different guard band values $\delta = 0$, 1, 5 and 20 subcarriers; we assume also that the timing offset τ is a uniform RV defined on [0,T]. Comparing the different curves, one can see that the performance improves with increasing δ. However, there is still a remaining gap with respect to the optimal case even with a guard-band of $\delta = 20$ subcarriers.

In contrast to the OFDM case, the FBMC waveforms present, in Fig. 4.6, an excellent performance and provide the same BER values as for the optimal case with a guard-band of a single subcarrier $\delta = 1$ in the case of PHYDYAS and 2 subcarriers $\delta = 2$ for the IOTA case. This result concords with those depicted in Fig. 3.10 that shows that in PHYDYAS-FBMC, the interference power does not exceed -60 dB when the interfering subcarrier and the victim one are separated by at least one subcarrier. The same remark can be noticed for IOTA-FBMC where the interference power is negligible compared to the noise level when

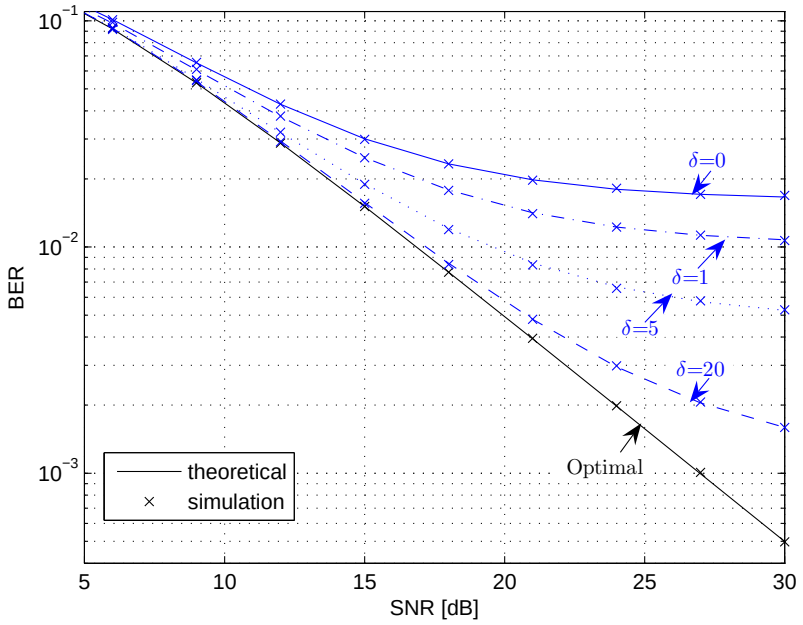

Figure 4.5: The OFDM average BER for different guard-band sizes $\delta = 0$, 1, 5 and 20, the timing offset interval $\tau \in$[0,T]

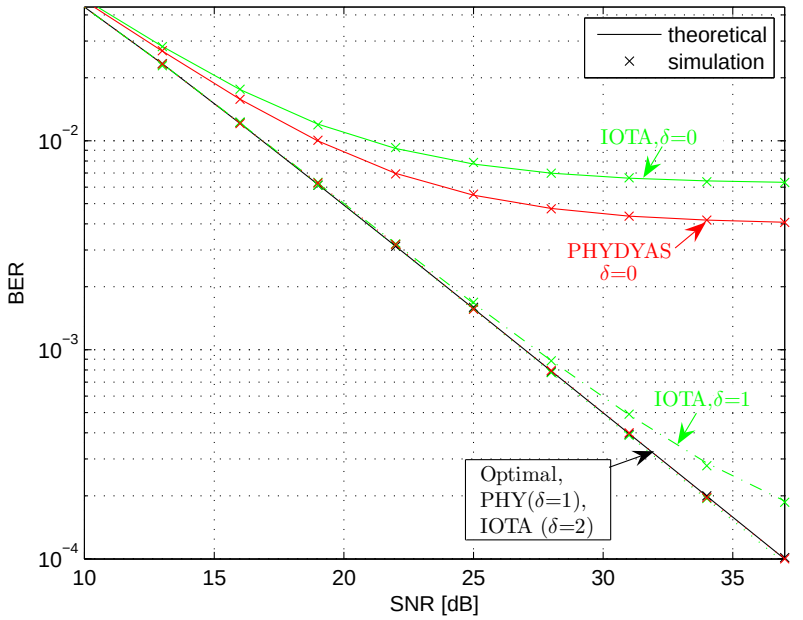

Figure 4.6: The FBMC average BER for different guard-band sizes $\delta = 0$,1 and 2, the timing offset interval $\tau \in$[0,T]

spectral distance between the interfering subcarrier and the victim one is greater or equal to 2 ($\delta \geq 2$).
Moreover, it should be noticed that Fig. 4.3, 4.4, 4.5 and 4.6 show also a perfect match between the simulation and theoretical results obtained by the closed-form expression of the average BER given by (4.24).

In what follows, we analyze the system performance in a partially loaded scenario. Fig. 4.7 and Fig. 4.8 depict the average error rates with respect to the load factor α for SNR = 20 and 25 dB, respectively. The timing offset τ is assumed uniformly distributed on [0,T]. From the obtained results, we find that the average BER increases when the load factor α increases. We observe also that the FBMC system still outperforms the OFDM system. Furthermore, simulation and theoretical results shown in Fig. 4.7 and 4.8 validate the accuracy of the average BER expression given in (4.34) for partially-loaded network.

4.6 Conclusion

In this chapter, we have investigated the impact of timing synchronization errors on the bit error rate performance of the downlink of OFDM and FBMC based multi-cellular networks. We have first given a literature review of average error rate analysis in the presence of asynchronous interference. Based on the interference tables introduced in the previous chapter, we have derived the analytical expression of the instantaneous SINR. We have then developed a theoretical derivation of the average error expressions for three scenarios: one interfering BS, several interfering BSs in a fully-loaded network and also several interfering BSs in a partially loaded network. Furthermore, the asymptotic behavior of the average error rate has been analyzed in two scenarios : the interference-less scenario and the noise-less one. Based on the interference tables and the frequency fading correlation between the interfering subchannels, we have derived the exact expression of the average error rate in the case of block subcarrier assignment. The accuracy of the obtained expressions has been validated through different simulation results. A global evaluation of the performance has been performed taking into account different parameters: the timing error range, the guard band length and the load factor of the network. Through this evaluation, we have shown that in OFDM case, timing errors between BSs cause a severe degradation in system performance. This result is explained by the loss of orthogonality between all system subcarriers. In contrast to the OFDM system, the FBMC waveforms are demonstrated to be less sensitive to timing errors between the different cells, due to the better frequency localization of the prototype filter.

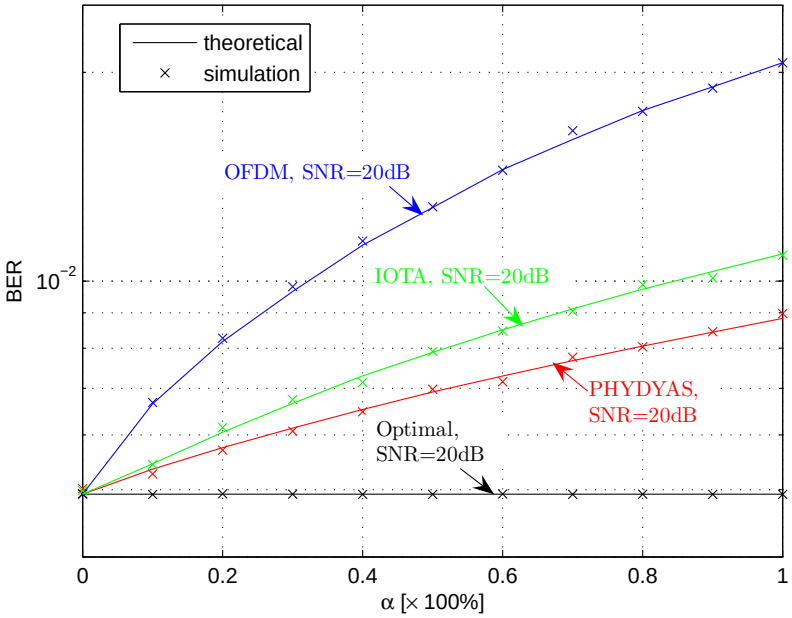

Figure 4.7: The average BER against the load factor α for SNR = 20 dB, the timing offset interval $\tau \in$[0,T]

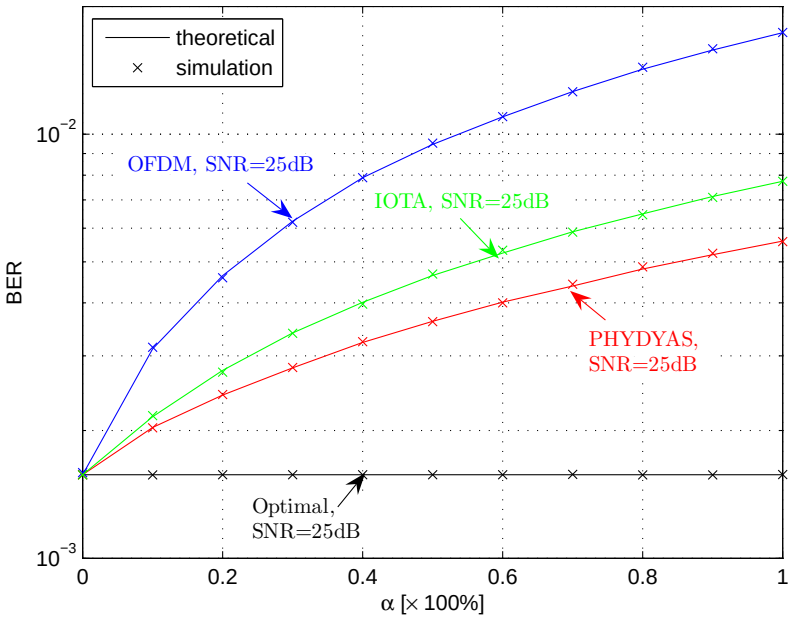

Figure 4.8: The average BER against the load factor α for SNR = 25 dB, the timing offset interval $\tau \in$[0,T]

Chapter 5

Spectral Efficiency Analysis in Asynchronous Cellular Networks

5.1 Introduction

One of the basic measure of performance is the channel capacity. The Shannon landmark paper established the significance of the capacity as the maximum rate of communication for which an arbitrarily small error probability can be achieved. The capacity of fading channels under various assumptions about transmitter and receiver channel knowledge has been examined in [97], [1], [98]. Several researches e.g [1], [97], [99] focus on the capacity analysis without interference whereas Monte-carlo simulations are performed in [100] to estimate the spectral efficiency of cellular systems in the presence of cochannel interference. An analytical expression of the average capacity of OFDM has been derived in [101] taking into account the carrier frequency offset.

However, to the best of our knowledge, there is no published work addressing the impact of the asynchronous interference on the spectral efficiency of OFDM/FBMC systems. This chapter presents an analytical interference analysis related to asynchronous downlink OFDM/FBMC in a multi-cellular environment. We provide here exact expressions of spectral efficiency in frequency selective fading channels. Based on the interference table model introduced in Chapter 3, we derive an explicit form of the spectral efficiency of time-asynchronous OFDM and FBMC systems. Two cases are investigated with respect to the interference source: the block interfering subcarrier in both fully and partially loaded networks. The computation of the average spectral efficiency is based on the moment generating function of the interference power.

The remainder of this chapter is organized as follows. In Section 5.2, a theoretical derivation of the spectral efficiency of asynchronous OFDM/FBMC systems in the presence of : block interfering subcarrier in both fully and partially loaded networks is presented. Section 5.3 is devoted to presenting and discussing the different simulation results. Finally, we review our main results and offer some concluding remarks in Section 5.4. In this chapter, we reuse the system model described in the previous chapter.

5.2 Spectral Efficiency Analysis

In this section, we consider deriving a closed-form expression of the spectral efficiency considering the asynchronous interference caused by the surrounding interfering transmitters. In the literature, the capacity is given by Shannon's well-known formula [102] if the decision variables are Gaussian random variables,

$$C(\mathrm{SNR}) = B \log_2 (1 + \mathrm{SNR}) \tag{5.1}$$

where B denotes the channel bandwidth.
Therefore, by conditioning on the set of variables $\mathcal{H} = \{H_0(m), H_k(m'), k \in \{1, ..., K\}, m' \in \mathcal{F}_k\}$ and substituting the instantaneous SINR expressed by (4.5) in equation (5.1), we can obtain the exact closed form expression for the conditional spectral efficient in presence of interference

$$C(\mathrm{SINR})|_{\mathcal{H}} = B \log_2 \left(1 + \frac{|H_0(m)|^2}{\sum\limits_{k=1}^{K} \sum\limits_{m' \in \mathcal{F}_k} A_{k,m,m'} |H_k(m')|^2 + b} \right) \tag{5.2}$$

We recall that b and $A_{k,m,m'}$ are given in (4.7) and (4.8), respectively.
The average spectral efficiency is thus given by

$$C_{\mathrm{average}} = \mathbb{E}_{\mathcal{H}} \left[B \log_2 \left(1 + \frac{|H_0(m)|^2}{\sum\limits_{k=1}^{K} \sum\limits_{m' \in \mathcal{F}_k} A_{k,m,m'} |H_k(m')|^2 + b} \right) \right] \tag{5.3}$$

The average over channel realizations $\mathcal{H}$ of this conditional spectral efficiency is excessively difficult to compute as it must be done over a $K \times |\mathcal{F}_k|$ complex fold.

$$C_{\mathrm{average}} = B \int_{\mathcal{H}} \log_2 \left(1 + \frac{|H_0(m)|^2}{\sum\limits_{k=1}^{K} \sum\limits_{m' \in \mathcal{F}_k} A_{k,m,m'} |H_k(m')|^2 + b} \right) p(\mathcal{H}) d\mathcal{H} \tag{5.4}$$

Here, $p(\mathcal{H})$ stands for the probability density function of the vector $\mathcal{H}$.

Recently, moment generating functions (MGF) have been demonstrated to be a powerful tool for an efficient performance analysis for generalized fading channels [22], [19]. In order to reduce the complexity of computing the average spectral efficiency into only one integration, we refer to the following lemma [19], which is based on the MGF of the interference power.

Lemma Let x be a unit-mean gamma random variable (RV) with parameter α and c is an arbitrary constant. Let g be an arbitrary non-negative random variable that is independent of x. Then

$$\mathbb{E}_{x,g}\left[\ln\left(1+\frac{x}{g+c}\right)\right] = \int_0^{+\infty}\left[\frac{1}{z}-\frac{1}{z(1+z)^{\alpha}}\right]\mathcal{M}_g(\alpha z)e^{-z\alpha c}dz \tag{5.5}$$

where $\mathcal{M}_g(z)=\mathbb{E}_g\left[e^{-zg}\right]$ is the MGF of g.
Let $x=|H_0(m)|^2$, since $|H_0(m)|$ is a Rayleigh random variable, x becomes an exponential RV with a probability density function (pdf) $f(x)=e^{-x}$, $x\geq 0$. In other words, x is a unit-mean gamma RV with $\alpha=1$.
Hence, according to (5.3) and (5.5), the average spectral efficiency becomes,

$$C_{\text{average}} = B\log_2(e)\int_0^{\infty}\frac{e^{-zb}}{1+z}\mathcal{M}_g(z)dz \tag{5.6}$$

Note that (5.6) could be directly obtained as shown in Appendix C.
For simplicity's sake, we will denote in the sequel of this chapter $|H_k(m')|^2$ by

$$g_{k,m'} = |H_k(m')|^2 \tag{5.7}$$

and the RV related to the total interference power by

$$g=\sum_{k=1}^{K}\sum_{m'\in\mathcal{F}_k}A_{k,m,m'}g_{k,m'} \tag{5.8}$$

Comparing (5.8) and (4.17), we notice that these two expressions are equivalent to a constant factor η. Moreover, the terms $A_{k,m,m'}$ are scalar factors that can absorb that constant η. In this case, $\eta=1/2$.
In order to obtain a more detailed expression, we distinguish two cases that depend on the activity of the surrounding interferers:

5.2.1 The multi-cell case

[103] Starting from (5.8) and based on the derivation of (4.23), the MGF of g can be expressed as follows

$$\mathcal{M}_g(z)=\prod_{k=1}^{K}\mathcal{M}_k(z)=\prod_{k=1}^{K}\left|\mathbf{I}_{L_k}+\mathbf{D}_k^A\,\mathbf{\Omega}_k\,z\right|^{-1} \tag{5.9}$$

We recall,

- $\mathbf{I}_{L_k}$ is the $L_k\times L_k$ identity matrix and L_k denotes the cardinal of $\mathcal{F}_k$
- $\left|\mathbf{I}_{L_k}+\mathbf{D}_k^A\,\mathbf{\Omega}_k\,z\right|$ stands for the determinant of the matrix $\mathbf{I}_{L_k}+2\mathbf{D}_k^A\,\mathbf{\Omega}_k\,z$

- $\mathbf{D}_k^A$ is a diagonal matrix with diagonal elements,

$$\mathbf{D}_k^A(i,i) = A_{k,m,i} \qquad i \in \mathcal{F}_k \tag{5.10}$$

- $\mathbf{\Omega}_k$ is the correlation matrix of the RVs $\{g_{k,m'}, m' \in \mathcal{F}_k\}$.

Therefore, using the expressions (5.6) and (5.9), the final expression of the average spectral efficiency for K interfering transmitters is shown in (5.11).

$$C_{\text{average}} = B\log_2(e) \int_0^{+\infty} \frac{e^{-zb}}{1+z} \prod_{k=1}^{K} \left|\mathbf{I}_{L_k} + \mathbf{D}_k^A\, \mathbf{\Omega}_k\, z\right|^{-1} dz \tag{5.11}$$

Two asymptotical cases of the average spectral efficiency given in (5.11) can be examined with respect to the correlation between the interfering subcarriers belonging to a given asynchronous transmitter: $\rho_{i,j\neq i} = 1$ and $\rho_{i,j\neq i} = 0$

Flat fading channels $\rho_{i,j\neq i} = 1$

In the case of flat fading channels, the interfering subcarriers of a given transmitter k experience the same power channel gain g_k,

$$g_{k,m'} = g_k \quad m' \in \mathcal{F}_k \tag{5.12}$$

As proceeded for equation (4.26), the MGF $\mathcal{M}_k(z)$ becomes

$$\mathcal{M}_k(z) = \left(1 + \sum_{m' \in \mathcal{F}_k} A_{k,m,m'} z\right)^{-1} \tag{5.13}$$

Therefore, the average spectral efficiency in the case of flat fading channels is given by

$$C_{\text{average}} = B\log_2(e) \int_0^{+\infty} \frac{e^{-zb}}{1+z} \prod_{k=1}^{K} \left(1 + \sum_{m' \in \mathcal{F}_k} A_{k,m,m'} z\right)^{-1} dz \tag{5.14}$$

Totally uncorrelated interfering subcarriers $\rho_{i,j\neq i} = 0$

Under the same conditions stated for the BER derivation in Chapter 4, the correlation matrix $\mathbf{\Omega}_k$ becomes the identity matrix. Thus, the MGF $\mathcal{M}_k(z)$ is

$$\mathcal{M}_k(z) = \prod_{m' \in \mathcal{F}_k} (1 + A_{k,m,m'} z)^{-1} \tag{5.15}$$

Consequently, the spectral efficiency in this case is given by

$$C_{\text{average}} = B\log_2(e) \int_0^{+\infty} \frac{e^{-zb}}{1+z} \prod_{k=1}^{K} \prod_{m' \in \mathcal{F}_k} (1 + A_{k,m,m'} z)^{-1} dz \tag{5.16}$$

5.2.2 The partially-loaded network

Following the same steps done in the derivation of the average BER in Section 4.3.2, the obtained MGF $\mathcal{M}_g(z)$ is

$$\mathcal{M}_g(z) = \prod_{k=1}^{K} \left(1 - \alpha_k + \alpha_k \left|\mathbf{I}_{L_k} + \mathbf{D}_k^A \, \mathbf{\Omega}_k \, z\right|^{-1}\right) \tag{5.17}$$

Therefore, using the expressions (5.6) and (5.17), the average spectral efficiency for a partially-loaded network of K interfering cells is shown in (5.18).

$$C_{\text{average}} = B \log_2(e) \int_0^{+\infty} \frac{e^{-zb}}{1+z} \prod_{k=1}^{K} \left(1 - \alpha_k + \alpha_k \left|\mathbf{I}_{L_k} + \mathbf{\Omega}_k \, \mathbf{D}_k^A z\right|^{-1}\right) dz \tag{5.18}$$

5.3 Simulation Results

In the previous section, we have derived closed-form expressions of the average spectral efficiency in the presence of the asynchronous interference. In contrast to direct complex analytical methods, these expressions constitute an efficient approach to compute the average spectral efficiency with a significantly reduced computational complexity. In this section, we present some numerical results for the OFDM and FBMC downlink systems based on the block subcarrier scheme described in Section 4.4. The details of the considered simulation setup are given in Section 4.5. It is worth mentioning that the following results are compared to the so-called optimal scenario where the orthogonality between the different subchannels is maintained.

In the first figrue, Fig. 5.1, the estimated spectral efficiency expression given by (5.11) is confronted with the real one. We consider here a configuration without guard bands between the clusters of the different cells ($\delta = 0$). The figure depicts the average spectral efficiency of OFDM and FBMC modulations as a function of the SNR for both theoretical and simulation performances. The theoretical results are evaluated based on (5.11). Fig. 5.1 shows a perfect match between the exact theoretical performances and the corresponding simulated ones. For these simulations, we have considered the timing offset τ as a uniformly distributed RV over [0,T]. Moreover, Fig. 5.1 shows the impact of the loss of synchronization. In fact, it can be seen that the average spectral efficiency is very sensitive to timing asynchronism. In addition, the observed degradation increases for an increasing SNR levels. The plotted curves show also, in the high SNR regime, the appearance of a spectral efficiency floor for asynchronous OFDM systems. This behavior can be explained by the dominance of the asynchronous interference caused by the other BSs over the considered noise levels. Such a case is expected to happen for the interference-limited scenarios. On the other hand, asynchronous FBMC performs quiet well and offers better performance compared to the asynchronous OFDM.

Such an important gain between FBMC and OFDM can be explained by the amount of interference collected. In fact, from figures Fig. 3.10 and Fig. 3.11 it can be seen that at

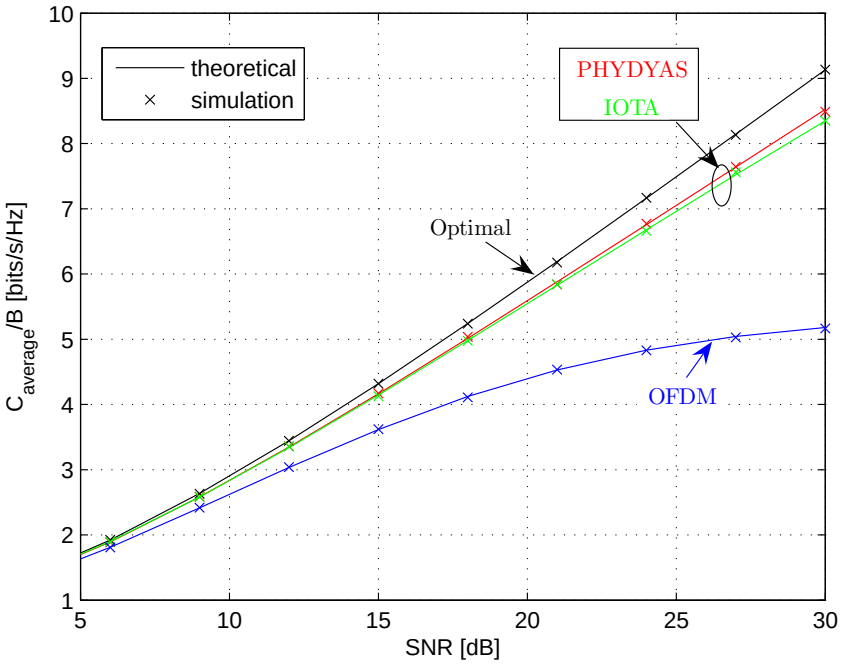

Figure 5.1: The OFDM/FBMC average spectral efficiency against the SNR for $\tau \in [0, T]$, the guard band size $\delta = 0$

each edge for FBMC systems only one single subcarrier suffers from a significant amount of interference caused by its adjacent subcarrier. However, in the OFDM case and as illustrated in figures Fig. 3.8, the entire cluster of subcarriers suffers from the interference caused by all the neighboring clusters. Finally, for the optimal case (perfect orthogonality maintained), both modulation schemes lead to identical results. But, taking into account the cyclic prefix used for the OFDM scheme, FBMC offers higher real bit rates compared to OFDM.

In the next figure, Fig. 5.2, we use the optimal case as a reference and plot the average spectral versus the SNR with different timing offset scenarios: [0,T/4] in scenario (a), [0,T/2] in scenario (b) and [0,T] in scenario (c).

We notice trough these plots a severe degradation for the OFDM system. This degradation grows with an increase of the timing error interval. This behavior can be explained by the fact that orthogonality depends on the timing offset. In fact, when the timing offset remains confined in the interval defined by the cyclic prefix duration (i.e. $\tau \in [0,\Delta]$), the orthogonality between the different clusters is maintained. In all other cases, the reference user suffers from the asynchronous interference. Considering now that the timing offset is a uniform random variable, we can compute the probability of obtaining the perfect synchronized case performances as the fraction of the CP duration over the entire considered timing offset interval (Δ/τ_{max}). It is strait forward that the probability of keeping the orthogonality is inversly proportional to τ_{max}. Therefore, the achievable average spectral efficiency decreases. On the other hand, for the FBMC systems, the amount of interference perceived at the two subcarriers of the cluster's edge remains roughly invariant with respect to the timing offset value. Consequently, FBMC systems are not sensitive to the length of the timing offset interval.

Up to now we have neglected the impact of the guard-band length δ. In the following we investigate the performance variations in function of the guard-band length δ. In fact, figure, Fig. 5.3 shows the OFDM and FBMC average spectral efficiency in function of the SNR for different guard band values δ =0, 1 and 5 subcarriers. As previously, we also assume that the timing offset τ is a uniform RV defined over [0,T]. The aim here is to get some insight about the evolution of the spectral efficiency for a variation of the spectral distance between the interfering subcarriers and the victim ones. As the spectral distance influences the asynchronous interference, the average spectral efficiency will be exclusively computed over the active subcarriers (subcarriers that are transmitting data). Comparing the different plots for the OFDM system, we clearly see a significant improvement of the performances as the spectral guard-band δ increases. However, there is still a significant remaining gap with the optimal case even for an important guard-band of 5 subcarriers.

Unlike the OFDM case, FBMC waveforms offer excellent performances as they are capable of achieving the optimal case performances just by leaving a guard-band of one single subcarrier δ =1. This observation is easily explainable when looking at figures Fig. 3.10 and 3.11. In fact, through these figures, it can be seen that for FBMC systems, the collected interference power becomes negligible compared to the noise level when the subcarrier block of interest is situated at just one subcarrier ($\delta = 1$) from the nearest interfering block.

Furthermore, it should also be noticed through figures Fig. 5.2 and 5.3 that the theoretical-

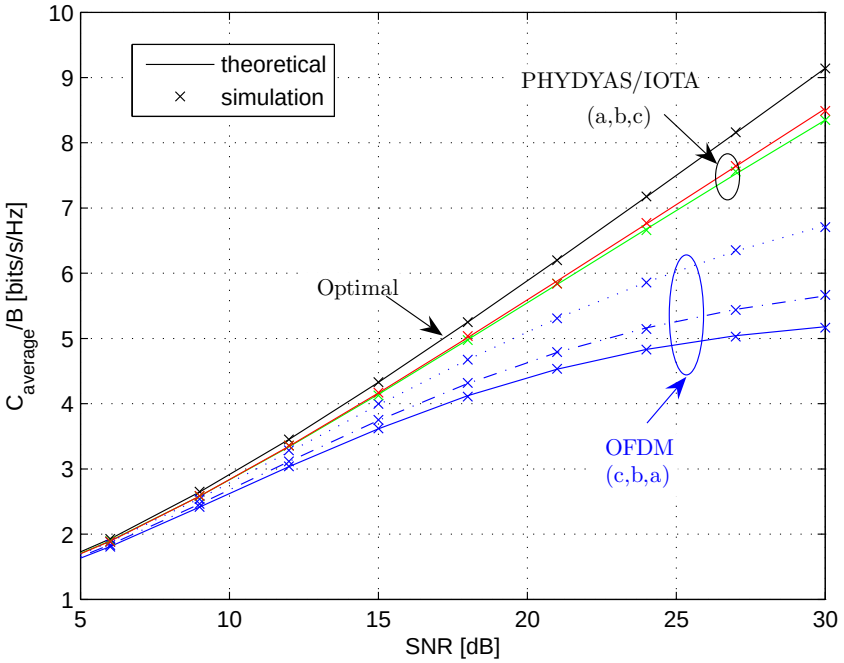

Figure 5.2: The OFDM average spectral efficiency for different timing offset intervals : Optimal case (a). $\tau \in$[0,T/4] (b). $\tau \in$[0,T/2] (c). $\tau \in$[0,T], the guard-band size δ =0

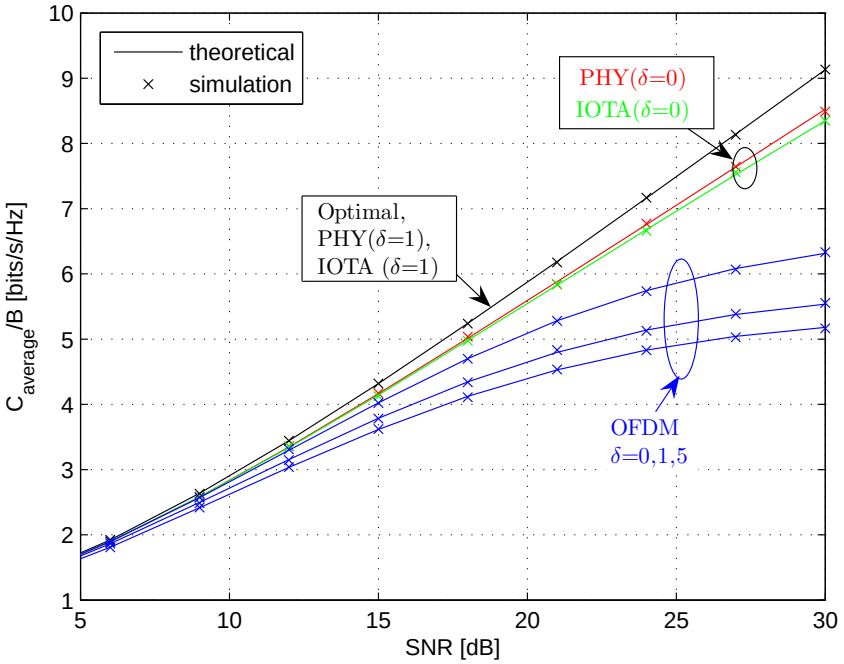

Figure 5.3: The OFDM average spectral for different guard-band sizes δ = 0, 1 and 5, the timing offset interval $\tau \in$[0,T]

based results obtained using the closed-form expression of the average spectral efficiency given in (5.11) constitute a perfect match to the simulated ones.

Finally, we focus on the system performances for a partially loaded scenario. Figures Fig. 5.4 and Fig. 5.5 gives the average spectral efficiency with respect to the load factor α for two SNR values = 20 and 25 dB, respectively. The random variable τ representing the timing offset is assumed to be uniformly distributed over [0,T]. These curves show that for an increasing load factor α, the average achievable spectral efficiency decreases. Moreover, all systems: FBMC, OFDM as well as the optimal case are starting from the same point as they offer the same performances for $\alpha = 0$. Nevertheless, the curves diverge with growing α where FBMC techniques remain close to each other and reasonably close to the optimal performances. The OFDM case, on the other hand, present performances largely below those achieved by FBMC. Furthermore, we note the excellent match between simulation and theoretical results presented in figures Fig. 5.4 and 5.5. This validates the accuracy of the computed average spectral efficiency expression for partially-loaded network given in (5.18).

5.4 Conclusion

In this chapter, we have considered the derivation of the spectral efficiency for OFDM and FBMC systems taking into account timing synchronization errors. We have started by giving a brief review of the impact of asynchronism on the spectral efficiency present in the literature. Several scenarios have been considered for the derivation of the theoretical average spectral efficiency closed-form expressions. Among them, we considered multiple interferers in both fully and partially loaded networks. The theoretical analysis has been finalized by the asymptotic behavior analysis for the noise-less and the interference-free scenarios. Then, some simulations have been carried out to validate these theoretically obtained expressions. We have taken into consideration various parameters such as: the timing error range, the guard band length and the load factor of the network. The obtained results show that the OFDM performance suffers from significant degradations due to timing misalignment between the interferers and the victim receiver. Theses degradations are mainly explained by the loss of orthogonality between all system subcarriers. On the opposite of OFDM systems, FBMC techniques have shown to be more robust to these timing synchronization errors. The better frequency localization of the used prototype filters (PHYDYAS and IOTA) constitutes the strength of FBMC systems against time asynchronism.

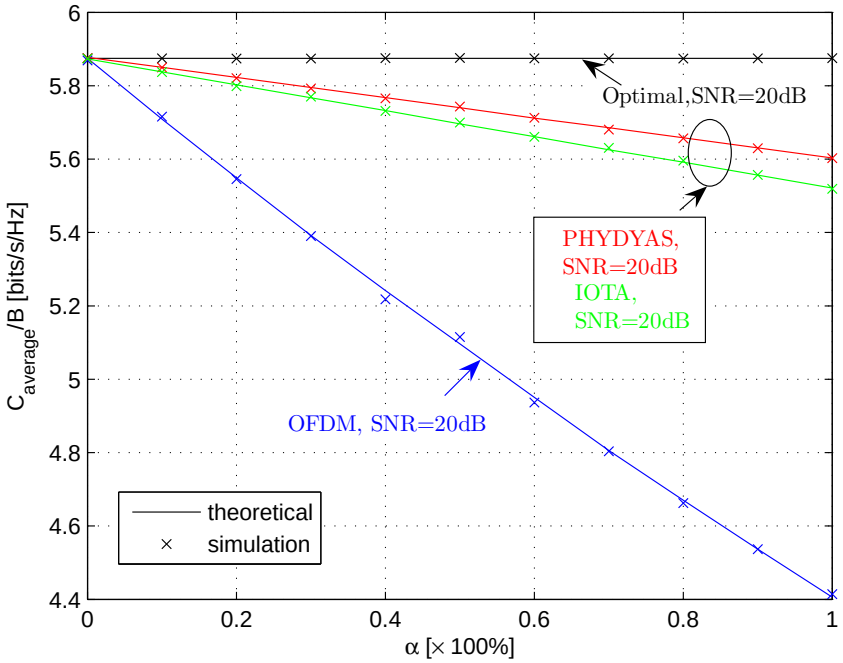

Figure 5.4: The average spectral efficiency against the load factor α for SNR = 20 dB, the timing offset interval $\tau \in$[0,T]

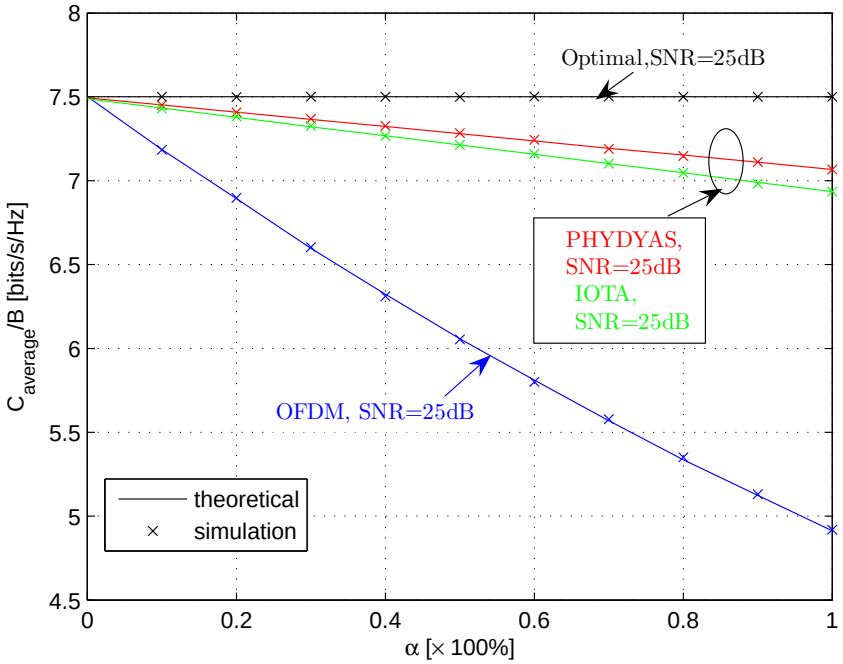

Figure 5.5: The average spectral efficiency against the load factor α for SNR = 25 dB, the timing offset interval $\tau \in$[0,T]

Chapter 6

Conclusions and Perspectives

6.1 Conclusions

This thesis mainly focuses on the impact of the timing asynchronism on the performances of OFDM and FBMC systems.

In the first part of the thesis, we have presented the research motivations and the background that resulted in the different contributions of this dissertation.

Since Multicarrier techniques are the heart of this thesis, the theory of OFDM and FBMC systems has been introduced as a basis for the rest of the thesis. Additionally, the asynchronism issue in multicarrier systems was discussed.

In Chapter 3, we have shown that the timing asynchronism can cause a loss of the orthogonality between subcarriers. This non-orthogonality results in the introduction of some amount of interference which is called asynchronous interference. First, a literature review of the asynchronous interference analysis has been presented. Then, we have introduced the concept of interference tables where the PSD-based interference tables have been derived for CP-OFDM and FBMC with IOTA and PHYDYAS waveforms. Since the PSD-based tables do not take into account the timing misalignment between the interfering signal and the reference one, we have proposed new interference tables called instantaneous interference tables. In this latter, the interference is modeled as a function of the timing offset between the interfering and the reference signals and the spectral distance between the interfering subcarrier and the victim one previously considered in the PSD-based model. Furthermore, we have extended the interference analysis to the case of frequency selective environments. Using the instantaneous tables, we have proposed a semi-analytical method to evaluate the average SINR and the spectral efficiency. We have finally examined the accuracy of the proposed model through different simulation results. In fact, simulation results have shown a

perfect match between the numerically computed performances and those obtained through the proposed interference tables. In contrast to these results, the PSD-based evaluated performance present a strong inaccuracy. Although the proposed model reduces the computation complexity compared to the numerical evaluation, there is still a need to simulate the different channel realizations. The computational complexity of the performance evaluation has been addressed in next chapters.

In Chapters 4 and 5, the analysis of the average error rate and the average spectral efficiency in the presence of the asynchronous interference is respectively addressed. We have first derived the analytical expression of the instantaneous SINR using the interference tables proposed in Chapter 3. We have thus demonstrated that the direct approach to compute the average BER and the average spectral efficiency leads to complex $(K \times |\mathcal{F}_k|^1)$-fold integrations which are analytically intractable in most cases. Then, based on the moment generating functions of the asynchronous interference power, we have developed a theoretical derivation of the expressions of the average of both the error rate and the spectral efficiency. The obtained expressions reduce the previous multiple integral to only a single integration. Moreover, three scenarios have been considered in this analysis : one interfering BS, several interfering BSs in fully and partially loaded networks. Furthermore, an asymptotic analysis has been developed for two cases: the interference-free case and the noise-less one. It is also worth mentioning that the obtained expressions consider in addition the frequency fading correlation between the interfering subcarriers.

The accuracy of the derived expressions has been validated through various simulation results. Taking into account different parameters such as: the timing error range, the network load factor and the length of the guard-band separating the interfering subcarrier blocks and the victim one. Through these evaluations, we have shown that:

- the timing asynchronism between the interfering signals and the reference one cause a severe degradation in the OFDM system performances. Such a result is explained by the high amount of the asynchronous interference power resulting from the loss of orthogonality between all system subcarriers

- thanks to the good frequency localization of both IOTA and PHYDYAS waveforms, the FBMC system is less sensitive to timing errors compared to OFDM systems.

- asynchronous FBMC systems can achieve the performances of the optimal case representing the lack of asynchronous interference. This can be achieved by inserting guard-band between the interfering subcarriers and the victim ones. Moreover, a single subcarrier is required for PHYDYAS and two for IOTA.

- OFDM systems are better than FBMC systems when the timing asynchronism is not very important.

[1] K is the number of interfering BSs and $|\mathcal{F}_k|$ the number of subcarriers allocated to the k-th BS

6.2 Suggestions for Future works

A number of interesting topics, based on the research issues studied in this thesis, could be addressed. We hereunder provide some suggestions of possible extensions to the work presented in this dissertation:

- The interference analysis in this work considers only time asynchronous interference. It is wise to extend this analysis to a global model that takes into account both timing and frequency offsets.

- We have shown in this thesis that one of the main advantages of FBMC modulation is its robustness to multiuser timing asynchronism. It has been demonstrated that, even for a large timing offset, a given subcarrier interferes at most the two adjacent ones. However, this property has only been confirmed for linear power amplifiers. The joint impact of the desynchronization and the non-linearity of power amplifiers on OFDM and FBMC performances has not been well investigated in the literature. The theoretical derivation developed in Chapters 4 and 5 could be extended to evaluate the performance of OFDM and FBMC considering both non-linearity and timing misalignments effects.

- Recently, many researches have focused on the problem of resource allocation in OFDM and FBMC cognitive radio networks. Various resource allocation algorithms considering the mutual interference between the primary system and the secondary one have been proposed [104], [105]. However in practice, it might happen that the nodes operating in the same system are not synchronized. In this context, the SINR is no more constant during the execution of the allocation algorithm but changes according to the current allocation state. Indeed, the SINR should be revised with respect to the interference caused by the new allocated resource (power and/or frequency bandwidth). Therefore, a new kind of optimization algorithms should be developed to deal with this problem.

Bibliography

[1] A. Goldsmith, *Wireless Communications*, Cambridge University Press, New York, NY, USA, 2005.

[2] H. Schulze and C. Lüders, *Theory and Applications of OFDM and CDMA: Wideband Wireless Communications*, John Wiley, 2005.

[3] K. Fazel and S. Kaiser, *Multi-Carrier and Spread Spectrum Systems: From OFDM and MC-CDMA to LTE and WiMax*, John Wiley & Sons, 2009.

[4] K. Etemad and M.-Y. Lai, *WiMAX Technology and Network Evolution*, John Wiley, 2011.

[5] WiMax Forum, *Mobile System Profile*, release 1.0 approved specification, Revision 1.5.0, Nov. 2007.

[6] 3GPP TS 36.211, *Evolved Universal Terrestrial Radio Access (E-UTRA); Physical Channels and Modulation (Release 8)*.

[7] R. Zakaria and D. Le Ruyet, "A Novel Filter-Bank Multicarrier Scheme to Mitigate the Intrinsic Interference: Application to MIMO Systems," *Wireless Communications, IEEE Transactions on*, vol. 11, no. 3, pp. 1112 –1123, march 2012.

[8] R. Zakaria and D. Le Ruyet, "Partial ISI cancellation with viterbi detection in MIMO filter-bank multicarrier modulation," in *Wireless Communication Systems (ISWCS), 2011 8th International Symposium on*, nov. 2011, pp. 322 –326.

[9] H. Zhang, D. Le Ruyet, and M. Terré, "Spectral Efficiency Comparison between OFDM/OQAM and OFDM based CR Networks," *Wireless Commun. and Mobile Computing Wiley*, vol. 9, pp. 1487–1501, Nov. 2009.

[10] T. Weiss, J. Hillenbrand, A. Krohn, and F.K. Jondral, "Mutual Interference in OFDM-based Spectrum Pooling Systems," in *IEEE Vehicular Technology Conference*, May 2004, vol. 4, pp. 1873–1877.

[11] S. Y. Shin, H. S. Park, and W. H. Kwon, "Mutual Interference Analysis of IEEE 802.15.4 and IEEE 802.11b," *Computer Networks: The International Jour. of Computer and Telecommunications Networking*, vol. 51, pp. 3338–3353, Aug. 2007.

[12] H.G. Feichtinger and T. Strohmer, *Gabor Analysis and Algorithms: Theory and Applications*, Applied and Numerical Harmonic Analysis. Birkhäuser, 1998.

[13] D. Tse and P. Viswanath, *Fundamentals of Wireless Communications* , Cambridge University Press, New York, NY, USA, 2004.

[14] B. Le Floch, M. Alard, and C. Berrou, "Coded Orthogonal Frequency Division Multiplex [TV broadcasting]," *Proceedings of the IEEE*, vol. 83, no. 6, pp. 982 –996, Jun. 1995.

[15] M. Alard, "Construction of a Multicarrier Signal," , no. WO/1996/035278, Nov. 1996.

[16] M.G. Bellanger, "Specification and Design of a Prototype Filter for Filter Bank based Multicarrier Transmission," in *IEEE Int. Conf. on Acoustics, Speech, and Signal Processing, 2001. Proceedings. (ICASSP '01).*, May 2001, vol. 4, pp. 2417 –2420.

[17] M. Morelli, C.-C.J. Kuo, and M.-O. Pun, "Synchronization Techniques for Orthogonal Frequency Division Multiple Access (OFDMA): A Tutorial Review," *Proceedings of the IEEE*, vol. 95, no. 7, pp. 1394 –1427, Jul. 2007.

[18] K. Cho and D. Yoon, "On the General BER Expression of one and two Dimensional Amplitude Modulation ," *IEEE Trans. on Commun.*, vol. 50, no. 7, pp. 1074–1080, Jul. 2002.

[19] K. A. Hamdi, "A Useful Technique for Interference Analysis in Nakagami Fading," *IEEE Trans. on Commun.*, vol. 55, no. 6, pp. 1120–1124, Jun. 2007.

[20] M. Abramowitz and I. A. Stegun, *Handbook of Mathematical Functions*, New York: Dover, 1965.

[21] A.S. Krishnamoorthy and M. Parthasarathy, "A Multi-Variate Gamma-Type Distribution," *Annals of Mathematical Statistics*, pp. 549–557, 1951.

[22] M.-S. Alouini and M.K. Simon, "An MGF-based Performance Analysis of Generalized Selection Combining over Rayleigh Fading Channels," *IEEE Trans. on Commun.*, vol. 48, no. 3, pp. 401 –415, Mar. 2000.

[23] T. Hidalgo Stitz, *Filter Bank Techniques for the Physical Layer in Wireless Communications*, Ph.D. thesis, Tampere University of Technology, 2010.

[24] *Radio Broadcasting Systems: Digital Audio Broadcasting (DAB) to mobile, portable and fixed receivers*, ETS 300 401, Eur. Telecommun. Standard Institute, May 1997.

[25] W. Hoeg and T. Lauterbach, *Digital Audio Broadcasting: Principles and Applications of DAB, DAB+ and DMB*, John Wiley & Sons, 2009.

[26] *Digital Video Broadcasting (DVB-T); Frame Structure, Channel Coding, Modulation for Digital Terrestrial Television*, ETS 300 744, Eur. Telecommun. Standard Institute, 2001.

[27] *Part 11: Wireless LAN Medium Access Control (MAC) and Physical Layer (PHY) specifications: Higher-Speed Physical Layer Extension in the 5 GHz Band*, IEEE802.11a, 1999.

[28] L. Deneire, "Beating the Wireless Channel," in *Wireless OFDM Systems*, Marc Engels, Ed., vol. 692, pp. 75–93. Springer US, 2002.

[29] B. Farhang-Boroujeny, "OFDM Versus Filter Bank Multicarrier," *IEEE Signal Processing Mag.*, vol. 28, no. 3, pp. 92 –112, May 2011.

[30] T. Strohmer and S. Beaver, "Optimal OFDM Design for Time-Frequency Dispersive Channels," *IEEE Trans. Commun.*, vol. 51, no. 7, pp. 1111 – 1122, Jul. 2003.

[31] S. Qiu and H.G. Feichtinger, "Discrete Gabor Structures and Optimal Representations," *IEEE Trans. Signal Processing*, vol. 43, no. 10, pp. 2258 –2268, Oct 1995.

[32] P. Jung and G. Wunder, "A Group-Theoretic Approach to the WSSUS Pulse Design Problem," in *International Symposium on Information Theory, 2005. ISIT 2005.*, Sept. 2005, pp. 870 –874.

[33] R. W. Chang, "High-Speed Multichannel Data Transmission with Bandlimited Orthogonal Signals," *Bell Syst. Tech. J.*, vol. 15, no. 6, pp. 1775–1796, Dec. 1966.

[34] B. Saltzberg, "Performance of an Efficient Parallel Data Transmission System," *IEEE Trans. Commun. Tech.*, vol. 15, no. 6, pp. 805 –811, Dec. 1967.

[35] M. Bellanger and J. Daguet, "TDM-FDM Transmultiplexer: Digital Polyphase and FFT," *IEEE Trans. Commun.*, vol. 22, no. 9, pp. 1199 – 1205, Sep. 1974.

[36] B. Hirosaki, "An Orthogonally Multiplexed QAM System Using the Discrete Fourier Transform," *IEEE Trans. Commun.*, vol. 29, no. 7, pp. 982 – 989, Jul. 1981.

[37] G. Cherubini, E. Eleftheriou, and S. Olcer, "Filtered multitone modulation for vdsl," in *Global Telecommunications Conference, 1999. GLOBECOM '99*, 1999, vol. 2, pp. 1139 –1144 vol.2.

[38] G. Cherubini, E. Eleftheriou, S. Oker, and J.M. Cioffi, "Filter bank modulation techniques for very high speed digital subscriber lines," *Communications Magazine, IEEE*, vol. 38, no. 5, pp. 98 –104, may 2000.

[39] G. Cherubini, E. Eleftheriou, and S. Olcer, "Filtered multitone modulation for very high-speed digital subscriber lines," *Selected Areas in Communications, IEEE Journal on*, vol. 20, no. 5, pp. 1016 –1028, jun 2002.

[40] S.D. Sandberg and M.A. Tzannes, "Overlapped Discrete Multitone Modulation for High Speed Copper Wire Communications," *IEEE J. Select. Areas Commun.*, vol. 13, no. 9, pp. 1571 –1585, Dec. 1995.

[41] B. Farhang-Boroujeny, "Multicarrier Modulation with Blind Detection Capability using Cosine Modulated Filter Banks," *IEEE Trans. Commun.*, vol. 51, no. 12, pp. 2057 – 2070, Dec. 2003.

[42] P. Amini, R. Kempter, and B. Farhang-Boroujeny, "A Comparison of Alternative Filter Bank Multicarrier Methods for Cognitive Radio Systems," in *Proc. of SDR Technical Conference and Product Exposition (SDR)*, Florida, USA, Jun. 2006.

[43] P. Siohan, C. Siclet, and N. Lacaille, "Analysis and Design of OFDM/OQAM Systems Based on Filter bank Theory,," *IEEE Trans. Signal Process.*, vol. 50, no. 5, pp. 1170–1183, May 2002.

[44] H. Bölcskei, "Orthogonal Frequency Division Multiplexing based on Offset QAM," *Advances in Gabor Analysis*, pp. 321–352, 2003.

[45] R. Zakaria, D. Le Ruyet, and M. Bellanger, "Maximum likelihood detection in spatial multiplexing with FBMC," in *Wireless Conference (EW), 2010 European*, april 2010, pp. 1038 –1041.

[46] R. Zakaria and D. Le Ruyet, "On spatial data multiplexing over coded filter-bank multicarrier with ML detection," in *Personal Indoor and Mobile Radio Communications (PIMRC), 2011 IEEE 22nd International Symposium on*, sept. 2011, pp. 1391 –1395.

[47] R. Zakaria, D. Le Ruyet, and Y. Medjahdi, "On ISI cancellation in MIMO-ML detection using FBMC/QAM modulation," in *Wireless Communication Systems (ISWCS), 2012 International Symposium on*, aug. 2012, pp. 949 –953.

[48] C. Lélé, *OFDM/OQAM : Méthodes d'Estimation de Canal, et Combinaison avec l'Accès Multiple CDMA ou les Systèmes Multi-Antennes*, Ph.D. thesis, Conservatoire National des Arts et Métiers, Paris, France, 2008.

[49] H. Lin, P. Siohan, P. Tanguy, and J-P. Javaudin, "An Analysis of the EIC Method for OFDM/OQAM Systems," *Journal of Communications*, vol. 4, no. 1, pp. 52–60, Feb. 2009.

[50] A. Vahlin and N. Holte, "Optimal Finite Duration Pulses for OFDM," *IEEE Trans. Commun.*, vol. 44, no. 1, pp. 10 –14, Jan. 1996.

[51] L. Vandendorpe, L. Cuvelier, F. Deryck, J. Louveaux, and O. van de Wiel, "Fractionally Spaced Linear and Decision-Feedback Detectors for Transmultiplexers," *IEEE Trans. Signal Processing*, vol. 46, no. 4, pp. 996 –1011, Apr. 1998.

[52] B. Hirosaki, "An Analysis of Automatic Equalizers for Orthogonally Multiplexed QAM Systems," *IEEE Trans. Commun.*, vol. 28, no. 1, pp. 73 – 83, Jan. 1980.

[53] S. Nedic, "An Unified Approach to Equalization and Echo Cancellation in OQAM-Based Multi-Carrier Data Transmission," in *IEEE Global Telecommunications Conference*, Nov. 1997, vol. 3, pp. 1519 –1523.

[54] K. Van Acker, G. Leus, M. Moonen, O. van de Wiel, and T. Pollet, "Per Tone Equalization for DMT-based Systems," *IEEE Trans. Commun.*, vol. 49, no. 1, pp. 109 –119, Jan. 2001.

[55] D.S. Waldhauser, L.G. Baltar, and J.A. Nossek, "MMSE Subcarrier Equalization for Filter Bank based Multicarrier Systems," in *IEEE 9th Workshop on Signal Processing Advances in Wireless Communications*, Jul. 2008, pp. 525 –529.

[56] D.S. Waldhauser, L.G. Baltar, and J.A. Nossek, "Adaptive Decision Feedback Equalization for Filter Bank based Multicarrier Systems," in *IEEE International Symposium on Circuits and Systems*, May 2009, pp. 2794 –2797.

[57] T. Ihalainen, T. Hidalgo Stitz, M. Rinne, and M. Renfors, "Channel Equalization in Filter Bank Based Multicarrier Modulation for Wireless Communications," *EURASIP Journal on Advances in Signal Processing*, p. 18, 2007.

[58] M. Bellanger, G. Bonnerot, and M. Coudreuse, "Digital Filtering by Polyphase Network: Application to Sample-Rate Alteration and Filter Banks," *IEEE Trans. Acoustics, Speech and Signal Processing*, vol. 24, no. 2, pp. 109 – 114, Apr. 1976.

[59] P. P. Vaidyanathan, *Multirate Systems and Filter Banks*, Prentice-Hall, Inc., Upper Saddle River, NJ, USA, 1993.

[60] B. Farhang-Boroujeny, *Signal Processing Techniques for Software Radios*, LuLu Publishing, Morrisville, North Carolina, USA, 2005.

[61] N. J. Fliege, *Multirate Digital Signal Processing: Multirate Systems, Filter Banks, Wavelets*, John Wiley, Hoboken, New Jersey, USA, 1994.

[62] G. Cariolaro and F.C. Vagliani, "An OFDM Scheme with a Half Complexity," *IEEE Jour. Select. Areas in Commun.*, vol. 13, no. 9, pp. 1586 –1599, Dec. 1995.

[63] L. Vangelista and N. Laurenti, "Efficient Implementations and Alternative Architectures for OFDM-OQAM Systems," *IEEE Trans. Commun.*, vol. 49, no. 4, pp. 664 –675, Apr. 2001.

[64] P. Siohan and C. Roche, "Cosine-Modulated Filterbanks based on Extended Gaussian Functions," *IEEE Trans. Signal Processing*, vol. 48, no. 11, pp. 3052 –3061, Nov. 2000.

[65] Delivrable D2.1, "Data-aided Synchronization and Initialization (Single Antenna)," Tech. Rep., European project ICT-211887 PHYDYAS, Jan. 2009.

[66] J. Proakis, *Digital Communications*, 4th ed. : McGraw- Hill, New York, USA, 1994.

[67] P. Chevillat and G. Ungerboeck, "Optimum FIR Transmitter and Receiver Filters for Data Transmission Over Band-Limited Channels," *IEEE Trans. on Commun.*, vol. 30, no. 8, pp. 1909 – 1915, Aug. 1982.

[68] Delivrable D5.1, "Prototype Filter and Structure Optimization," Tech. Rep., European project ICT-211887 PHYDYAS, Jan. 2009.

[69] H. Sari and G. KARAM, "Orthogonal Frequency-Division Multiple Access and its Application to CATV Networks," *Eur. trans. telecommun.*, vol. 9, no. 6, pp. 507–516, Nov-Dec. 1998.

[70] *Interaction Channel for Digital TerrestrialTelevision (RCT) Incorporating MultipleAccess OFDM*, ETS 301 958 Eur. Telecommun. Standard Institute, Mar. 2001.

[71] "IEEE Standard for Local and Metropolitan Area Networks — Part 16: Air Interface for Fixed Broadband Wireless Access Systems— Amendment 2: Medium Access Control Modifications and Additional Physical Layer Specifications for 2-11 GHz," *IEEE Std 802.16a-2003 (Amendment to IEEE Std 802.16-2001)*, 2003.

[72] A.M. Tonello and S. Pupolin, "Performance of Single User Detectors in Multitone Multiple Access Asynchronous Communications," in *Vehicular Technology Conference, 2002. VTC Spring 2002. IEEE 55th*, 2002, vol. 1, pp. 199 – 203.

[73] A. M. Tonello, "Asynchronous Multicarrier Multiple Access: Optimal and Sub-Optimal Detection and Decoding," *Bell Labs Tech. Jour.*, vol. 7, no. 3, pp. 191–217, Mar. 2003.

[74] S. Haykin, "Cognitive Radio: Brain-Empowered Wireless Communications," *IEEE J. Select. Areas Commun.*, vol. 23, no. 2, pp. 201 – 220, feb. 2005.

[75] J. Mitola and Jr. Maguire, G.Q., "Cognitive Radio: Making Software Radios More Personal," *IEEE Personal Commun.*, vol. 6, no. 4, pp. 13 –18, aug 1999.

[76] Ian F. Akyildiz, Won-Yeol Lee, Mehmet C. Vuran, and Shantidev Mohanty, "NeXt Generation/Dynamic Spectrum Access/Cognitive Radio Wireless Networks: A survey," *Computer Networks*, vol. 50, no. 13, pp. 1389–1286, 2006.

[77] T.A. Weiss and F.K. Jondral, "Spectrum Pooling: an innovative strategy for the enhancement of spectrum efficiency," *IEEE Commun. Mag.*, vol. 42, no. 3, pp. S8 – S14, mar 2004.

[78] K.A. Hamdi and Y.M. Shobowale, "Interference Analysis in Downlink OFDM Considering Imperfect Intercell Synchronization," *IEEE Trans. Veh. Technol.*, vol. 58, no. 7, pp. 3283 –3291, sept. 2009.

[79] M. Shaat and F. Bader, "An Uplink Resource Allocation Algorithm for OFDM and FBMC based Cognitive Radio Systems," in *Proceedings of Conference on Cognitive Radio Oriented Wireless Networks Communications (CROWNCOM)*, Jun. 2010, pp. 1 –6.

[80] Y. Medjahdi, M. Terré, Le Ruyet, D., D. Roviras, J.A. Nossek, and L. Baltar, "Inter-cell interference analysis for OFDM/FBMC systems," in *IEEE 10th Workshop on Signal Processing Advances in Wireless Communications, 2009. SPAWC '09.*, Jun. 2009, pp. 598 –602.

[81] Y. Medjahdi, M. Terré and, D. Le Ruyet, and D. Roviras, "Asynchronous OFDM/FBMC interference analysis in selective channels," in *Personal Indoor and Mobile Radio Communications (PIMRC), 2010 IEEE 21st International Symposium on*, sept. 2010, pp. 538 –542.

[82] *Universal Mobile Telecommunications System (UMTS); Radio Frequency (RF) system scenarios*, ETS TR 125 942, Eur. Telecommun. Standard Institute, 2010.

[83] K. Raghunath and A. Chockalingam, "SIR Analysis and Interference Cancellation in Uplink OFDMA with Large Carrier Frequency/Timing Offsets," *IEEE Trans. Wireless Commun.*, vol. 8, no. 5, pp. 2202 –2208, May 2009.

[84] Y. Medjahdi, M. Terré, D. Le Ruyet, and D. Roviras, "A New Model for Interference Analysis in Asynchronous Multi-Carrier Transmission," *submitted to IEEE Trans. Veh. Technol. and available at arXiv*, vol. 1006.4278v1 [cs.NI], 2012.

[85] X. Wang, T.T. Tjhung, Yiyan Wu, and B. Caron, "SER Performance Evaluation and Optimization of OFDM System with Residual Frequency and Timing Offsets from Imperfect Synchronization," *IEEE Trans. Broadcast.*, vol. 49, no. 2, pp. 170 – 177, jun. 2003.

[86] Y. Mostofi and D.C. Cox, "Mathematical Analysis of the Impact of Timing Synchronization Errors on the Performance of an OFDM System," *IEEE Trans. on Commun.*, vol. 54, no. 2, pp. 226 – 230, Feb. 2006.

[87] T. Pollet, M. Van Bladel, and M. Moeneclaey, "BER Sensitivity of OFDM Systems to Carrier Frequency Offset and Wiener Phase Noise," *IEEE Trans. on Commun.*, vol. 43, no. 234, pp. 191 –193, feb/mar/apr 1995.

[88] T. Pollet and M. Moeneclaey, "The Effect of Carrier Frequency Offset on the Pperformance of Band Limited Single Carrier and OFDM Signals," in *Proc. IEEE GLOBECOM*, nov 1996, vol. 1, pp. 719 –723 vol.1.

[89] T. Pollet, P. Spruyt, and M. Moeneclaey, "The BER Performance of OFDM Systems using Non-Synchronized Sampling," in *Proc. IEEE GLOBECOM*, nov 1994, pp. 253 –257 vol.1.

[90] N.C. Beaulieu, "The Evaluation of Error Probabilities for InterSymbol and Cochannel Interference," *IEEE Trans. on Commun.*, vol. 39, no. 12, pp. 1740 –1749, dec 1991.

[91] N.C. Beaulieu, "An Infinite Series for the Computation of the Complementary Probability Distribution Function of a Sum of Independent Random Variables and its Application to the Sum of Rayleigh Random Variables," *IEEE Trans. on Commun.*, vol. 38, no. 9, pp. 1463 –1474, sep 1990.

[92] S. Verdú, *Multiuser Detection*, Cambridge University Press, 1998.

[93] Y. Medjahdi, M. Terre, D. Le Ruyet, D. Roviras, and A. Dziri, "Performance analysis in the downlink of asynchronous ofdm/fbmc based multi-cellular networks," *Wireless Communications, IEEE Transactions on*, vol. 10, no. 8, pp. 2630 –2639, august 2011.

[94] Y. Medjahdi, M. Terre, D. Le Ruyet, D. Roviras, and A. Dziri, "The Impact of Timing Synchronization Errors on the Performance of OFDM/FBMC Systems," in *Communications (ICC), 2011 IEEE International Conference on*, june 2011, pp. 1 –5.

[95] Y. Medjahdi, D. Le Ruyet, D. Roviras, H Shaeik, and R Zakaria, "On the Impact of the Prototype Filter on FBMC Sensitivity to Time Asynchronism," in *ISWCS 2012*, Aug. 2012, pp. 1–5.

[96] *Guidelines for evaluation of radio transmission technologies for IMT-2000*, Rec. ITU-R M.1225 1, 1997.

[97] W.C.Y. Lee, "Estimate of Channel Capacity in Rayleigh Fading Environment," *IEEE Trans. on Veh. Technol.*, vol. 39, no. 3, pp. 187 –189, Aug 1990.

[98] G. Caire and S. Shamai, "On the Capacity of Some Channels with Channel State Information," *IEEE Trans. on Inform. Theory*, vol. 45, no. 6, sep 1999.

[99] J. Li, A. Bose, and Y.Q. Zhao, "Rayleigh Flat Fading Channels Capacity," in *Proc. 3rd Annual Commun. Networks Services Research Conf.*, May 2005, pp. 214 – 217.

[100] M.-S. Alouini and A.J. Goldsmith, "Area Spectral Efficiency of Cellular Mobile Radio Systems," *IEEE Trans. on Veh. Technol.*, vol. 48, no. 4, pp. 1047 –1066, Jul. 1999.

[101] K.A. Hamdi, "Average Capacity Analysis of OFDM with Frequency Offset in Rician Fading," in *Proc. IEEE GLOBECOM*, Nov. 2007, pp. 1678 –1682.

[102] C. E. Shannon, "A Mathematical Theory of Communication," *Bell. Sys. Tech. Journal*, pp. 379–423, 1948.

[103] Y. Medjahdi, M. Terre, D. Le Ruyet, and D. Roviras, "On spectral efficiency of asynchronous OFDM/FBMC based cellular networks," in *Personal Indoor and Mobile Radio Communications (PIMRC), 2011 IEEE 22nd International Symposium on*, sept. 2011, pp. 1381 –1385.

[104] M Shaat and F Bader, "Computationally Efficient Power Allocation Algorithm in MultiCarrier-based Cognitive Radio Networks: OFDM and FBMC systems," *EURASIP J. Adv. Signal Process*, vol. 2010, pp. 13, Jan 2010.

[105] H. Zhang, D. Le Ruyet, D. Roviras, and Hong Sun, "Noncooperative Multicell Resource Allocation of FBMC-based Cognitive Radio Systems," *IEEE Trans. on Veh. Technol.*, vol. 61, no. 2, pp. 799 –811, Feb. 2012.

Appendices

Appendix A

Relative Appendix in Section 3.4

A.1 Proof of the expressions (3.24) and (3.25)

Substituting the expression (2.50) in (3.23), we obtain when $l = 0$

$$\begin{aligned}\Psi(t,\tau,0)\Big|_{t=t_1}^{t_2} &= \int_{t_1}^{t_2} g(t-\tau)g(t)dt \\ &= \int_{t_1}^{t_2} \left[1 + 2\sum_{n=1}^{K-1}(-1)^n G_n \cos\left(\frac{2\pi}{KT}nt\right)\right]\left[1 + 2\sum_{n=1}^{K-1}(-1)^n G_n \cos\left(\frac{2\pi}{KT}n(t-\tau)\right)\right]dt\end{aligned}$$

Using some trigonometric transformations, the integral $\Psi(t,\tau,0)\Big|_{t=t_1}^{t_2}$ can be written in the following form

$$\begin{aligned}\Psi(t,\tau,0)\Big|_{t=t_1}^{t_2} &= \int_{t_1}^{t_2} 1 + 2\sum_{n=1}^{K-1}(-1)^n G_n \left[\cos\left(\frac{2\pi}{KT}nt\right) + \cos\left(\frac{2\pi}{KT}n(t-\tau)\right)\right] \\ &+ 2\sum_{n=1}^{K-1}\sum_{m=1}^{K-1}(-1)^{n+m} G_n G_m \left[\cos\left(\frac{2\pi}{KT}\left((n+m)t - n\tau\right)\right) + \cos\left(\frac{2\pi}{KT}\left((n-m)t - n\tau\right)\right)\right]dt\end{aligned}$$

After integration, we get

$$\begin{aligned}\Psi(t,\tau,0)\Big|_{t=t_1}^{t_2} &= \frac{t}{A}\left[1+2\sum_{n=1}^{K-1}G_n^2\cos\left(\frac{2\pi}{KT}n\tau\right)\right] \\ &+ \frac{KT}{\pi A}\left\{\sum_{n=1}^{K-1}\sum_{m=1}^{K-1}(-1)^{n+m}\ \frac{G_nG_m}{n+m}\sin\left(\frac{2\pi}{KT}((n+m)t-n\tau)\right)\right. \\ &\quad + \sum_{n=1}^{K-1}\sum_{\substack{m=1\\ n\neq m}}^{K-1}(-1)^{n+m}\frac{G_nG_m}{n-m}\sin\left(\frac{2\pi}{KT}((n-m)t-n\tau)\right) \\ &\quad \left.+\sum_{n=1}^{K-1}(-1)^n\frac{G_n}{n}\left[\sin\left(\frac{2\pi}{KT}n\tau\right)+\sin\left(\frac{2\pi}{KT}n(t-\tau)\right)\right]\right\}\Big|_{t=t_1}^{t_2}\end{aligned}$$

when $l\neq 0$,

$$\begin{aligned}&\Psi(t,\tau,l)\Big|_{t=t_1}^{t_2} = \int_{t_1}^{t_2} g(t-\tau)g(t)e^{j\frac{2\pi}{T}lt}dt \\ &= \int_{t_1}^{t_2} e^{j\frac{2\pi}{T}lt}\left\{1+2\sum_{n=1}^{K-1}(-1)^nG_n\left[\cos\left(\frac{2\pi}{KT}nt\right)+\cos\left(\frac{2\pi}{KT}n(t-\tau)\right)\right]\right. \\ &\left.+\,2\sum_{n=1}^{K-1}\sum_{m=1}^{K-1}(-1)^{n+m}G_nG_m\left[\cos\left(\frac{2\pi}{KT}\left((n+m)t-n\tau\right)\right)+\cos\left(\frac{2\pi}{KT}\left((n-m)t-n\tau\right)\right)\right]\right\}dt\end{aligned}$$

After integration, we obtain

$$\begin{aligned}\Psi(t,\tau,l)\Big|_{t=t_1}^{t_2} &= \frac{T}{j2\pi lA}e^{j\frac{2\pi}{T}lt} \\ &+ \frac{KT}{j2\pi A}\sum_{n=1}^{K-1}(-1)^nG_n\left[\frac{1+e^{-j\frac{2\pi}{KT}n\tau}}{n+Kl}e^{j\frac{2\pi}{KT}(n+Kl)t}-\frac{1+e^{j\frac{2\pi}{KT}n\tau}}{n-Kl}e^{-j\frac{2\pi}{KT}(n-Kl)t}\right] \\ &+ \frac{KT}{j2\pi A}\sum_{n=1}^{K-1}\sum_{m=1}^{K-1}(-1)^{n+m}G_nG_m\left[e^{-j\frac{2\pi}{KT}n\tau}\left(\frac{e^{j\frac{2\pi}{KT}(n+m+Kl)t}}{n+m+Kl}+\frac{e^{j\frac{2\pi}{KT}(n-m+Kl)t}}{n-m+Kl}\right)\right. \\ &\qquad \left.-\,e^{j\frac{2\pi}{KT}n\tau}\left(\frac{e^{-j\frac{2\pi}{KT}(n+m-Kl)t}}{n+m-Kl}+\frac{e^{-j\frac{2\pi}{KT}(n-m-Kl)t}}{n-m-Kl}\right)\right]\Big|_{t=t_1}^{t_2}\end{aligned}$$

Appendix B

Relative Appendix in Section 4.4

B.1 Proof of the expression (4.15)

In this section, we establish the theoretical derivation of the expression (4.15). We write the following conditional expectation

$$\mathbb{E}_x\left[\text{erfc}\left(\frac{x}{y+b}\right)^{1/2}\right] = \int_0^{+\infty} \text{erfc}\left(\frac{x}{y+b}\right)^{1/2} e^{-x}dx \tag{B.1}$$

where x is an exponential RV which is independent of y.
Using a suitable change of variables $z = x/(y+b)$, equation (B.1) becomes

$$\mathbb{E}_x\left[\text{erfc}\left(\frac{x}{y+b}\right)^{1/2}\right] = \int_0^{+\infty} \text{erfc}(\sqrt{z})e^{-z(y+b)}(y+b)dz$$

Applying the rules of integration by parts, we obtain

$$\mathbb{E}_x\left[\text{erfc}\left(\frac{x}{y+b}\right)^{1/2}\right] = -\text{erfc}(\sqrt{z})e^{-z(y+b)}\Big|_{z=0}^{+\infty} + \int_0^{\infty} e^{-z(y+b)}\left[\frac{d}{dz}\text{erfc}\sqrt{z}\right]dz \tag{B.2}$$

Since y and b are positive, $-\text{erfc}(\sqrt{z})e^{-z(y+b)}\Big|_{z=0}^{+\infty} = 1$. Furthermore, the derivative of $\text{erfc}\sqrt{z}$ is given by

$$\frac{d}{dz}\text{erfc}\sqrt{z} = -\frac{1}{\sqrt{\pi}}\frac{e^{-z}}{\sqrt{z}} \tag{B.3}$$

Substituting (B.3) in (B.2), we obtain

$$\mathbb{E}_x\left[\operatorname{erfc}\left(\frac{x}{y+b}\right)^{1/2}\right] = 1 - \frac{1}{\sqrt{\pi}}\int_0^{+\infty}\frac{e^{-z(1+b)}}{\sqrt{z}}e^{-zy}dz \tag{B.4}$$

By averaging on y, we get

$$\begin{aligned}\mathbb{E}_{x,y}\left[\operatorname{erfc}\left(\frac{x}{y+b}\right)^{1/2}\right] &= 1 - \frac{1}{\sqrt{\pi}}\int_0^{+\infty}\frac{e^{-z(1+b)}}{\sqrt{z}}\mathbb{E}_y\left[e^{-zy}\right]dz \\ &= 1 - \frac{1}{\sqrt{\pi}}\int_0^{+\infty}\frac{e^{-z(1+b)}}{\sqrt{z}}\mathcal{M}_y(z)dz \end{aligned}\tag{B.5}$$

B.2 Proof of the expression (4.26)

The proof of (4.26) can be reduced to demonstrate that

$$\mathcal{M}_k(z) = \begin{vmatrix} 1+\alpha_1 & \alpha_1 & \cdots & \alpha_1 \\ \alpha_2 & 1+\alpha_2 & \cdots & \alpha_2 \\ \vdots & \vdots & \vdots & \\ \alpha_{L_k} & \alpha_{L_k} & \cdots & 1+\alpha_{L_k} \end{vmatrix} = 1 + \sum_{i=1}^{L_k}\alpha_i \tag{B.6}$$

where α_i represents $2A_{k,m,m'_i}z$.
In what follows, we demonstrate that the statement given in (B.6) holds for any positive integer $L_k > 1$:

Basis($L_k = 2$): In this case, we have

$$\begin{vmatrix} 1+\alpha_1 & \alpha_1 \\ \alpha_2 & 1+\alpha_2 \end{vmatrix} = (1+\alpha_1)(1+\alpha_2) - \alpha_1\alpha_2 = 1 + \sum_{i=1}^{2}\alpha_i \tag{B.7}$$

Inductive step: Assume that the statement in (B.6) holds for $L_k = N$,

$$\begin{vmatrix} 1+\alpha_1 & \alpha_1 & \cdots & \alpha_1 \\ \alpha_2 & 1+\alpha_2 & \cdots & \alpha_2 \\ \vdots & \vdots & \vdots & \\ \alpha_N & \alpha_N & \cdots & 1+\alpha_N \end{vmatrix} = 1 + \sum_{i=1}^{N}\alpha_i \tag{B.8}$$

It must then be shown that (B.6) holds for $L_k = N+1$, that is:

$$\begin{vmatrix} 1+\alpha_1 & \alpha_1 & \cdots & \alpha_1 \\ \alpha_2 & 1+\alpha_2 & \cdots & \alpha_2 \\ \vdots & \vdots & \vdots & \\ \alpha_{N+1} & \alpha_{N+1} & \cdots & 1+\alpha_{N+1} \end{vmatrix} = 1 + \sum_{i=1}^{N+1}\alpha_i \tag{B.9}$$

The left-hand side in (B.9) can be rewritten as

$$\begin{vmatrix} 1+\alpha_1 & \alpha_1 & \cdots & \alpha_1 \\ \alpha_2 & 1+\alpha_2 & \cdots & \alpha_2 \\ \vdots & \vdots & \vdots & \\ \alpha_{N+1} & \alpha_{N+1} & \cdots & 1+\alpha_{N+1} \end{vmatrix}$$

$$= \underbrace{\begin{vmatrix} 1+\alpha_1 & \alpha_1 & \cdots & \alpha_1 \\ \alpha_2 & 1+\alpha_2 & \cdots & \alpha_2 \\ \vdots & \vdots & \vdots & \\ \alpha_N & \alpha_N & \cdots & 1+\alpha_N \end{vmatrix}}_{\mathrm{T}_1} + \underbrace{\begin{vmatrix} 1+\alpha_1 & \alpha_1 & \cdots & \alpha_1 \\ \alpha_2 & 1+\alpha_2 & \cdots & \alpha_2 \\ \vdots & \vdots & \vdots & \\ \alpha_{N+1} & \alpha_{N+1} & \cdots & \alpha_{N+1} \end{vmatrix}}_{\mathrm{T}_2} \tag{B.10}$$

Based on the induction hypothesis given in (B.8), T_1 becomes

$$\mathrm{T}_1 = 1 + \sum_{i=1}^{N} \alpha_i \tag{B.11}$$

Now, doing the following linear transform on columns $C_{i=1,\ldots,N}$ of T_2

$$C_i = C_i - C_{N+1} \tag{B.12}$$

we get,

$$\mathrm{T}_2 = \begin{vmatrix} 1 & 0 & \cdots & 0 & \alpha_1 \\ 0 & \ddots & \ddots & \vdots & \vdots \\ \vdots & \ddots & \ddots & 0 & \vdots \\ \vdots & & \ddots & 1 & \alpha_N \\ 0 & \cdots & \cdots & 0 & \alpha_{N+1} \end{vmatrix} = \alpha_{N+1} \tag{B.13}$$

Consequently, (B.11) and (B.13) show that indeed the statement in (B.9) holds. Since both the basis and inductive steps have been validated, it has now been proved by mathematical induction that (B.6) holds for any positive integer $L_k > 1$.

Appendix C

Relative Appendix in Section 5.2

C.1 Proof of the expression (5.6)

In this section, we provide the proof of the expression (5.6), that is equivalent to

$$\mathbb{E}_{x,g}\left[\ln\left(1+\frac{x}{g+c}\right)\right] = \int_0^\infty \frac{e^{-zb}}{1+z}\mathcal{M}_g(z)dz \tag{C.1}$$

where x is an exponential RV which is independent of g.
The expectation in left-hand side of (C.1) can be written as a double conditional expectation,

$$\mathbb{E}_{x,g}\left[\ln\left(1+\frac{x}{g+c}\right)\right] = \mathbb{E}_g\left[\mathbb{E}_x\left[\ln\left(1+\frac{x}{g+c}\right)\right]\right] \tag{C.2}$$

Since the pdf of x is $f(x) = e^{-x}$, $x \geq 0$, the following conditional expectation can be expressed by

$$\mathbb{E}_x\left[\ln\left(1+\frac{x}{g+c}\right)\right] = \int_0^{+\infty} \ln\left(1+\frac{x}{g+c}\right) e^{-x}dx \tag{C.3}$$

Substituting $x/(g+b)$ by z, equation (C.3) becomes

$$\mathbb{E}_x\left[\ln\left(1+\frac{x}{g+c}\right)\right] = \int_0^{+\infty} \ln\left(1+z\right) e^{-z(g+b)}(g+b)dz$$

Here, the integral limits remain the same because g and b are positive.
Applying the rules of integration by parts, we obtain

$$\mathbb{E}_x\left[\ln\left(1+\frac{x}{g+c}\right)\right] = -\ln(1+z)\,e^{-z(g+b)}\Big|_{z=0}^{+\infty} + \int_0^{+\infty} e^{-z(g+b)}\left[\frac{d}{dz}\ln(1+z)\right]dz \quad \text{(C.4)}$$

Since g and b are positive, $-\ln(1+z)\,e^{-z(g+b)}\Big|_{z=0}^{+\infty} = 0$. Furthermore, the derivative of $\ln(1+z)$ is given by

$$\frac{d}{dz}\ln(1+z) = \frac{1}{1+z} \quad \text{(C.5)}$$

Substituting (C.5) in (C.4), we get

$$\mathbb{E}_x\left[\ln\left(1+\frac{x}{g+c}\right)\right] = \int_0^{+\infty} e^{-z(g+b)}\frac{1}{1+z}dz \quad \text{(C.6)}$$

By averaging on g, we obtain

$$\begin{aligned}\mathbb{E}_{x,g}\left[\ln\left(1+\frac{x}{g+c}\right)\right] = &= \int_0^{+\infty}\frac{e^{-zb}}{1+z}E_g\left[e^{-zg}\right]dz \\ &= \int_0^{+\infty}\frac{e^{-zb}}{1+z}\mathcal{M}_g(z)dz \quad \text{(C.7)}\end{aligned}$$